UNIVERSIDADE D
COIMBRA

João Tomás da Silva Barros

CHANGES IN THE GUT-BRAIN AXIS DURING AGING

Dissertação no âmbito do Mestrado em Biologia Celular e Molecular com especialidade em Neurobiologia orientada pela Professora Doutora Raffaella Gozzelino e pelo Professor Doutor Carlos Jorge Alves Miranda Bandeira Duarte apresentada ao Departamento de Ciências da Vida da Universidade de Coimbra.

Outubro de 2020

Changes in the Gut-Brain axis during aging

João Tomás da Silva Barros

Dissertação no âmbito do Mestrado em Biologia Celular e Molecular com especialidade em Neurobiologia orientada pela Professora Doutora Raffaella Gozzelino e pelo Professor Doutor Carlos Jorge Alves Miranda Bandeira Duarte apresentada ao Departamento de Ciências da Vida da Universidade de Coimbra.

Outubro de 2020

UNIVERSIDADE D
COIMBRA

AGRADECIMENTOS

Em primeiro lugar, gostaria de agradecer à minha orientadora, a Doutora Raffaella Gozzelino, por me ter dado esta oportunidade e por tudo o que me ensinou ao longo do ano, tanto a nível científico como profissional. Obrigado por todo o apoio.

Quero agradecer também aos restantes membros do nosso grupo, principalmente à Ana e à Ilyane. Já sabem que não há espaço suficiente nesta página para poder agradecer por tudo. Obrigado pelo que me ensinaram, pela ajuda, pela paciência e até pelos sermões. Estabeleceram um nível ao qual um dia gostaria de chegar, e sem bocês esta tese não seria feita. Talvez um dia destes vos pague um almoço…..

Agradeço também a todo o pessoal que me apoiou ao longo deste percurso. Percebessem, ou não, o que andava a fazer, deram-me sempre motivação e mostraram-se disponíveis para ajudar no que fosse. Mesmo que fosse só para ouvir as minhas frustrações, estiveram sempre lá. São demasiados para vos poder listar a todos individualmente, mas a carapuça serve a quem já sabe. Obrigado, sem a vossa amizade não seria a mesma coisa.

Por fim, gostaria de agradecer às pessoas que são sem sombra de dúvida os pilares que me aguentam nos bons e nos maus momentos. Para qualquer um de vocês um 'obrigado' nunca será suficiente. Aos meus pais agradeço o apoio incondicional que sempre me deram. Discordamos em alguns aspectos e estes 3 anos foram tudo menos fáceis, mas nunca desistiram. É um orgulho ser vosso filho, e se alguma vez conseguir alcançar na vida metade do que vocês conseguiram, serei sem dúvida uma pessoa feliz. São o melhor exemplo que podia ter pedido. Falando em exemplos, quero também deixar um agradecimento especial ao meu irmão. O meu melhor amigo desde sempre, pronto para me ajudar seja no que for, mesmo quando o que faço está errado. Saber que tenho alguém comigo que independemente do que acontecer, estará sempre lá dá-me a maior segurança que podia ter. És um excelente exemplo, 'e quando for grande quero ser como tu!'. Obrigado, a sério, não podemos escolher a nossa família, mas mesmo que pudesse não a mudava por nada.

Tenho de deixar também o meu maior agradecimento à melhor de sempre. Catarina, sinceramente não sei o que dizer. És o meu maior motivo de orgulho e de motivação. Estiveste sempre lá ao longo de todo este percurso, mesmo quando nem eu sabia que precisava de apoio. É o meu maior prazer poder partilhar contigo as tuas vitórias, e muitas mais ainda hão de vir. Sabes que da minha parte estarei sempre lá para ti, tal como estás incondicionalmente para mim. Obrigado por seres a minha melhor amiga, a minha namorada, e por ter a oportunidade de caminhar a teu lado. Sem ti, a vida não seria igual.

A todos, muito, muito obrigado. Esta vitória é tanto minha como vossa, e espero ter-vos deixado orgulhoso.

Obrigado!

ABSTRACT

Low-grade chronic inflammation and altered composition of gut microbiota have been suggested to underlie the pathogenesis of neurodegenerative diseases, such as Parkinson's disease (PD). An increased level of pro-inflammatory cytokines was found in both peripheral blood and colonic biopsies of PD patients, an observation that allowed linking gut immunity and inflammation. The notion that PD patients usually present intestinal dysfunction and constipation further strengthens the importance of a gut-brain interaction during the development of neurodegenerative diseases, like PD. Since gastro-intestinal (GI) manifestations often occur a decade before the appearance of severe motor deficits, changes in gut microbes can be identified as early PD symptoms. Hence, the disruption between commensal and pathogenic bacteria in the gut, as physiologically occurs during aging, is thought to favor an increased susceptibility to PD. This study aimed to verify that changes occurring in the gut microbiota during aging rendered mice more susceptible to PD. Moreover, we hypothesized that the accumulation of iron could be the underlying cause of this unbalance.

C57BL/6 mice were used, as a pre-clinical animal model, to address the objectives of this study. Comparisons between relatively young (8-12-weeks old) and old (52-60-weeks old) mice were carried out, in terms of neuroinflammation and iron accumulation. The gut-brain axis was evaluated by associating the results obtained in the gut with an increased neuroinflammation and iron accumulation in the brain. A pharmacological model of PD was induced by the administration of 1-methyl-4-phenyl-1,2,3,6-tetrahydropyridine (MPTP), a neurotoxin known to target exclusively dopaminergic neurons in the substantia nigra of the brain. Fecal transplantation was also used to address whether changing the composition of the gut microbiota could influence the neuro-inflammatory profile of aged mice and, subsequently, the severity of PD.

Preliminary data supporting the hypotheses put forth were already obtained in the laboratory, so it was crucial their validation with the experimental plan proposed to complete my studies. This research was expected to prove that changes in gut microbiota occurring during aging were capable to influence the neuro-inflammatory phenotype of older mice and to increase the severity of PD. Furthermore, it was also expected to show that the molecular mechanism underlying this phenomenon relied on the accumulation of iron in the gut, a process known to increase bacteria pathogenicity and to modulate the inflammatory response.

Keywords: Aging; Gut Microbiota; Iron; Inflammation; Parkinson's disease.

RESUMO

Atualmente, pensa-se que inflamação sub-crónica e um microbioma intestinal alterado poderão estar subjacentes à patogénese de doenças neurodegenerativas, tais como na doença de Parkinson. O descrito aumento do número de citocinas pró-inflamatórias tanto no sangue, como em biópsias colónicas de doentes de Parkinson permitiu conectar, assim, imunidade gastrointestinal com inflamação. Uma vez que os pacientes desta doença muitas vezes apresentam disfunção intestinal acrescenta peso à importância da interação intestino-cérebro no desenvolvimento da neurodegeneração. Uma vez que perturbações gastrointestinais podem ocorrer até décadas antes do aparecimento de sintomas motores, mudanças no microbioma intestinal poderão ser identificadas como prognóstico antecipado. Assim, a disrupção entre bactérias comensais e patogénicas no intestino, tal como acontece com o envelhecimento, poderá aumentar a suscetibilidade à doença de Parkinson.

Este estudo teve como objetivo verificar que as alterações que ocorrem no microbioma com o envelhecimento, deixam ratinhos mais suscetíveis ao desenvolvimento da doença de Parkinson. Mais, ponderamos que a acumulação de ferro no intestino durante o envelhecimento possa ser a causa deste desequilíbrio.

Ratinhos C57BL/6 foram usados como modelo pré-clínico de modo a alcançar os objetivos deste estudo. Comparações entre ratinhos relativamente novos (8-12 semanas) e velhos (52-60 semanas) foram realizadas de forma a analisar a neuro-inflamação e a acumulação de ferro.As interações intestino-cérebro foram avaliadas associando os resultados obtidos no intestino com um aumento na neuroinflamação e acumulação de ferro no cérebro. Um modelo farmacológico da doença de Parkinson foi induzido através da administração de 1-methyl-4-phenyl-1,2,3,6-tetrahydropyridine (MPTP), uma neurotoxina exclusiva dos neurónios dopaminérgicos da substantia nigra cérebro. Transplantes fecais também foram efetuados para avaliar se a alteração do microbioma intestinal influencia o perfil neuro inflamatório de ratos velhos e, consequentemente, a severidade da doença.

Dados preliminares a suportar a hipótese colocada já foram adquiridos pelo mesmo laboratorio, tendo sido crucial a sua validação com o plano experimental proposto. Esta tese almejou conseguir provar que as mudanças no microbioma com o envelhecimento são capazes de influenciar o fenótipo neuro-inflamatório de ratinhos velhos, aumentando a sua suscetibilidade à doença. Esperou-se também mostrar que os mecanismos moleculares subjacentes a este fenómeno, necessitavam de acumulação de ferro no intestino, um processo que aumenta a patogenicidade bacteriana e modula a resposta imune.

Palavras-chave: Envelhecimento; Microbioma; Ferro; Inflamação; Doença de Parkinson

CONTENT/INDEX

List of Figures

ABBREVIATIONS

ATP - Adenosine triphosphate
AD - Alzheimer's disease
APCs - Antigen presenting cells
BBB - Blood-brain-barrier
CNS - Central nervous system
CTLs - Cytotoxic T lymphocytes
DcytB - Duodenal cytochrome B reductase
EGCs - Enteric glial cells
ENS - Enteric nervous system
Ft - Ferritin
Fe - Iron
Fe^{2+} - Ferrous iron
Fe^{3+} - Ferric iron
GF - Germ-free
GI - Gastrointestinal
HCP-1 - Heme carrier protein-1
HO-1 - Heme oxygenase-1
IRE - Iron responsive element
IRP - Iron responsive protein
ISC - Iron-sulfur cluster
MHCII - Major histocompatibility complex class II
MPTP - 1-methyl-4-phenyl-1,2,3,6-tetrahydropyridine
NBIA - Neurodegeneration with brain iron accumulation
ND - Neurodegenerative disorders
NM - Neuromelanin
PD - Parkinson's disease
PKAN - Pantothenate kinase-associated neurodegeneration
SCFA - Short-chain fatty acids
SPF - Specific pathogen free
Tf - Transferin
TfR1 - Transferin receptor-1
Th - T helper lymphocytes
TLR - Toll-like receptors
UPDRS - Unified parkinson's disease rating score

INTRODUCTION

1. AGING

Life expectancy is a statistical measure of the average time that an organism is predicted to live, taking into account a wide variety of several different aspects. Human life expectancy has been rising since the early 19th century, and it almost doubled during the 20th. This massive increase in life expectancy can be attributed to major technological and scientific advances such as the development of vaccines, improved sanitation, and the development of antibiotics. Together, these and other factors led to a generalized improvement in populations' health.

Between 2000 and 2016, global life expectancy for both sexes increased from 66.5 to 72.0 years,[1], and in 2017 the average life expectancy in EU countries was 78.3 years. In Portugal, in particular, a marked increase from 64.0 to 81.5 occurred between 1960 and 2018, respectively [2]. Additionally, from 2010 to 2050 the number of people aged 65 years, or more, is predicted to triple, leaving this group representing 16% of the world population [3].

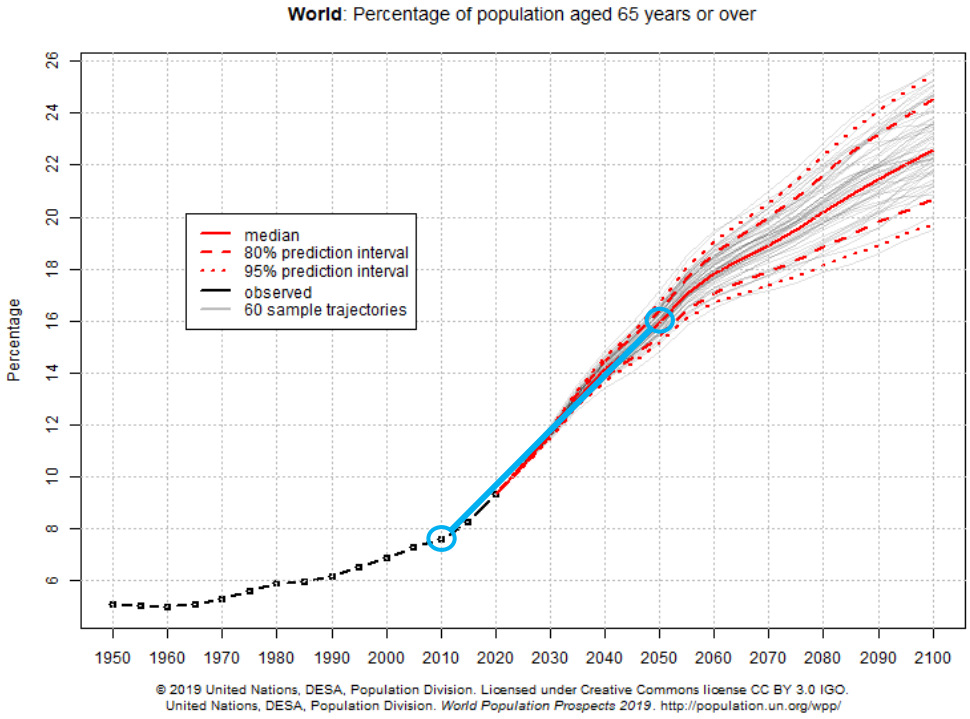

Figure 1 Estimates and probabilistic projections of people with 65 or more years for this century. The population projections are based on the probabilistic projections of total fertility and life expectancy at birth which were carried out with a Bayesian Hierarchical Model. The uninterrupted red line displays the probabilistic median, while the dashed and dotted red lines represent the 80 and 95 per cent prediction intervals of the probabilistic population projections, respectively. The light blue circles and line emphasize the values for 2010 and 2050 [119].

Aging is a genetically encoded, environmentally modulated, biological process through which we get older. For humans, until young adulthood, it can be viewed as a beneficial

phenomenon, responsible for driving the developmental process through which we grow and develop. However, as life expectancy increases, a generalized decline in bodily functions is usually observed as several systemic and cellular systems become compromised. Hence, aging is the highest risk factor for several diseases, as cells begin to show deficits in several key processes and start accumulating mutations. In fact, advancing age increases susceptibility to develop a number of different age-related diseases that can range from cardiovascular diseases and cancer, to metabolic syndromes and neurodegenerative diseases [4]. Different theories, such as the Free Radical or the Cell Senescence Theory, have been developed trying to explain why we age, and the research on this topic continues with some authors even arguing that it should be seen as a disease in itself [5][6][7].
A prodigious review has identified and categorized nine cellular and molecular hallmarks of aging, which can be classified into three categories. The primary hallmarks represent the negative impact of aging on cellular processes, which include genomic instability, telomere attrition, epigenetic alterations, and loss of proteostasis. Mitochondrial dysfunction, deregulated nutrient-sensing and cellular senescence constitute the antagonistic hallmarks [8]. These are characterized by their ability to engage defense mechanisms against nutrient scarcity or against cell damage. However, the aging process disturbs this balance, leading to the chronic activation of specific signaling pathways that exacerbate oxidative stress and cause cytotoxicity. Lastly, integrative hallmarks influence the aging process by directly affecting tissues, i.e. disrupting their function and homeostasis. These include stem cell exhaustion and altered intercellular communication. Among these latter, the best example, in humans, is a phenomenon known as 'Inflammaging' ([9]; [8]; [10]), which refers to the observed low-grade chronic inflammation that occurs with advancing age. Whether accumulated damaged molecules, or interactions and products from microbial communities colonizing the human body could be the underlying cause for the observed increase in a pro-inflammatory status, is likely the case.

With the estimated increase in world aged population, noncommunicable diseases are predicted to account for more than 50% of the disease burden in middle-income countries [3]. Among these, neurodegenerative diseases are a major health concern. Not only are they chronic and long-lasting, but also, their diagnosis is frequently hard to obtain at early stages. As such, therapies to prevent disease progression often fail and patients end up getting symptomatic treatment while the disease progresses. With this in mind, researcher's efforts have focused on comprehending these age-related pathologies, being that several research studies in the last decade were conducted to better understand disease mechanisms and pathophysiology.

Figure 2 The Hallmarks of Aging. This scheme lists the nine hallmarks described in this thesis and in the review. Primary Hallmarks → Genomic Instability; Telomere Attrition; Epigenetic Alterations; Loss of Proteostasis. Antagonistic Hallmarks → Deregulated Nutrient Sensing; Mitochondrial Dysfunction; Cellular Senescence. Integrative Hallmarks → Stem Cell Exhaustion; Altered Intercellular Communication [8].

1.1 PARKINSON'S DISEASE

Characterized for the 1st time more than 200 years ago as a shaking palsy by the English surgeon James Parkinson, Parkinson's Disease (PD, as it would later be renamed) is the 2nd most common neurodegenerative disorder (ND) worldwide. It affects 2-3% of the population over 65 years old and a small study showed that the incidence of the disease may double in individuals aged 75-84 years [11]. As observed in other NDs, this pathology is characterized by the formation of protein aggregates which are known as Lewy bodies, composed of oligomeric bundles of misfolded α-synuclein. These aggregates lead to the selective neurodegeneration of the midbrain dopaminergic neurons in the substantia nigra pars compacta of the brain, located in the basal ganglia. Ultimately, this results in a decreased cortex excitation which is responsible for motor symptoms such as bradykinesia and rigidity.

A well-established element that is known to play a major role in disease progression is the mitochondrial dysfunction observed in PD-affected neurons [12]. This is a

physiological process occurring with advancing age which leads to a decreased production of ATP and increased probability of oxidative damage. PD patients were shown to present both mitochondrial impairment and oxidative damage [12]; [13]. By originating a positive feedback loop, this compromises several vital central nervous system (CNS) functions, in view of the constant Adenosine triphosphate (ATP) supply needed by the brain to meet energy demands. Whether α-synuclein aggregation might foster these responses in PD patients, promoting in turn neuroinflammation and neuronal death, seems indeed the case [14]; [15]; [16].

Besides being considered a movement disorder, it was also well established that PD is characterized by a wide array of non-motor symptoms that can appear several years before the onset of motor dysfunction. These include sleep disturbances, constipation, and gastro-intestinal (GI) dysfunction, thus proving the multifactorial nature of the disease [17]. Interestingly, GI dysfunction may affect PD patients, even decades before the appearance of motor symptoms [18]; [19] [20]. Prospective and retrospective studies demonstrated that constipation may be observable up to 2 decades before PD onset, making it possibly one of the earliest markers of disease progression [21]; [22]; [23]; [18]. Therefore, this implies that the pathogenic trigger for the progression of this neurological disorder might occur several years before the appearance of detectable motor deficits. As such, the development of better and more efficient diagnostic methods is highly important, also to identify populations at risk and, if possible, prevent PD progression by decreasing PD incidence. Recently, particular interest has been given to the gut microbiota.

1.2 THE GUT MICROBIOTA AND NEURODEGENERATION

The human GI tract, along with skin, lungs and vaginal epithelia, constitutes one of the major interfaces between the host and the environment. Its proper function is crucial, as it is responsible for proper nutrient absorption. Starting at birth, the GI tract is colonized by a large number of commensal bacteria referred to as the ‘gut microbiota’. Although particular interest is given to the microbial community, the microbiome also includes viruses, fungus and archae. This intestinal flora takes approximately 3 years to develop. It acquires a similar function and composition to those of adults [24] and has been shown to be involved in several processes, such as regulating host immunity [25]. Another crucial function of gut microbes is the synthesis of key metabolites and anti-inflammatory compounds capable to regulate lipid metabolism and the production of cytokine involved in the maintenance and repair of epithelial integrity [26]. Likewise, vitamin production is influenced by the gut microbiota, and folate plays important roles as co-factor in vital metabolic processes like DNA repair and protein synthesis [25]. Although the results are mere estimates and microbiota composition may vary between individuals, compiled data of two different projects identified that gut microbes are mainly constituted of four different bacterial phyla: Proteobacteria, Firmicutes, Actinobacteria and Bacteroidetes [27] [28].

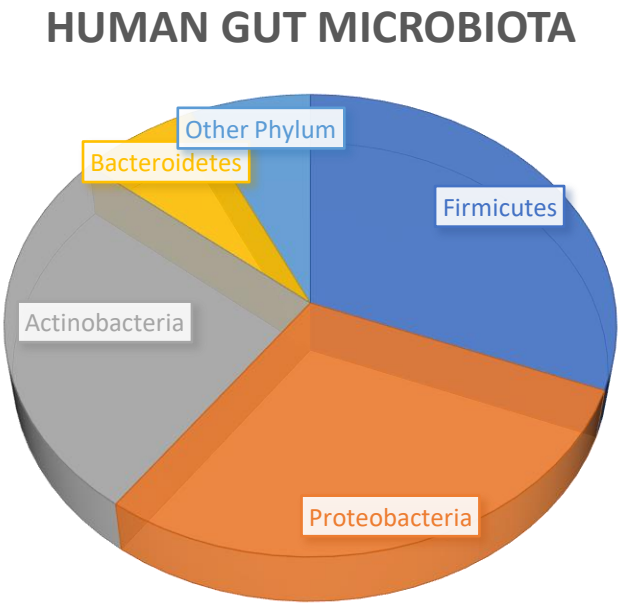

Figure 3 Composition of the human gut microbiota. Characterization of the human gut residing bacterial species by phylum. Firmicutes ≈ 31%; Proteobacteria ≈ 29%; Actinobacteria ≈ 26%; Bacteroidetes ≈ 7% [27].

As occurs with many other systems in our body, the microbial composition of the gut changes with age, and microbial diversity declines with advancing age. However, these changes are not widely observed or reported, since there have not been many investigations looking into this subject. However, it is safe to assume that controversies between conducted researches may arise from different methodologies, study groups or their respective diets [29]; [30]. Moreover, the elderly are usually affected by many simultaneous comorbidities. Therefore, these and other systemic changes associated with aging might play a crucial role in altering the gut microbiota [30]. In general, proteolytic bacteria seem to increase, while the levels of saccharolytic bacteria are likely to decrease [31].

The continuous interaction of gut microbes with the host opened a new field of investigations, aimed at better understanding possible routes of communication, among these the 'gut-brain axis'. This is a bidirectional communication system that links the brain to the gut, defined as our 'second' brain via the enteric nervous system (ENS). These commensal interactions that occur between the two compartments are responsible for a wide variety of responses affecting both organs as the gut microbiota has been shown to be able to modulate the profile expression not only of cytokines, but also of neurotransmitters [32] [33].

The ENS is part of the peripheral nervous system and is organized in two major ganglionated plexus that contain enteric glial cells (EGCs) and neuronal cell bodies connected through a complex net of nerve processes. Through the expression of toll-like receptors (TLRs), these cells have been linked to the recognition of immune cues from the gut [34]. Since EGCs also express molecules important to initiate immune

responses, like major histocompatibility complex class II (MHC II), they have been proposed to function as antigen presenting cells (APCs) to lymphocytes located at the gut epithelial barrier [35]. As such, the role that these cells play in controlling immune homeostasis is highly important, being reasonable to assume that EGCs may act as 'neuronal-glial-immune' units. The ENS may also directly affect CNS health through the afferent neurons from the vagal nerve [36].

Since immune signaling from the gut to the brain has been discovered, several new pieces of evidence started linking a microbiota dysbiosis with neurodegenerative diseases and their progression. Both Alzheimer's disease (AD) and PD studies demonstrated the correlation between a dysregulated composition of gut resident microbes, to GI dysfunction symptoms that usually accompany these diseases [37]; [38]; [39]. However, as degeneration of the ENS occurs parallel to CNS impairment, many GI abnormalities may be attributed to the degeneration of these nerve cells [40].

Taking this into account, Braak and colleagues, proposed that PD pathology might start in the gut, affecting first the ENS as a result of the inflammatory insult caused by changes in gut microbiota or the release of their metabolites [41]; [18] [19].

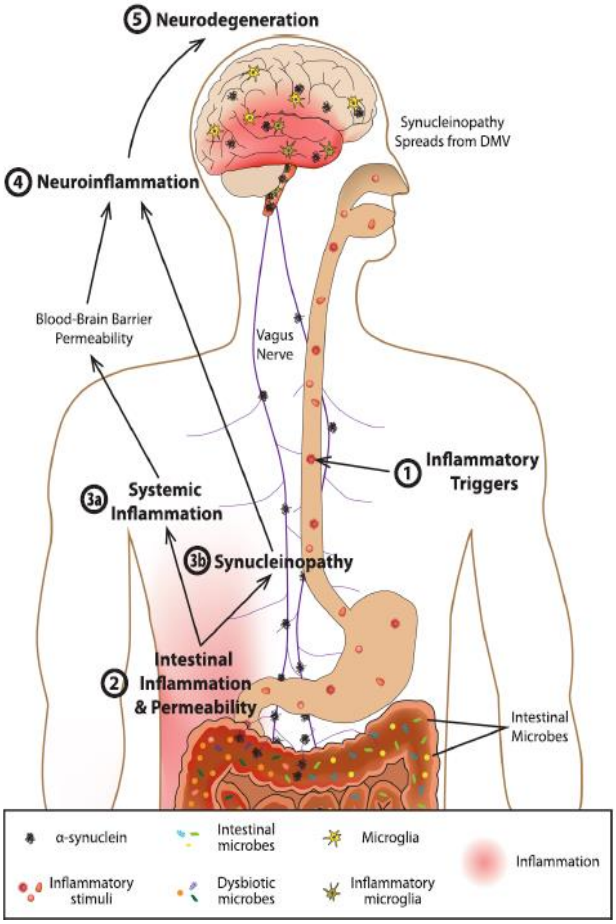

Figure 4 Model of gut-originating, inflammation-driven PD pathogenesis. Inflammatory triggers in the gut (1) initiate immune responses that deleteriously impact the microbiota, and intestinal permeability, inducing increased expression and aggregation of αSYN (2). The misfolded protein may then be transmitted from the gut to the brain via the vagus nerve (3b). Moreover, chronic intestinal inflammation and permeability promote systemic inflammation, which, among other elicited effects, can also increase blood-brain barrier permeability (3a). This pro-inflammatory status along with synucleinopathy promotes neuroinflammation (4), which drives the neurodegeneration that characterizes PD (5) [18]

The compromised intestinal permeability affecting PD patients promotes gut inflammation, shifting the equilibrium in gut microbial community towards a more pathogenic composition. The growth of bacterial populations that are responsible for eliciting a local pro-inflammatory response are then believed to be capable of dictating PD progression [42]; [18].

Thus, several studies have sought to characterize the differences in gut microbes in PD patients, by comparing profiles obtained with healthy controls. At taxa level, no big differences are observed, however the diversity of gut microbe's composition is significantly altered. A decrease in the diversity of Firmicutes and Bacteroidetes is often observed, with particular emphasis on the diminished Short-Chain Fatty Acids (SCFA) producing strains. SCFAs are major metabolic products of gut microbiota that are involved in several processes and signaling roles, such as microglial activation and neuroinflammation. Many studies also emphasize the role of bacteria taxa in the development of motor deficits and PD severity [40]; [18]; [19]; [43]; [44]. Among these,

it is worth mentioning the investigation proving how gut microbiota influences the outcome of a PD-induced mouse model. When comparing wild-type (i.e. specific pathogens free) vs. gnotobiotic (GF) animal models, it was shown that GF mice present a reduced locomotor dysfunction, accompanied by less microglia activation and dopamine neuronal loss. However, this effect was abolished not only by colonizing GF mice with gut microbiota, but also by administering SCFAs. The study also shows that mice colonized with microbiotas derived from human PD-patients present enhanced motor dysfunction, linking once again gut dysbiosis with the neuropathological progression and severity of PD [45], furtherly underlining the importance of keeping a healthy gut. To this end, pre- and probiotic formulas are being developed to restore gut microbiota and so far, have been shown to provide beneficial effects, especially to the elderly. Nevertheless, further research into this field still needs to be performed.

2. IRON METABOLISM

Iron (Fe) is in the 4th period of the 8th group of the periodic table, being categorized as a transition metal. It is one of the most common elements in the Earth's crust, and like many other metals, it is indispensable to life. Being involved in vital functions such as cell respiration, it can stably interconvert between its two most common oxidative states, ferrous (Fe2+) and ferric (Fe3+), giving it high propensity to participate in the Fenton and Haber-Weiss reactions, generating ROS [46]. The metabolic necessity of Fe for key processes as well as, the ability to become highly toxic make both bodily and cellular Fe homeostasis a tightly controlled process [47]; [48].

Dietary inorganic Fe is absorbed by gut enterocytes through the actions of DcytB (duodenal cytochrome B reductase) and DMT1 (divalent metal transporter 1), which enable its reduction and absorption, respectively [49]. On the other hand, organic Fe is absorbed and subsequently degraded by heme carrier protein-1(HCP1) and HO-1 (heme oxygenase-1) and HO-2 [50]. Once inside the cell, Fe is either: i) stored into ferritin (Ft) a hetero-polymer that stores Fe in nanocages; ii) directed to mitochondrial bio-synthetical pathways (heme synthesis and Iron-Sulfur Cluster (ISC) biogenesis) or iii) exported by the only and so far described Fe efflux pump, ferroportin (FPN) [47]; [48] [51]; [52].

In order to reach circulation, Fe must be oxidized back to its ferric form and it is then chaperoned by transferrin (Tf), a plasma glycoprotein [47]. The main Fe uptake mechanism utilized by most cells involves Tf-bound Fe internalization via its receptor, transferrin receptor 1 (TfR1). This clathrin-coated endocytosis is followed by a low pH-dependent dissociation of Fe and Tf in the endosome, with the latter being released back into circulation and TfR1 being recycled back to the membrane. A metalloreductase, known as Steap3, reduces Fe back to its ferrous state and DMT1 transports it to the cytosol [47]; [48]; [52].

Once inside cells, iron metabolism is post-transcriptionally regulated by the Fe regulatory protein (IRP)-Fe responsive element (IRE) system. In mammals, two isoforms of IRPs have been described, IRP1 and IRP2, both of which promote rapid alterations in the synthesis of key proteins involved in Fe metabolism [47] [52]. By binding to IREs that are present in the mRNAs of the genes encoding for those proteins, they can either inhibit translation or promote it by protecting the nucleic acids against the actions of endonucleases [47] [52]. So, in Fe-deficient cells, IRP1 binds to the 3'UTR of the mRNA of TfR1 or DMT1 to increase cellular uptake. Simultaneously, it also binds the 5'UTR of the mRNA of ferritin, decreasing Fe storage, and increasing its cellular availability. Once Fe reaches the needed levels, the ISC (iron-sulfur cluster, a prosthetic group composed of non-heme Fe and inorganic sulfide) of IRP1 is reconstituted. As so, it loses its binding affinity to the IREs of the mentioned mRNAs increasing ferritin expression and decreasing transferrin receptor expression (**Figure 5**).

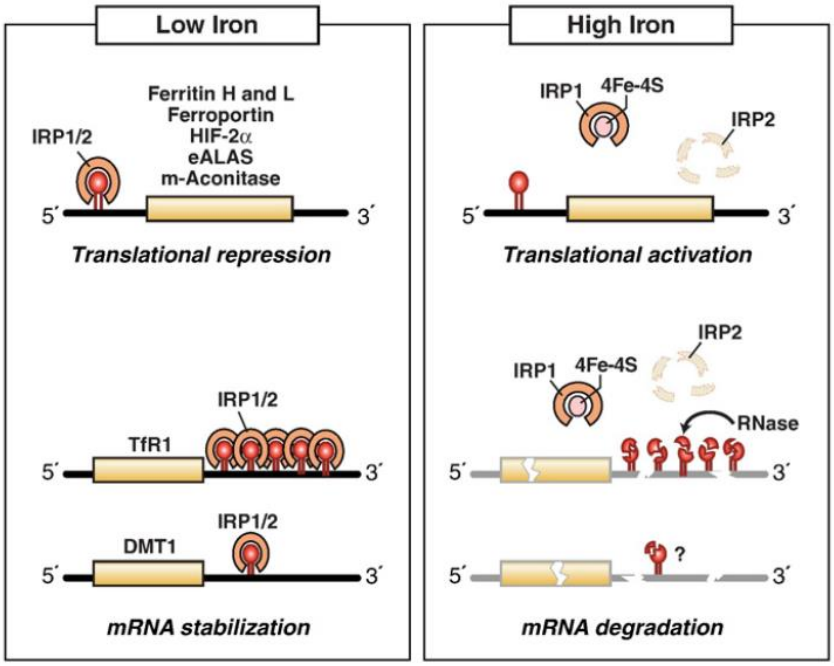

Figure 5 IRPs regulate translation and stability of IRE-containing mRNAs. The levels of proteins involved in cellular Fe uptake, storage or utilization are controlled by IRP/IREs system. When cells are Fe depleted, IRP1 does not have a Fe-S center, thus becoming an active IRE binding protein. By binding to it in 3'UTR, it stabilizes the mRNAs of Fe importers, like DMT1 and TFR1. When IRP1 binds to IRE in 5'UTr, mRNAs translation is inhibited, leading to a negative regulation of genes promoting Fe storage, such as ferritin. When cells are loaded with Fe, this leads to opposite result. In case of IRP2, despite the similarity to IRP1, the regulation of gene expression is based on its own degradation [120].

At systemic level, serum and tissue Fe homeostasis are maintained through the release of the Fe regulatory hormone hepcidin, which when produced by the liver enters the blood circulation. When the levels of Tf-Fe increase, a signaling cascade is initiated and this culminates in hepatocytes hepcidin expression through the activation of the BMP-SMAD pathway [47]. Hepcidin activity is the main regulator of Fe dietary absorption. It exerts its effects by binding to the extracellular portion of ferroportin, promoting its endocytosis and subsequent degradation. Thus, the levels of circulating Fe decrease, contrarily to intracellular levels. Apart from circulating levels of Fe, hepcidin production can also be stimulated by other factors, such as inflammation [53]; [48].

Both inflammation and infection are known to alter Fe homeostasis through proinflammatory cytokines that bind to the promoters of aforementioned genes [47]; [54]. Hepcidin also plays a crucial role by preventing Fe access to pathogens, which manipulating Fe metabolism require this metal for their growth and proliferation [55]. Our immune cells need Fe to function properly, with different responses being reported in both iron-loaded and iron-deficient pathological conditions. Although disrupting iron homeostasis might be a beneficial first strategy deployed by our immune system to minimize pathogen burden, long-term chronic activation of such processes (as observed in aging) becomes detrimental and increases our propensity to develop several disorders [56]; [47].

2.1 IRON and NEURODEGENERATION

The brain is a highly demanding metabolic organ, accounting for at least 20% of total energy expenditure. Being that Fe is a structural component of cytochromes, mitochondrial proteins involved in the process of cellular respiration, adequate supply, and homeostasis of this vital metal to the brain is of the utmost importance [56] [57]. The maintenance of iron homeostasis in the brain is essential for this organ to exert proper functions, since this metal plays a crucial role in processes, such as catecholamine biosynthesis. The iron transported into this compartment must cross the BBB (blood-brain barrier) and most certainly enters the epithelial barrier through the Tf-to-cell cycle. Regarding its font, Fe recycling seems to be the main source for brain Fe [58].

Accumulation of Fe in tissues with advancing age has been well established. In the brain, Fe accumulation in areas susceptible to neurodegeneration has been long recognized, and it is highly related to their pathology [58].

Microglia, the resident brain immune cells, are involved in the process of Fe recycling, due to their ability to phagocytose dying cells. These cells can shift between two known and characterized activation states. The M1 phenotype synthesizes and secretes pro-inflammatory cytokines in order to increase the inflammatory response, while in turn, the M2 phenotype releases anti-inflammatory cytokines to resolve the inflammation. An increase in pro-inflammatory mediators increases DMT1 expression and increases cellular free Fe accumulation. This may cause oxidative damage and promote chronic neuroinflammation, which ultimately exacerbates neuronal damage and neuronal death. On the other hand, M2 microglia releasing anti-inflammatory cytokines increase Tf expression and release ferritin stores, possibly to support the protection and regeneration of neurons and other glial cells [57].

Additionally, a group of rare and genetic diseases known as Neurodegeneration with Brain Iron Accumulation (NBIA), where Fe accumulation in the brain was first described, provided a strong link between Fe dyshomeostasis and its ability to cause neurodegeneration. While several mutations causing NBIA are not directly involved in Fe metabolism, aceruloplasminaemia and neuroferritinopathy are two NBIAs caused by mutations in genes encoding for the ferroxidase ceruloplasmin and the ferritin light chain, respectively. Other known NBIAs are caused by mutations in genes related to lipid metabolism, like Pantothenate Kinase-Associated Neurodegeneration (PKAN), thus linking once again Fe accumulation to oxidative stress and lipid peroxidation [59].

The relevance of this Fe-dependent cell death has been provided by discovering the existence of ferroptosis, a new form of regulated death that plays an important role in

neurodegeneration [60]; [61]. Although it is still a poorly elucidated process, when regarding mechanisms or physiological role, the elevated levels of lipid peroxidation and diminished expression of antioxidant defenses have been shown as the main requirements for it to occur.

2.2 IRON AND PARKINSON'S DISEASE

Fe accumulation in neurons and glia has been described in several neurodegenerative disorders (ND), such as AD and PD, where it acts as early indicator of disease progression and severity [62]; [63]; [64]. Human analyses positively correlate total Fe accumulation in the basal ganglia with age [65]. Moreover, studies show that the concentration of Fe and Ft linearly increases in the substantia nigra with advancing age, hence highlighting a linking role with PD.

It is thought to be the leading cause of neuronal death [66] [58] as showed by PD samples, where excess Fe is found mainly in the substantia *nigra* [67].). In this region, Fe is primarily stored in neuromelanin (NM), which, seeking to confer protection to dopaminergic neurons, sequesters labile Fe and prevents it from generating ROS. However, NM expression has been shown to decrease with age, hence, these neurons become more susceptible. Moreover, as Fe is capable to promote the release of pro-inflammatory cytokines from microglia, these resident immune cells will exacerbate neuroinflammation, which in turn enhances neuronal death. Also, since microglia phagocytose the Fe deriving from dying neurons, while patrolling the brain, this metal accumulates in these cells, fostering a never-ending pathological cycle.
It is also known that, Fe favors the aggregation of α-synuclein, as observed in post-mortem PD samples [68]. More studies corroborate these findings, showing that Fe-driven α-synuclein aggregation exerts cytotoxic effects on neuronal cells [69]. Moreover, a recent study showed that ferroptosis inhibitors were able to rescue the deficits induced in an MPTP pharmacological PD-mouse model [70] and possibly the accumulation of α-synuclein in genetically mutated PD animal models. Hence, this Fe-mediated cell death and the influence of ferroptosis on brain normal functioning are likely to play major roles in neuronal death and, as such, investigated in a number of ND pathologies, like PD and [70][71].

Ferroptosis can be experimentally induced and its toxicity in neuronal cells is observed by the appearance of many alterations in mitochondrial morphology [72] This Fe-mediated cell death mainly occurs when key players of other cell death modalities are suppressed and deeply affects mitochondria functioning. Given that mitochondria are the organelle with the highest concentration of Fe, its age-related accumulation may increase ROS production, promoting oxidative stress and mitochondrial dysfunction, in an auto-feeded process that keeps exacerbating neuronal loss [73][65]. These effects can be reversed by treating cells with ferroptosis inhibitors or ROS scavengers, showing

again a causal link between neuronal death and Fe accumulation. Our lab has written an extensive review on the role that ferroptosis, along with other types of cell death, plays in PD with these and other topics being deeply explained, which is enclosed to this dissertation in the appendix session.
Hence, the data collected from these studies, have linked the disruption of Fe homeostasis to an ever-growing puzzle underlying the pathogenesis of PD. Although it is still not clear whether Fe accumulation is the cause or consequence of disease progression, it is known that it exacerbates the neurodegeneration observed in PD.

2.3 IRON AND THE GUT MICROBIOTA

As almost all organisms, gut bacteria are also dependent on Fe to survive. However, this metal has a direct impact on host-microbiota interactions as both its depletion or excess can alter mucosal immune responses, which in turn influence Fe metabolism. This notion is supported by studies showing that the expression of Fe transporters (DMT1 and DcytB) in mice maintained in gnotobiotic conditions, germ-free (GF)-mice is increased. Contrarily, the levels of FPN decreased. Therefore, under these conditions, intestinal cells showed a diminished capacity to store and transport Fe [74] showing a reduced Fe absorption and retention in GF animal models [75]. Interestingly, gut colonization experiments were able to increase cellular Fe storages and ferritin expression.
The observed increase in age-related Fe accumulation throughout the body also plays a detrimental role at the gut epithelium as microorganisms develop strategies to capture and bind Fe by using chelator molecules known as siderophores. A number of evidences also show that Fe accumulation increases pathogenicity of gut bacteria, promoting their growth and replication [76][77][78]. As such, Fe retention is a defense strategy used by the host to fight infection, as bacterial growth is limited in low-Fe conditions. Hence, the content of Fe in the gut may have a significant impact on gut microbiota and their ability to turn it more pathogenic [79].

Several authors have also tried to appreciate the impact in the gut microbiota composition, due to differences in dietary Fe uptake. The most consistent finding refers to an increase in potentially pathogenic Enterobacteriaceae with a simultaneous decrease in commensals Lactobacillaceae and Bifidobacteriaceae [80][81].
Taken together, these results suggest a role for Fe in regulating the composition of gut microbiota, possibly through the modulation of the metabolic profile of said microbes. Nevertheless, further work is still required to corroborate this statement.

2.4 IRON CHELATION THERAPY

Accumulating evidence linking Fe deposition with several diseases indicated that re-establishing Fe homeostasis can be used as possible therapeutic approach. Fe chelators

in thalassemia major and hemochromatosis, two systemic diseases with Fe dyshomeostasis, have been proven beneficial and are used as therapeutics, indicating that their use can be extended to other clinical conditions.

The accumulation of Fe in the brain and the role it might have in promoting mitochondrial dysfunction and oxidative stress, particularly in areas affected by ND[58], have highlighted the salutary role of Fe chelators in these pathologies. An Fe chelator is a molecule presenting the ability to bind labile free Fe. However, in order to properly function in the brain, these compounds must enter neural cells, cross the BBB and transfer their chelated Fe to either Fe depleted brain regions or biological acceptors. However, given its vital importance for several key cellular metabolic pathways, Fe chelators must also have an intermediate affinity for this metal as to avoid excessive iron depletion [82].

Recent clinical trials have been studying the effect of Fe chelators in the treatment of ND [83] [84]. Particularly, in the case of PD, treatment with the brain permeable Fe chelator deferiprone has showed promising results [85]. Most data obtained from clinical trials revealed that PD-patients treated with deferiprone have decreased Fe accumulation in the substantia *nigra*, when compared to patients given placebo. This resulted in a concomitant improvement of motor functions and UPDRS (Unified Parkinson's Disease Rating Scale) scores [82]. Moreover, a Phase-II clinical trial examined the effect that a different Fe-Cu chelator, clioquinol, had on the treatment of AD patients. The authors reported that the Alzheimer's Disease Assessment Scale scores stabilized and that the plasma Aβ levels were decreased, showing once again the therapeutic effect of Fe chelation on pathologies affecting the brain [86].

Overall, these studies show that Fe chelators might constitute a new therapeutic strategy against neurodegeneration. However, the notion that after treatment some patients tend to revert back to a pathological state, makes this an area of constant improvement. The need to develop more efficient Fe chelators drives the research in this field, as compounds like the M30 are promising in animal models, due to their Fe chelation activity and ability to induce expression of antioxidant enzymes [82].

3. AIMS

Given all previous information, one of the objectives of this study was to assess the association between aging and changes in gut microbiota, knowing that iron metabolism significantly influences both phenomena. The importance of disruption of iron homeostasis and gut dysbiosis in the pathogenesis of PD was also analyzed.

Hence, this thesis aims to contribute to better understand to the molecular mechanisms underlying the development of PD by:

i. assessing the correlation between gut microbiota and neuroinflammation during aging;

ii. investigating whether this association might influence the susceptibility to develop PD;

iii. evaluating brain iron accumulation with aging.

METHODOLOGY

Animals

C57BL/6 mice were used as *in vivo* model and bred and maintained in ventilated cages under specific pathogen-free barrier (SPF) conditions. Animal care and experimental procedures were conducted according to protocols approved by local (Champalimaud Foundation) and national (DGAV) ethics committees. Comparisons between different age groups were carried out, by using eight to twelve-week-old mice *vs.* fifty-two to sixty-week-old mice.

The gut-colonization model of SPF mice was achieved by the administration of streptomycin (5 g/L) in drinking water, for 7 days. The animals were then inoculated with 2 pellets of stool samples from old animals, homogenized in 100 µL of saline buffer, by gavage. This experimental procedure was repeated for 5 consecutive days. One week after, the effects of this gut colonization were evaluated, as described in the following sessions. The data obtained were compared to the results achieved by colonizing mice that were born and always mantained in gnotobiotic conditions and known as germ-free (GF), using the same procedure of sample preparation and route of administration.
Stool samples were collected from SPF or GF C57BL/6 mice, aged 8-12 or 52-60 weeks old. Two pellets per eppendorf were stored at -80ºC, until being resuspended and used for further analyses.

Pathological model

Mice were injected intraperitoneally (i.p.) with 200µl of 1-methyl-4-phenyl-1,2,3,6-tetrahydropyridine (MPTP; 15mg/kg, 3 injections every 2 h) to induce PD. The animals were monitored daily for 30 days and motor dysfunction was assessed as time of performance, as follows.

Behavioral tests

In order to assess motor coordination, mice were submitted to the pole descending test. Mice were placed up-side-down on a vertical pole. The time was measured by stopwatch, when mice descend the pole and place the four paws on the ground. The cut off time of the test was 120 seconds. The average times to descent the pole are reported in the results.

Evaluation of gut barrier disruption

Mice were injected intravenously (i.v.) with 100 µl of 2% Evans Blue (Sigma), dissolved in saline solution. Mice were sacrificed 1 hour later, and the gut were harvested, weighed, placed in 2ml of formamide (Merck) and left 48 hours at 37 ºC to extract Evans blue dye. Absorbance was then measured at λ = 620 nm (Bio Rad SmartSpec 3000). A standard curve with fixed concentrations of Evans blue was used to calculate dye extravasation into the gut.

Single cell suspension for flow cytometry analysis of immune cells

Mice were sacrificed by CO_2 inhalation and blood was immediately collected in 1.5mL eppendorf, containing 10 µl of heparin, by cardiac puncture, using a 1mL siringe and a 25G needle. The, mice were perfused with 20mL cold saline solution, using a 20mL syringe and a 21G needle, placed directly in the heart. At the end of this procedure, brain and spleen were harvested and analyzed as explained in the next sessions. Brain samples were collected to study the animals' neuroinflammatory profile. In a 6mm uncoated petri dish, the brain was smashed and homogenized between two glass slides in a Collagenase VIII solution. After homogenization the samples were incubated for 30 minutes at 37ºC, and then transferred to cold 50mL falcons through a 100µm strainer. Afterwards, samples were centrifuged for 12 minutes at 1500rpm, at 4ºC. The supernatant was discarded, and the cells were washed two times in PBS 1x. Then, the samples were re-suspended in a Percoll gradient solution. After a centrifugation of 22 minutes at 2500rpm (22ºC), the myelin and the Percoll solution were carefully removed, and the cell pellet was re-suspended in 25mL of PBS 1x. The samples were then centrifuged for 12 minutes at 1500rpm, at 4ºC, the supernatant discarded, and the cells transferred to a 1.5mL Eppendorf tube. Finally, cells were centrifuged for 3 minutes at 2000rpm at 4ºC and re-suspended in FACS buffer.

Counting cells for flow cytometry analysis

For all cell suspensions, a specific sample volume was transferred to a counting mix containing FACS buffer, propidium iodide (PI - a viability dye) (Fluka) and reference beads with known concentration (Bangs Laboratories, SureCountTM, Ref. No. CC10N). In order to obtain the best possible results, each counting mix was run in the BD FACSCanto II Flow Cytometer (BD Bioscience) and the number of cells per µL was obtained based on the following equation:

$$Cells\ per\ \mu L = \frac{Nº\ cells\ counted * Volume\ added\ beads}{Nº\ beads\ counted * Volume\ cells\ added} * Beads\ concentrations$$

Cell differentiation and cell surface phenotype analysis by flow cytometry

According to the **Aims** of this study, the purpose of this flow cytometric analysis served: 1) to characterize the neuroinflammatory profile of ageing GF animals, 2) to assess if gut microbiota modulates this process and, 3) to establish a possible underlying link between iron metabolism, the gut microbiota and neuroinflammation, in the CNS. Hence, different mixes of antibodies against surface antigens were created for each purpose.

Antibody mixes

The first mix named "T mix" was composed by antibodies allowing to identify cells from the lymphoid lineage. This mix was used in all samples, as enabling to distinguish T cells from B cell populations, and included: Pacific Blue anti-mouse CD45 Antibody (BD Bioscience, Ref. No. 558107), FITC anti-mouse TCR β chain Antibody (BioLegend, Ref No. 109208), Brilliant Violet 510 anti-mouse CD19 Antibody (BioLegend, Ref. No. 115545), PE anti-mouse CD4 antibody and APC/Cy7 anti-CD8 (BioLegend, Ref. No. 100714),Pacific Blue anti-mouse CD45 Antibody (BD Bioscience, Ref. No. 558107), PE/Cy7 anti-mouse CD62L Antibody (BioLegend, Ref. No. 104417), and APC anti-mouse/human CD44 Antibody (BioLegend, Ref. No. 103012). Anti-TCR β and anti-CD19 allowed the identification of T cells and B cells, respectively. Within the T cell family, it was possible to identify the cytotoxic and helper T cell subpopulations by using anti-CD8 and anti-CD4, respectively. Anti-CD44 and anti-CD62L were used to determine the levels of activation of the CD4+, CD8+ and CD19+ cell population.
The second mix called "M mix" was composed by a number of antibodies allowing to identify different immune cell populations and it was used in all samples. This mix contained: PE/Cy7 anti-mouse/human CD11b Antibody (BioLegend, Ref. No. 101216), APC-Cy7 anti-x CD45 Antibody, PE anti-x CCR2 Antibody, APC anti-x NK11 Antibody, Brilliant Violet 510 anti-x CD19+TCRβ Antibody (BioLegend, Ref. No. 115545), Pacific Blue anti-x MHCII Antibody, and FITC anti-x Ly6C Antibody. Anti-CD45 allowed to distinguish between leukocytes ($CD45^{+}$) and the brain resident immune cell, microglia ($CD45^{Int}$); while the anti-Ly6C and anti-NK11 antibodies enable identifying monocytes and natural killer cells. Anti-CD19+TCRβ was used to separate the lymphocytic populations, whereas anti-CCR2 was used to monitor the recruitment of infiltrating monocytes and anti-MHCII their activation.
Calcein assays were also performed, using the 'Calcein Mix'. This molecule is a cell-permeant dye that can aid to determine cell viability. Yet, it has been clearly established that it can also act as an iron chelator, thus serving as a probe to measure intracellular iron levels, namely the amount of iron available in the labile iron pool (LIP). This mix also contained the CD19, CD11b, TCR-β, CD4, NK1.1 and CD45 markers in order to discriminate in which cellular populations there were increasing their Fe levels.

Surface staining and flow cytometry analysis

Flow cytometry analyses were also used to assess cell differentiation and to determine the percentage of cell subpopulations that are activated upon treatment. For this purpose, cells were seeded in a 96-well plates at $1x10^6$ cells/well. The plate was centrifuged for 2 min at 2000rpm, at 4ºC, and the supernatant was removed. Fc-block (BD Bioscience, Ref. No. 553141) was added for 15 min, at 4º, with the aim to block unspecific immunoglobulin binding. After a centrifugation of 2 min at 2000rpm, the antibodies mix was added to the respective well and the plate was left for 30mim, at 4º, in the dark. After this incubation period, fluorescence-activated cell sorting (FACS) buffer was added to the wells and the plate was centrifuged for 2 min at 2000 rpm. Cells were washed two more times with FACS buffer; as for FACS data acquisition, stained cells were resuspended in FACS buffer and PI in a 1 to 1 proportion and collected in FACS tubes. Unstained sample was used as a negative control and to set-up the acquisition parameters in BD FACSCanto II Flow Cytometer. Data analysis was performed using FlowJo software (version 10.0.7, Tree Star Inc.) and GraphPad Prism (v. 8.0) (GraphPad Software).

Statistical analysis

Data was expressed as mean values ± standard deviation. Statistically significant differences between indicated conditions were assessed using One-way non-parametric ANOVA (Kruskal-Wallis test). When significant, this was indicated as *$p < 0.05$; ** $p < 0.01$; ***$p < 0.001$. All statistical analysis was performed using GraphPad Prism (v. 8.0) (GraphPad Software).

RESULTS

Preliminary data from our lab, in the context of gut barrier disruption, revealed the link between gut microbiota and aging. These results showed that non-manipulated old mice had an increased gut barrier disruption and motor dysfunction, upon PD induction, when compared to their young counterparts (**Figure 6 – A** and **B)**. Additionally, it was found that non-manipulated, old animals, maintained in SPF (**Figure 7 A**) and GF (**Figure 7 B**), presented a significant increased gut barrier disruption, when compared to non-manipulated young animals. However, when young mice are colonized with the stools

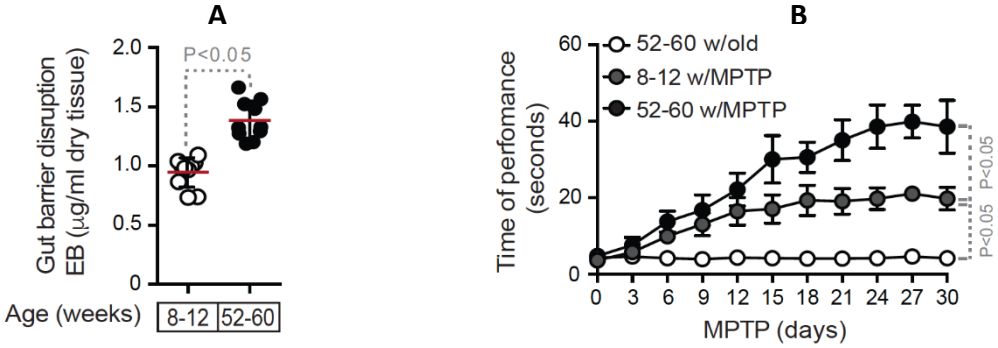

Figure 6 Gut barrier disruption and motor dysfunction. **(A)** Gut permeability was evaluated by measuring the extravasation of Evans Blue dye, administered intravenously, into the gut, in the indicated groups of mice and the results were expressed as mean standard deviation (n=10-15 mice per group). Significance has been observed between conditions according to t-test. **(B)** Exacerbated motor dysfunction was measured as time of performance of mice placed up-side-down on a vertical pole upon MPTP treatment, which was used as pharmacological model of PD induction (n=10-15 mice per group). Significance has been observed, according to t-test.

of old mice, their phenotype significantly changes, resembling that observed in non-manipulated old mice (**Figure 7**). Gut barrier disruption was measured by quantifying the extravasation of Evans Blue dye, administered intravenously, into the gut, as described in material and methods.

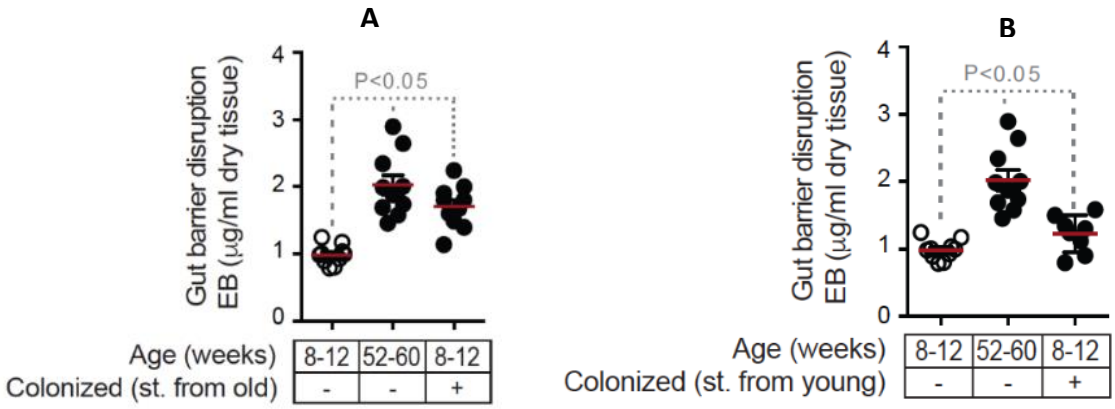

Figure 7 Gut barrier disruption – gut colonization Gut permeability was evaluated in the indicated groups of mice for (A) SPF (control) and (B) GF. The results were expressed as mean standard deviation (n=10-15 mice per group). Significance has been observed between conditions according to t-test.

The neuroinflammatory profile of SPF-Old colonized mice also seemed to show an increase in immune cells but further characterization is still required to assess the reproducibility of the results obtained (*data not shown*).

Taking this into account, this study was conducted with the objective to further understand how changes in gut microbiota could modulate PD susceptibility. Therefore, motor dysfunction and neuroinflammation were evaluated in aging animals, colonized or not with stool samples collected from older mice.

In order to prove the involvement of Fe in changing gut microbiota and, as such, increasing the incidence and severity to PD, the potential of iron chelators as reversion mechanism was also evaluated.

Neuroinflammatory profile in animals maintained in specific pathogen free (SPF) vs. germ-free (GF) conditions

C57BL/6, GF mice are bred in controlled environments and fully prevented from exposure to detectable bacteria, viruses, and eukaryotic microbes. This is an ideal model to study the role of microbes on the progression of specific pathologies, given the possibility to colonize gnotobiotic animals exclusively with specifically identified pathogens. Thus, GF mice are a good model to study the mechanism underlying aged gut microbiota and neuroinflammation, as capable to pinpoint only microbial effects on the brain. It should be noted that in these studies, we compared the results obtained to those collected from animals maintained in SPF conditions, i.e. with a healthy gut.

In the first set of experiments, the initial goal was to confirm existence of differences in the neuroinflammatory profile of non-manipulated animals. Brain samples from 52-60-

week-old mice, both GF and SPF, were collected and analyzed by flow-cytometry with the aim of identifying different innate and adaptive immune populations.

Taking into account that the brain was for long time considered an 'immune privileged' organ, we analyzed both microglial ($CD45^{Int}$) and peripheral leukocyte ($CD45^{Hi}$) levels. In this last compartment, by using different antibody mixes, particular focus was given to lymphoid and myeloid populations. Hence, two antibody mixes (M and T mix) were used in the analysis presented hereafter.

To sort and characterize the myeloid lineage we used the M mix. With this mix, the objective was to evaluate the prevalence of population subsets in the myeloid compartment of the immune system, also using CD11b and Ly6C as markers expressed in a wide variety of immune cells. However, when used in combination, they allow to discriminate between different types of monocyte, such as: 'classical' pro-inflammatory monocytes ($CD11b^{+}Ly6C^{Hi}$) and 'non-classical' patrolling monocytes ($CD11b^{+}Ly6C^{Low}$). This gating strategy may also discriminate eosinophils ($CD11b^{Int}$ $Ly6C^{Int}$) and neutrophils ($CD11b^{+}$ $Ly6C^{Int}$). Yet, for these last cells, other markers or strategies, such as the expression of Ly6C in function of Ly6G, prove to be more efficient [87].

Distinct functions are attributed to different subsets of monocytes. In case of infection, classical monocytes are recruited to inflammation sites, where acting as the first line of defense they start to secrete pro-inflammatory cytokines, to recruit other immune cells and to differentiate into macrophages [88], [89]. Non-classical monocytes, on the other hand, seem to act as surveillance and patrolling cells of the vascular tissue, although some pro-inflammatory responses have been also reported [90].

The gating strategies, used in our analysis and concerning this mix, are shown in **Figure 8.**

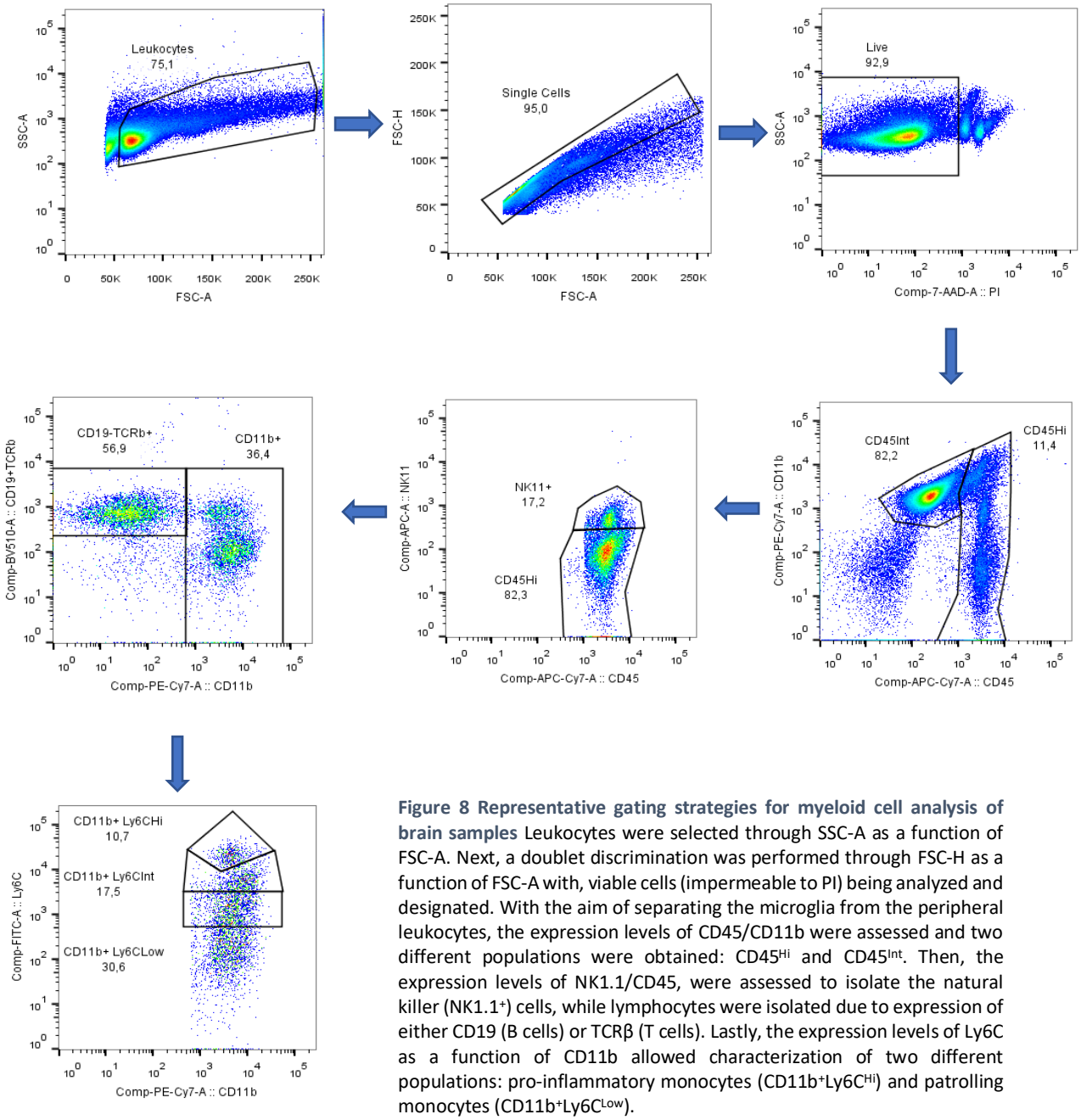

Figure 8 Representative gating strategies for myeloid cell analysis of brain samples Leukocytes were selected through SSC-A as a function of FSC-A. Next, a doublet discrimination was performed through FSC-H as a function of FSC-A with, viable cells (impermeable to PI) being analyzed and designated. With the aim of separating the microglia from the peripheral leukocytes, the expression levels of CD45/CD11b were assessed and two different populations were obtained: $CD45^{Hi}$ and $CD45^{Int}$. Then, the expression levels of NK1.1/CD45, were assessed to isolate the natural killer ($NK1.1^{+}$) cells, while lymphocytes were isolated due to expression of either CD19 (B cells) or TCRβ (T cells). Lastly, the expression levels of Ly6C as a function of CD11b allowed characterization of two different populations: pro-inflammatory monocytes ($CD11b^{+}Ly6C^{Hi}$) and patrolling monocytes ($CD11b^{+}Ly6C^{Low}$).

The results obtained from the described experiences are presented as follows**.**

The first populations identified, with the mix of antibodies described, correspond to the microglia ($CD45^{Int}$) and the peripheral leukocytes ($CD45^{Hi}$). We can see in **Figure 9** that our axenic animal model showed a drastic decrease in microglial numbers, when compared to their SPF counterpart (**Figure 9 – A and B**). Importantly and despite the variability observed when assessing different animals, the statistical analysis supports

these results, as the numbers of brain resident immune cells were significantly higher in SPF mice ($1.65*10^4$) in relation to non-modulated GF animals ($9.1*10^3$) (**Figure 9 – C**). Meanwhile, when analyzing their peripheral leukocytes, although we could observe a slight increase in the SPF animals (**Figure 9 – A and B**), there was no statistical difference reported between the two conditions (**Figure 9 – D**).

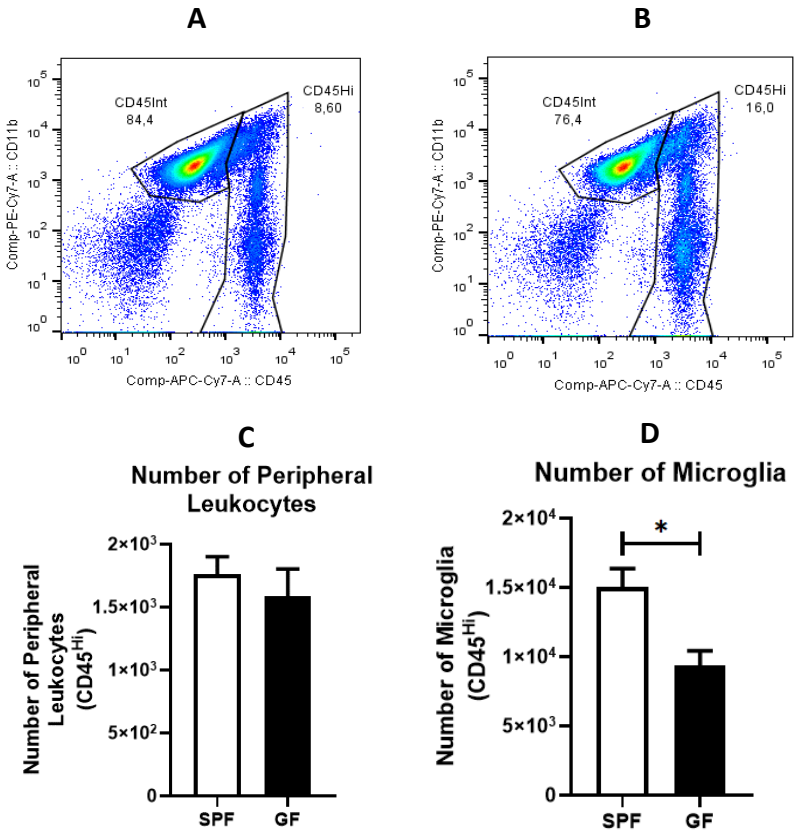

Figure 9 Fluorescence activated cell sorting analysis of brain immune cells. Mice were kept in GF and flow cytometry was used to compare immune cells brain profiles to SPF animal models. Gating strategy for isolation of microglia and peripheral leukocytes from **(A)** SPF (control) and **(B)** GF mice. Histograms represent the number of cells obtained for each population: **(C)** Peripheral Leukocytes, **(D)** Microglia. Microglial numbers showed a significant decrease in cell numbers between SPF and GF mice. In the case of peripheral leukocytes, there was no significant change. Mean values of 4 mice for each animal group. Error bars indicate standard deviation, while the asterisk refers to a statistically significant difference. *p<0.05; **p<0.01.

After the exclusion of the natural killer and the lymphocyte population, different monocyte populations were evaluated. By analyzing **Figure 10 A and B,** it is clear that the pro-inflammatory monocytes ($CD11b^{+}Ly6C^{Hi}$) presented a similar behavior to the previous populations analyzed. Once again, GF animals, when compared to their SPF counterparts, show a 50% decrease in the number of the pro-inflammatory cells (**Figure 10 C**), while no changes were observed for patrolling monocytes ($CD11b^{+}Ly6C^{Low}$) (**Figure 10 D**).

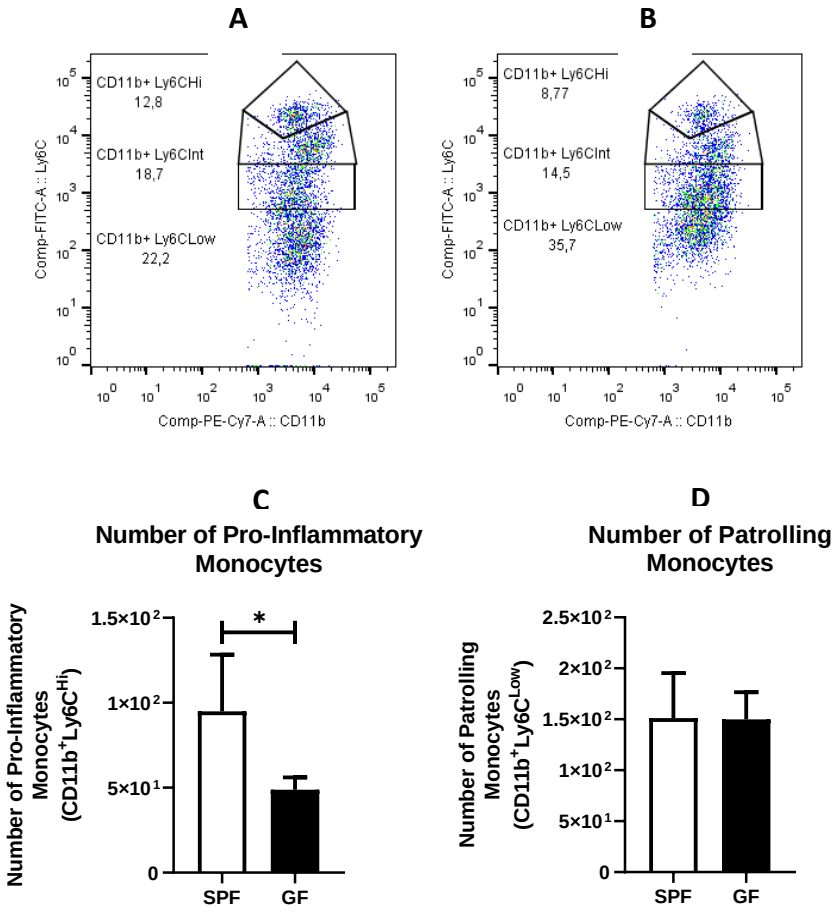

Figure 10 Fluorescence activated cell sorting analysis of myeloid immune cells in the brain. Mice were kept in GF conditions and flow cytometry was used to compare immune cells brain profiles to SPF animal models. Gating strategy for isolation of pro-inflammatory monocytes and patrolling monocytes from **(A)** SPF (control) and **(B)** GF mice. Histograms represent the number of cells obtained for each population: **(C)** Pro-inflammatory monocytes, **(D)** patrolling monocytes. Pro-inflammatory monocyte numbers showed a significant decrease in the numbers of cells between SPF and GF mice. In the case of patrolling monocytes, there was no significant change. Mean values of 4 mice for each animal group. Error bars indicate standard deviation, while the asterisk refers to a statistically significant difference. *p<0.05; **p<0.01.

To conclude the analysis of cells from the myeloid lineage, we also analyzed the number of recruited monocytes using the CCR2 marker. CCR2 (or CD192) is a chemokine receptor that can have two alternatively spliced variants. Since it is a specific monocyte recruiter, we analyzed its expression levels inside the monocytic populations.

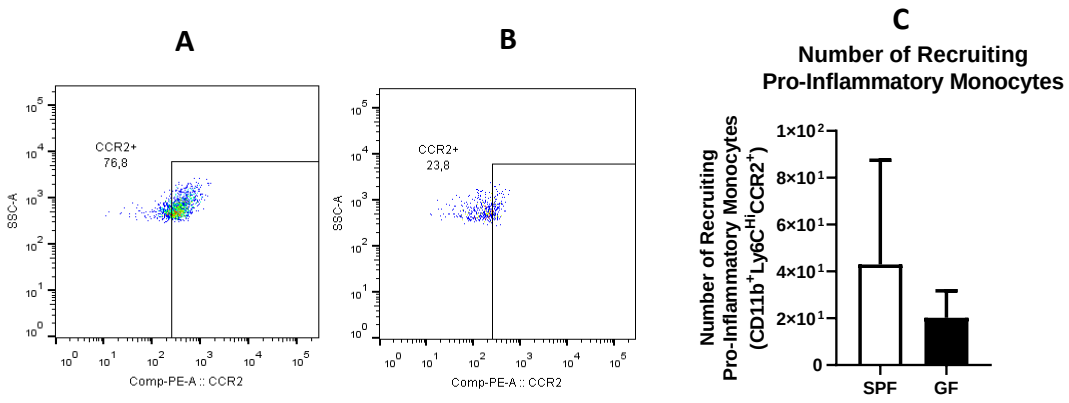

Figure 11 Fluorescence activated cell sorting analysis of myeloid immune cells in the brain. Mice were kept in GF conditions and flow cytometry was used to compare immune cells brain profiles to SPF animal models. Gating strategy for isolation of recruiting pro-inflammatory monocytes for **(A)** SPF (control) and **(B)** GF mice. Histograms represent the number of cells obtained for the studied population: **(C)** Recruiting pro-inflammatory monocytes. Recruited cell numbers showed no significant difference between conditions tested. Mean values of 4 mice for each animal group. Error bars indicate standard deviation, while the asterisk refers to a statistically significant difference. *p<0.05; **p<0.01.

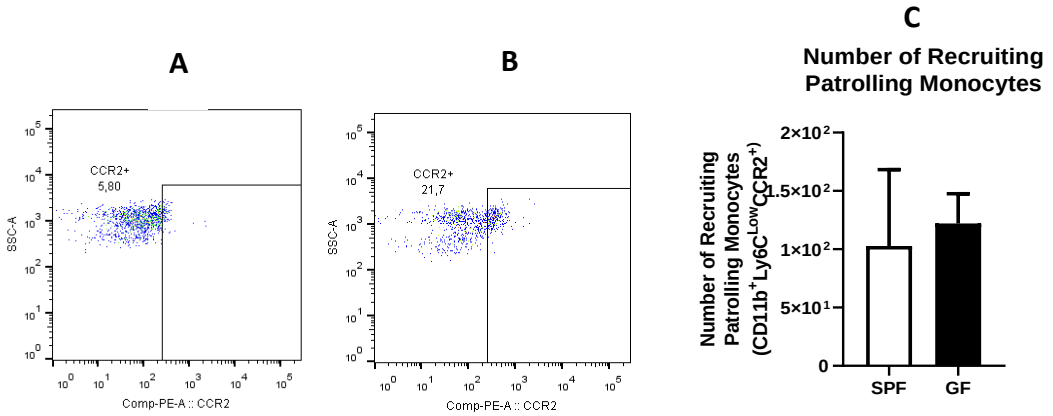

Figure 12 Fluorescence activated cell sorting analysis of myeloid immune cells in the brain. Mice were kept in GF conditions and flow cytometry was used to compare immune cells brain profiles to SPF animal models. Gating strategy for isolation of recruiting patrolling monocytes for **(A)** SPF (control) and **(B)** GF mice. Histograms represent the number of cells obtained for the studied population: **(C)** Recruiting patrolling monocytes. Recruited cell numbers showed no significant difference between conditions tested. Mean values of 4 mice for each animal group. Error bars indicate standard deviation, while the asterisk refers to a statistically significant difference. *p<0.05; **p<0.01.

At first glance, there was a small observable difference between conditions regarding the pro-inflammatory monocytes (**Figure 11 A and B**). Although not statistically significant, GF mice appear to have a pronounced decrease in the number of these cells when compared to their colonized counterparts. Regarding patrolling monocytes, a marked increase is apparent in their number in the GF mice (**Figure 12 A and B)**. However, statistical analysis of these results showed no significant changes. Moreover, the number of cells obtained for both populations is extremely low, possibly providing erroneous suggestions. Experiment repetition would be necessary to further validate these results.

Having characterized the myeloid compartment, we then proceeded to categorize the lymphoid cells using the T mix.

To better discriminate the lymphoid compartment, we wanted to characterize both B and T lymphocytes, paying particular focus to the latter. As such, we were capable of discerning between T helper (Th) cells ($CD4^+$) or cytotoxic T cells (CTLs) ($CD8^+$). Conversely, B lymphocytes were identified based on their expression of CD19, which is a transmembrane protein expressed in all B lineage cells.

Th cells recognize peptides in MHCII molecules, thus having an active role in shaping the immune response. While, on the other hand, cytotoxic T lymphocytes (CTLs) identify peptides presented by the MHC molecules and induce cell death when they recognize the corresponding antigens, as their name implies. B cells on the other hand, are part of the adaptive immune response and, among other functions, are responsible for antibody secretion.

Moreover, we also wanted to evaluate the activation status of the mentioned cellular populations. This was accomplished by analyzing the function of the expression levels of the adhesion molecules CD62L over CD44. In mice, these markers can be used to discriminate between activated ($CD44^+CD62L^-$) and naive ($CD44^-CD62L^+$) lymphocytes.

Using the T mix in the same brain samples previously presented, we obtained the following results. The gating strategies for said mix are shown in **Figure 13**.

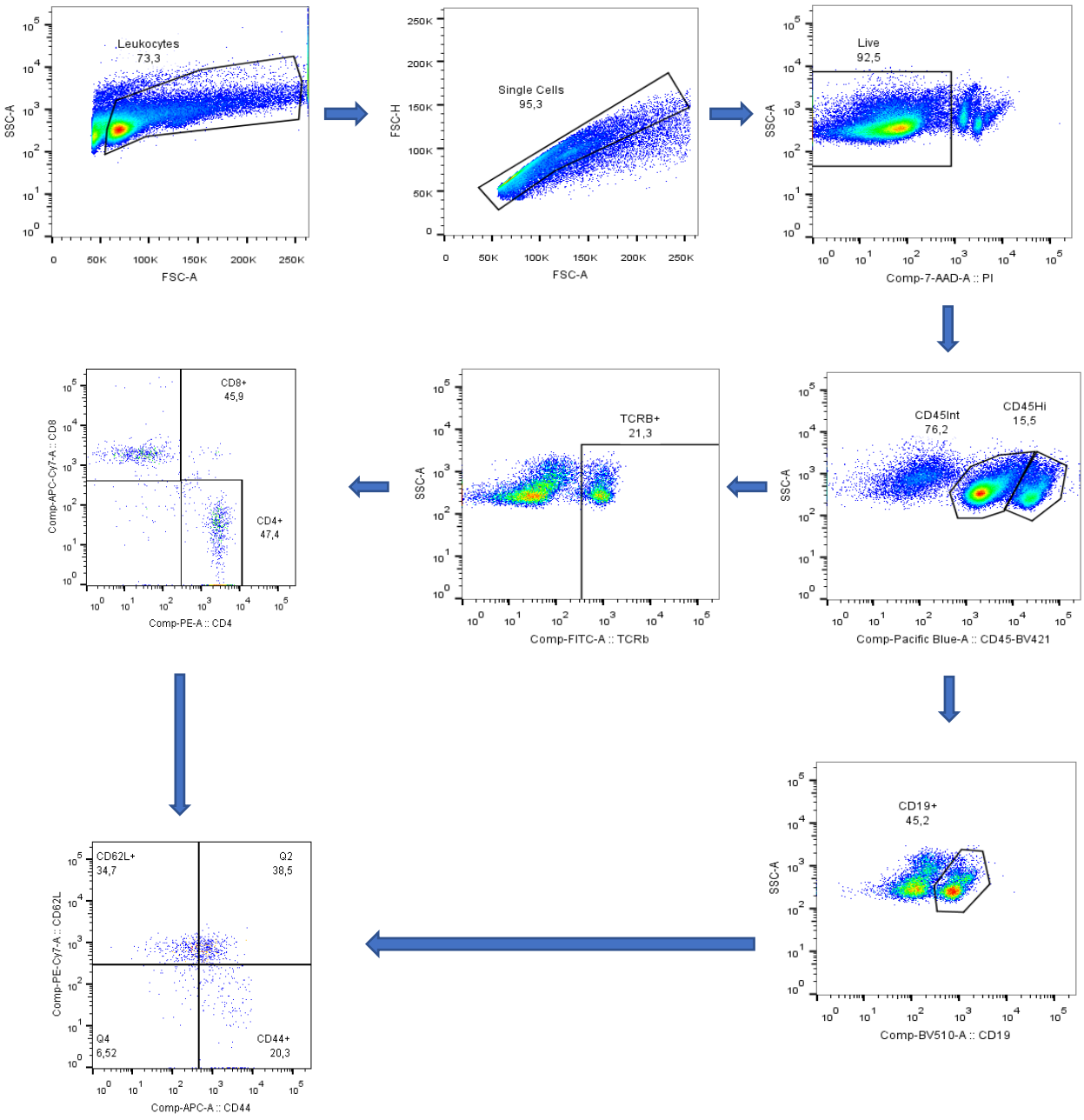

Figure 13 Representative gating strategies for lymphoid cell analysis of brain samples. . Leukocytes were selected through SSC-A as a function of FSC-A. Next, a doublet discrimination was performed through FSC-H as a function of FSC-A, with viable cells (impermeable to PI) being analyzed and designated. With the aim of separating the microglia from the peripheral leukocytes, the expression levels of CD45 were assessed and two different populations obtained: $CD45^{Hi}$ and $CD45^{Int}$. Then, the expression levels of CD19 and TCRβ were assessed individually to isolate the B lymphocytes ($CD19^{+}$) and T lymphocytes ($TCR\beta^{+}$), respectively. The $TCR\beta^{+}$ population was further divided based on the expression of CD4 as a function of CD8, allowing the identification of Th cells ($TCR\beta^{+}$ $CD4^{+}$) or CTLs ($TCR\beta^{+}$ $CD8^{+}$). Lastly, the activation status of all lymphocytic populations ($CD19^{+}$; $TCR\beta^{+}$ $CD4^{+}$; $TCR\beta^{+}$ $CD8^{+}$) was assessed by discriminating CD62L as a function of CD44, thus allowing the identification of naïve ($CD44^{-}CD62L^{+}$) and activated ($CD44^{+}CD62L^{-}$) lymphocytes.

With this mix we first analyzed the two subsets of lymphocytes, B and T cells. The results are presented in **Figures 16 and 17,** respectively.

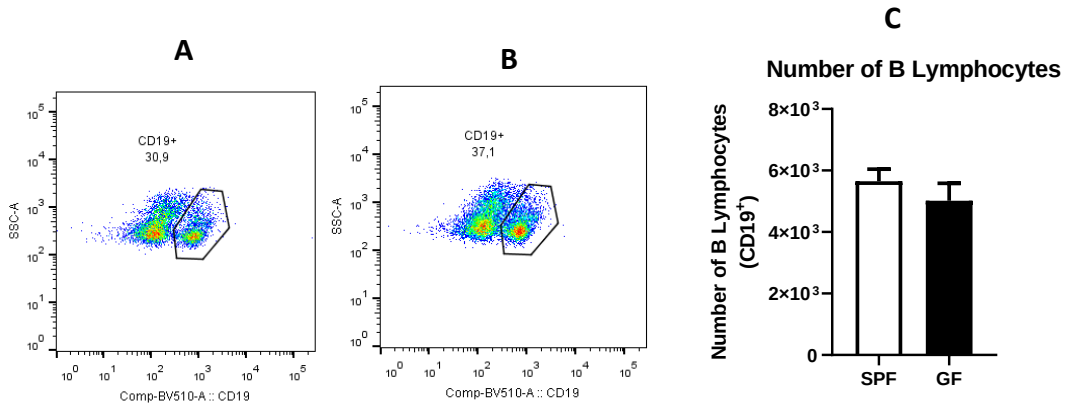

Figure 14 Fluorescence activated cell sorting analysis of lymphoid immune cells in the brain. Mice were kept in GF conditions or treated with antibiotic in order to eliminate possible pathogenic bacteria (SPF). Flow cytometry was used to study cells of the immune system in the brain of our animal models. Gating strategy for isolation of B lymphocytes for **(A)** SPF (control) and **(B)** GF mice. Histograms represent the number of cells obtained for the studied population: **(C)** B lymphocytes. Cell numbers showed no significant difference between conditions tested. Mean values of 4 mice for each animal group. Error bars indicate standard deviation, while the asterisk refers to a statistically significant difference. *p<0.05; **p<0.01.

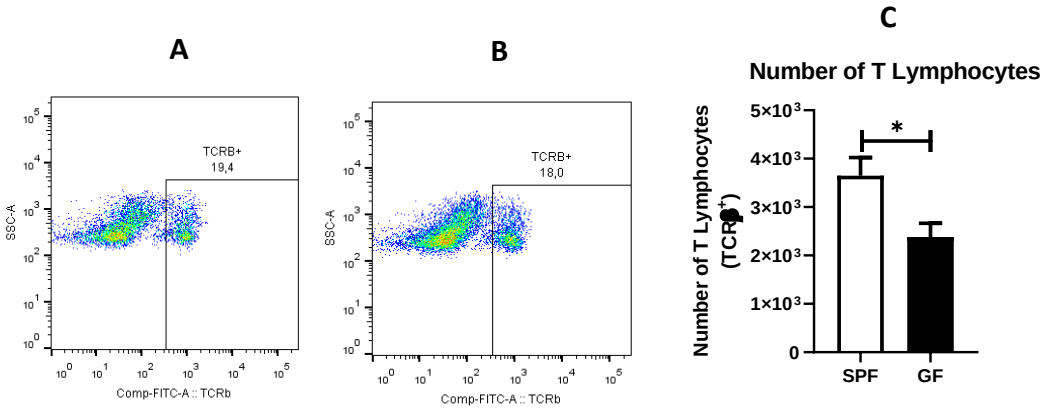

Figure 15 Fluorescence activated cell sorting analysis of lymphoid immune cells in the brain. Mice were kept in GF conditions or treated with antibiotic in order to eliminate possible pathogenic bacteria (SPF). Flow cytometry was used to study cells of the immune system in the brain of our animal models. Gating strategy for isolation of T lymphocytes for **(A)** SPF (control) and **(B)** GF mice. Histograms represent the number of cells obtained for the studied population: **(C)** T lymphocytes. Cell numbers showed a significant decrease between SPF and GF mice. Mean values of 4 mice for each animal group. Error bars indicate standard deviation, while the asterisk refers to a statistically significant difference. *p<0.05; **p<0.01.

Despite the lack of statistical significance between SPF and GF mice, the results show a slight decrease in the number of B cells (CD19+) of the GF mice (**Figure 14C**). The opposite behavior was observed for the T cell (TCRβ$^+$). Although flow cytometry analysis showed little difference between cellular percentages, statistical analysis allowed to observe that, when compared to their SPF counterpart, GF animals present a reduction in the number of T lymphocytes (**Figure 15C**).

Afterwards, our analyses focused on the different subsets of T cells ($CD4^+$ and $CD8^+$ T cells) and respective activation profiles (**Figure 16**).

By examining this figure, we observe that the results obtained were similar to those acquired in previous analyses (**Figure 15**). Indeed, both helper ($CD4^+$) and cytotoxic ($CD8^+$) T cells show a decrease in the number of cells when comparing GF mice with SPF mice (**Figure 16 C** and **D**). In the case of the $CD8^+$ cells, that difference translates into a statistical significance (**Figure 16 D**).

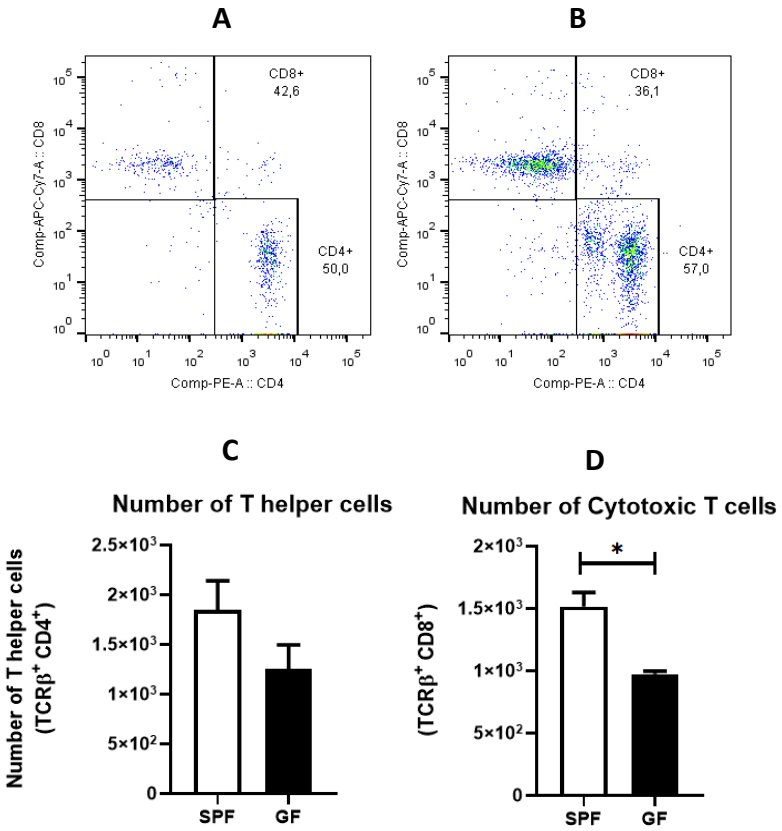

Figure 16 Fluorescence activated cell sorting analysis of lymphoid immune cells in the brain. Mice were kept in GF conditions and flow cytometry was used to compare immune cells brain profiles to SPF animal models. Gating strategy for isolation of Th cells and CTLs for **(A)** SPF (control) and **(B)** GF mice. Histograms represent the number of cells obtained for the various population: **(C)** T helper cells; **(D)** Cytotoxic T cells. CTL cell numbers showed a significant decrease between the SPF and GF mice. Th cell numbers showed no significant difference. Mean values of 4 mice for each animal group. Error bars indicate standard deviation, while the asterisk refers to a statistically significant difference. *p<0.05; **p<0.01.

Lastly, we sought to characterize the activation status of the different lymphocytic populations.

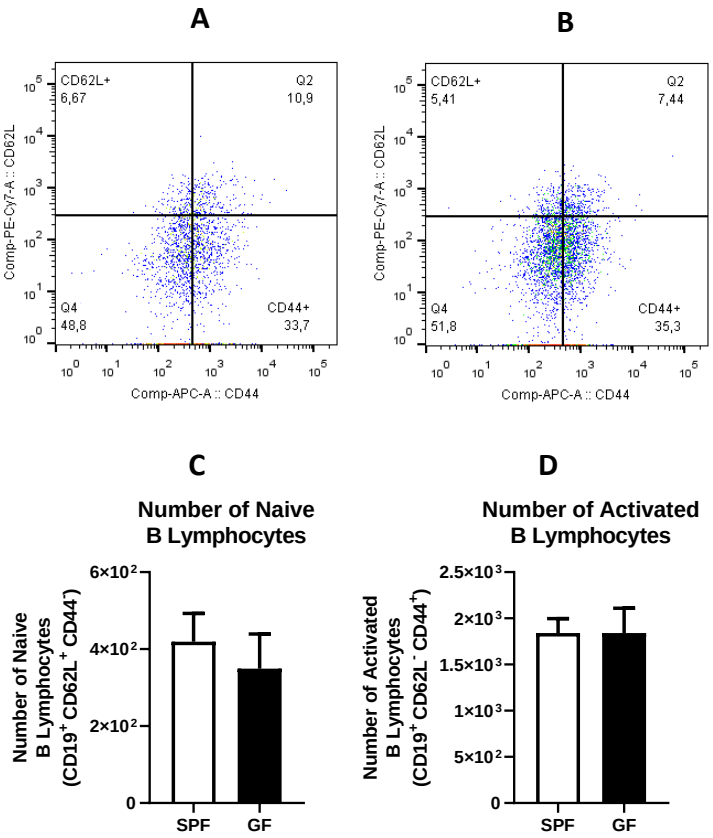

Figure 17 Fluorescence activated cell sorting analysis of lymphoid immune cells in the brain. Mice were kept in GF conditions and flow cytometry was used to compare immune cells brain profiles to SPF animal models. Gating strategy for isolation of naïve and activated B lymphocytes for **(A)** SPF (control) and **(B)** GF mice. Histograms represent the number of cells obtained for the various population: **(C)** Naïve B cells; **(D)** Activated B cells. Cell numbers showed no significant difference between conditions tested. Mean values of 4 mice for each animal group. Error bars indicate standard deviation, while the asterisk refers to a statistically significant difference. *p<0.05; **p<0.01.

No significant changes were detected in terms of B cells activation (**Figure 17**). The number of naïve B lymphocytes (CD19+CCD62L+CD44-) and activated B lymphocytes (CD19+CCD62L-CD44+) remain quite similar when comparing SPF and GF (**Figure 17C and D**).

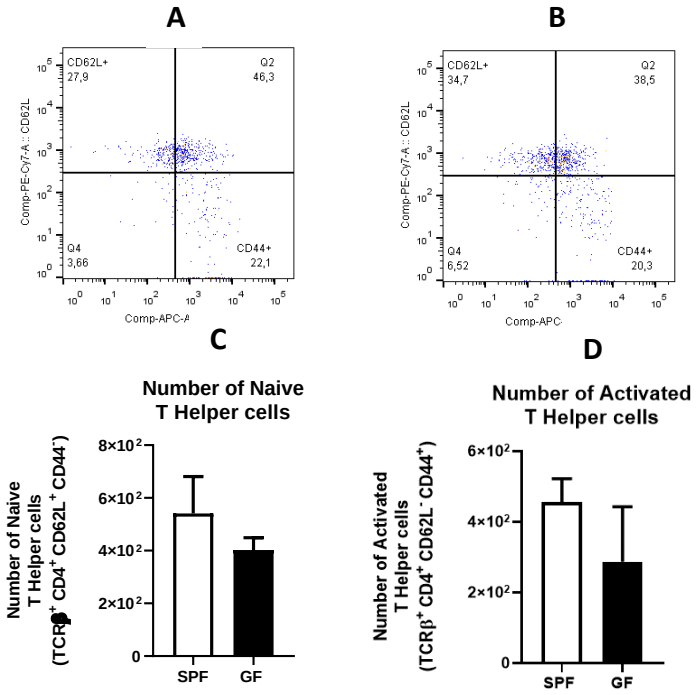

Figure 18 Fluorescence activated cell sorting analysis of lymphoid immune cells in the brain. Mice were kept in GF conditions and flow cytometry was used to compare immune cells brain profiles to SPF animal models. Gating strategy for isolation of naïve and activated Th lymphocytes for **(A)** SPF (control) and **(B)** GF mice. Histograms represent the number of cells obtained for the various population: **(C)** Naïve Th cells; **(D)** Activated Th cells. Cell numbers showed no significant difference between conditions tested. Mean values of 4 mice for each animal group. Error bars indicate standard deviation, while the asterisk refers to a statistically significant difference. *p<0.05; **p<0.01.

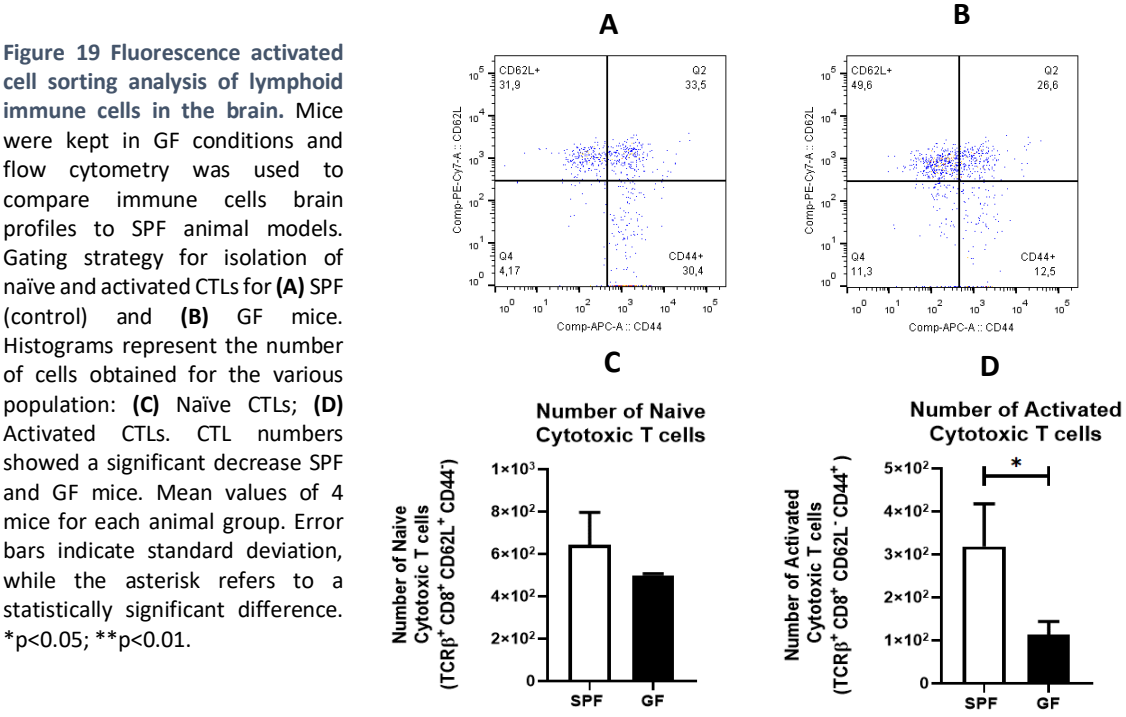

Figure 19 Fluorescence activated cell sorting analysis of lymphoid immune cells in the brain. Mice were kept in GF conditions and flow cytometry was used to compare immune cells brain profiles to SPF animal models. Gating strategy for isolation of naïve and activated CTLs for **(A)** SPF (control) and **(B)** GF mice. Histograms represent the number of cells obtained for the various population: **(C)** Naïve CTLs; **(D)** Activated CTLs. CTL numbers showed a significant decrease SPF and GF mice. Mean values of 4 mice for each animal group. Error bars indicate standard deviation, while the asterisk refers to a statistically significant difference. *p<0.05; **p<0.01.

In terms of T cell sub-populations, despite not having significant changes in Th cells activation (**Figure 18 C** and **D**), their number seemed decreased when compared to the SPF model. Regarding CTLs, while naïve ($TCR\beta^+CD8^+CD62L^+CD44^-$) cells followed a similar pattern seen in **Figure 18** the activated ($CD8^+CD62L^-CD44^+$) population showed a significant decrease when comparing GF mice with SPF animals (**Figure 19 C and D**). This

decrease in both sub-populations of T lymphocytes might suggest a role for the microbiota during their maturation and activation.

Neuroinflammatory profile in animals maintained in specific pathogen free (SPF) vs. germ-free (GF) conditions, upon PD induction

As it is known, gut microbiota changes over time and microbial diversity declines with advancing age. This association between aging and the microbiome allow to open new fields of investigation, with the aim to deepen the association between this compartment and the severity and progression of specific diseases. Particularly important became to study the 'gut-brain axis', due to its link to neurodegenerative disorders, like PD. Several studies sought to characterize the differences between gut microbes in PD patients, by comparing the profiles obtained with healthy controls. The role of bacteria taxa in the development of motor deficits and PD severity was also highlighted [40]; [18]; [19]; [43]; [44]. However, further research still needs to be conducted to understand, especially, how changes in the gut microbiota composition might modulate neuroinflammation and contribute to increase the susceptibility to PD. Thus, we proceeded to investigate the role that MPTP treatment, a neurotoxin commonly used for the induction of a pharmacological PD model, exerts on the neuroinflammatory profile of our GF animals.
In this set of experiments, we once again compared the neuroinflammatory profile of 52-60-week-old mice, both GF and SPF upon MPTP treatment. Non-manipulated mice were used as controls. Motor dysfunction assays were performed during the entire experiment and after PD induction. The results obtained are shown in **Figure 20.**

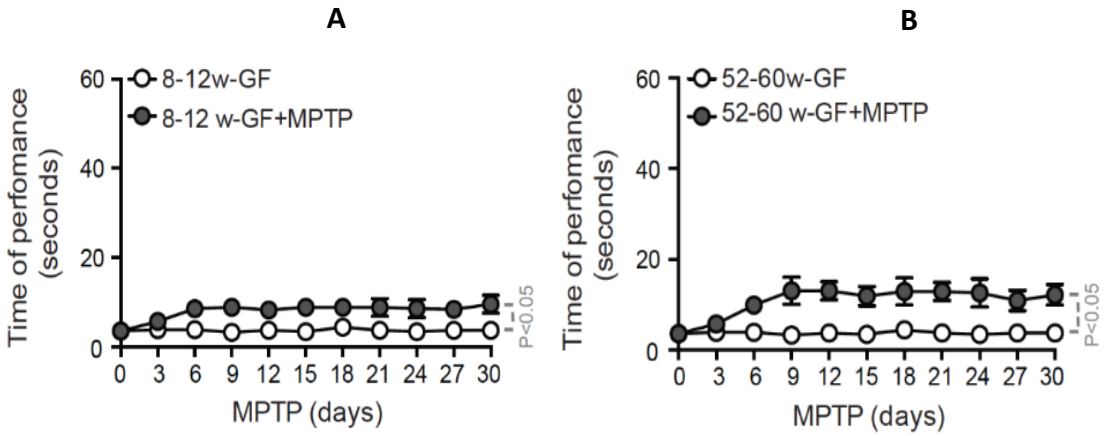

Figure 20 Motor dysfunction assessment. Exacerbated motor dysfunction was measured as time of performance of mice placed up-side-down on a vertical pole. Motor performance evaluated for both **(A)** young GF and **(B)** old GF mice. 10 mice per group. Significance was observed, according to the t-test.

These results indicate that MPTP-treated GF mice showed little motor dysfunction, although significantly different from non-treated mice. This indicate that these mice are resistant to the induction PD, an effect that is not modulated by age. Indeed, both young animals (**Figure 20 A**) and old mice appear to be pretty resistant to PD severity (**Figure 20 B**).

Once sacrificed, brain samples were collected from experimental animals and analyzed by flow-cytometry, with the aim of evaluate the prevalence of different innate and adaptive immune populations. Using the gating strategy shown in **Figure 8**, distinct myeloid cell subsets were characterized.

The first populations to be analyzed were microglia ($CD45^{Int}$) and infiltrated leukocytes ($CD45^{Hi}$) (**Figure 21).** As shown in **Figure 21 F**, the number of microglial cells in non-manipulated GF animals is higher when compared to SPF and GF mice treated with MPTP. The same profile was observed for peripheral leukocytes (**Figure 21 E**) although not to that extent. No significant results were obtained.

The monocytic population was also studied by combining the CD11b and Ly6C markers.

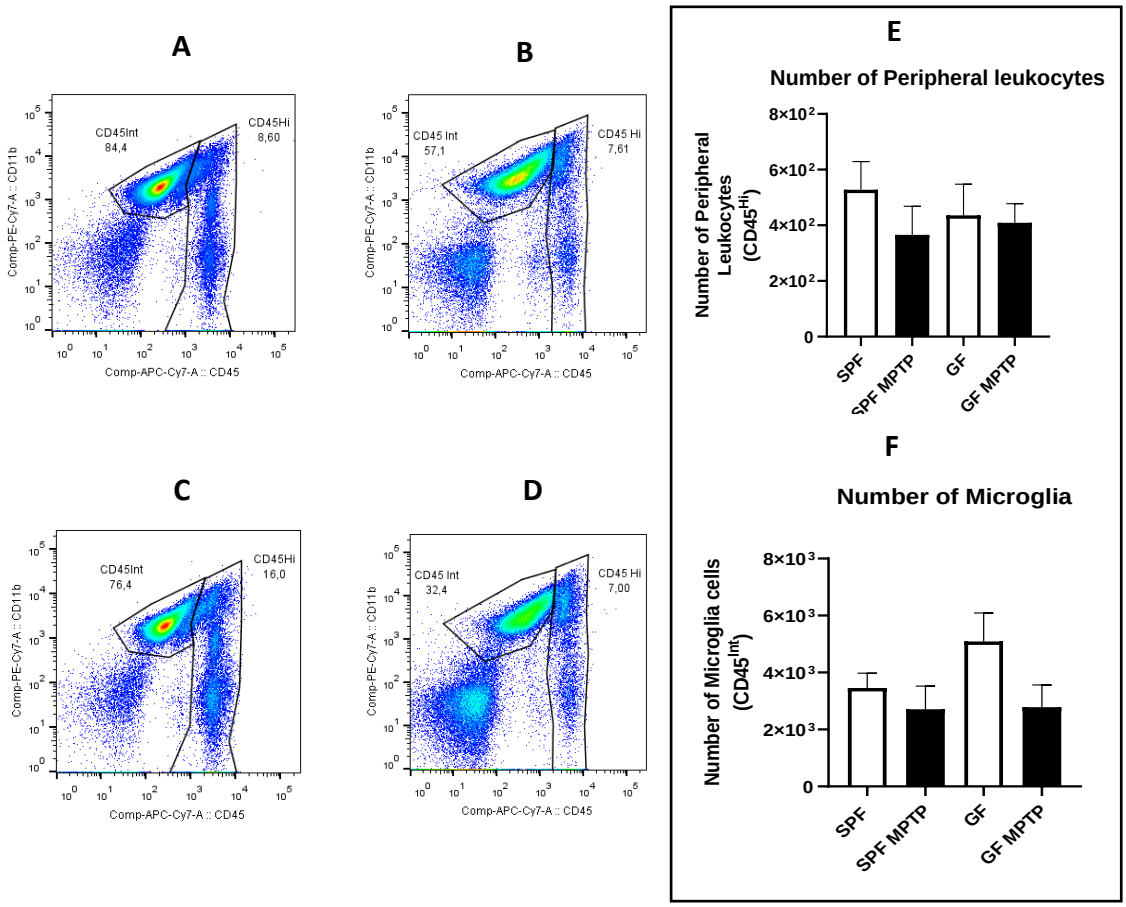

Figure 21 Fluorescence activated cell sorting analysis of brain immune cells. Mice were kept in GF conditions and flow cytometry was used to compare immune cells brain profiles to SPF animal models, upon being treated with MPTP. Gating strategy for isolation of microglia and peripheral leukocytes from **(A)** SPF (control) and **(B)** SPF-MPTP; **(C)** GF and **(D)** GF-MPTP mice. Histograms represent the number of cells obtained for each population: **(E)** Peripheral Leukocytes, **(F)** Microglia. There was no significant change between conditions tested. Mean values of 2 to 4 mice for each animal group. Error bars indicate standard deviation, while the asterisk refers to a statistically significant difference. *p<0.05; **p<0.01.

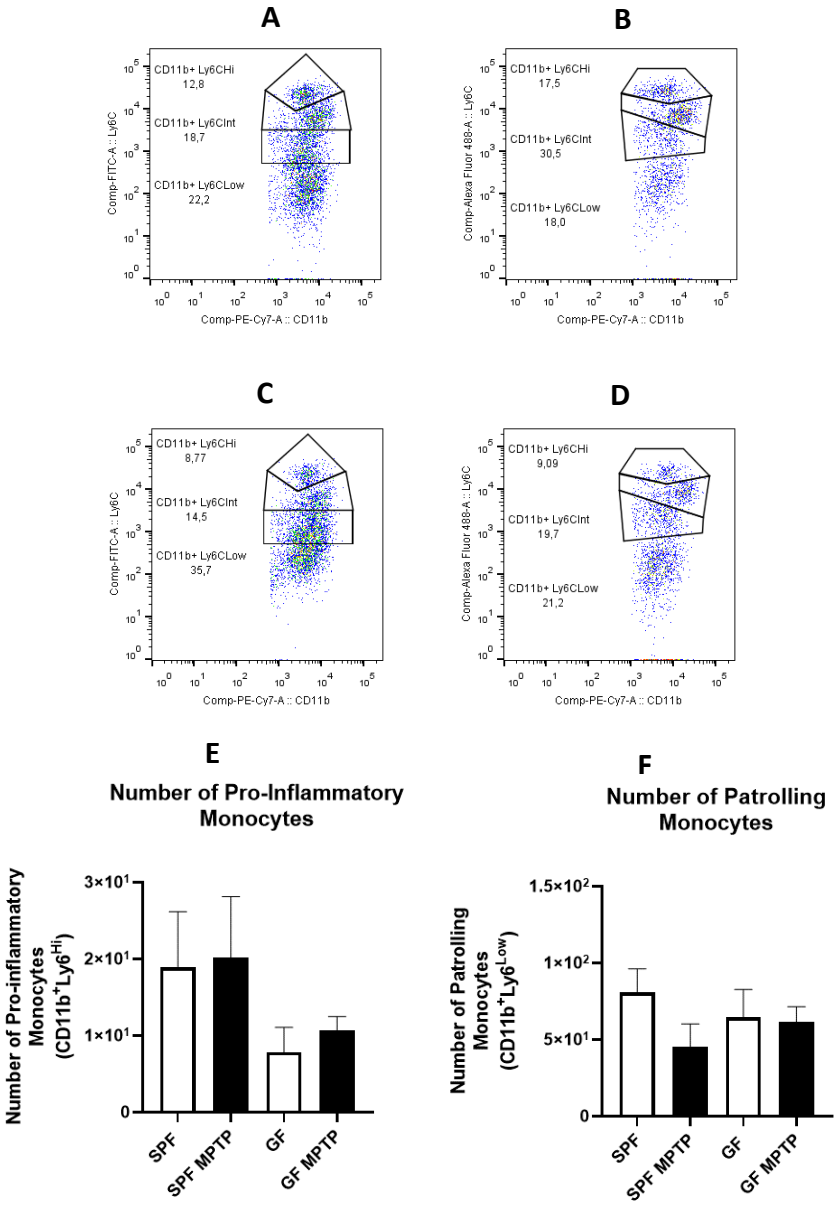

Figure 22 Fluorescence activated cell sorting analysis of myeloid immune cells in the brain. Mice were kept in GF conditions and flow cytometry was used to compare immune cells brain profiles to SPF animal models, upon being treated with MPTP. Gating strategy for isolation of pro-inflammatory monocytes and patrolling monocytes from **(A)** SPF (control), **(B)** SPF-MPTP, **(C)** GF and **(D)** GF-MPTP mice. Histograms represent the number of cells obtained for each population: **(E)** Pro-inflammatory monocytes, **(F)** patrolling monocytes. There was no significant change between conditions tested. Mean values of 2 to 4 mice for each animal group. Error bars indicate standard deviation, while the asterisk refers to a statistically significant difference. *p<0.05; **p<0.01.

There were no significant statistical differences between the conditions tested (**Figure 22**). However, by looking at the graphs presented, we can see that the pro-inflammatory monocytes seem to be increased in the SPF-MPTP mouse model when compared with the GF-MPTP (**Figure 22 E**). Patrolling monocytes on the other hand, seem to follow a reverse tendency, i.e. these cells increased in the GF-MPTP model to levels similar of the

non-modulated GF model (**Figure 22 F**). However, to uphold these suggestions, a new experiment should be conducted, as the numbers of obtained cells were low.

To conclude the myeloid characterization of this animal model, we assessed the values of recruiting cells in the populations above. The results obtained for the $CCR2^{+}$ monocytes are shown in **Figures 23** and **24.**

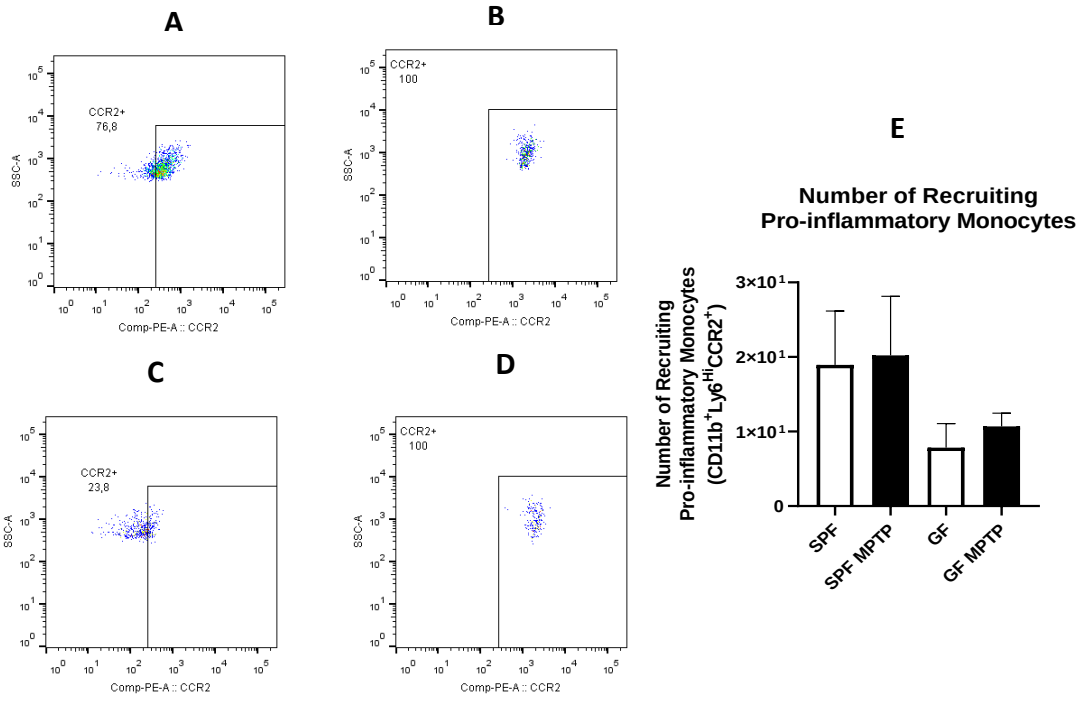

Figure 23 Fluorescence activated cell sorting analysis of myeloid immune cells in the brain. Mice were kept in GF conditions and flow cytometry was used to compare immune cells brain profiles to SPF animal models, upon being treated with MPTP. Gating strategy for isolation of recruiting pro-inflammatory monocytes from **(A)** SPF (control), **(B)** SPF-MPTP, **(C)** GF and **(D)** GF-MPTP mice. Histograms represent the number of cells obtained for each population: **(E)** Pro-inflammatory monocytes. There was no significant change between conditions tested. Mean values of 2 to 4 mice for each animal group. Error bars indicate standard deviation, while the asterisk refers to a statistically significant difference. *p<0.05; **p<0.01.

Although a statistical significance was not observed between the conditions tested, the SPF-MPTP mice seem to exhibit an increase in pro-inflammatory status, as the levels of recruiting pro-inflammatory monocytes are increased, when compared to other conditions (**Figures 23 A and B**). Regarding the patrolling monocytes (**Figure 24),** it seems that these cells are following the reverse trend to that observed for pro-inflammatory monocytes. Even though there is no statistical significance, the number of recruited cells seem to be increased in the GF-MPTP model, approaching levels similar of the non-modulated GF model (**Figure 24 C**). However, it is important to underline that some groups have very few mice. Thus, further experiments are necessary to support the results obtained.

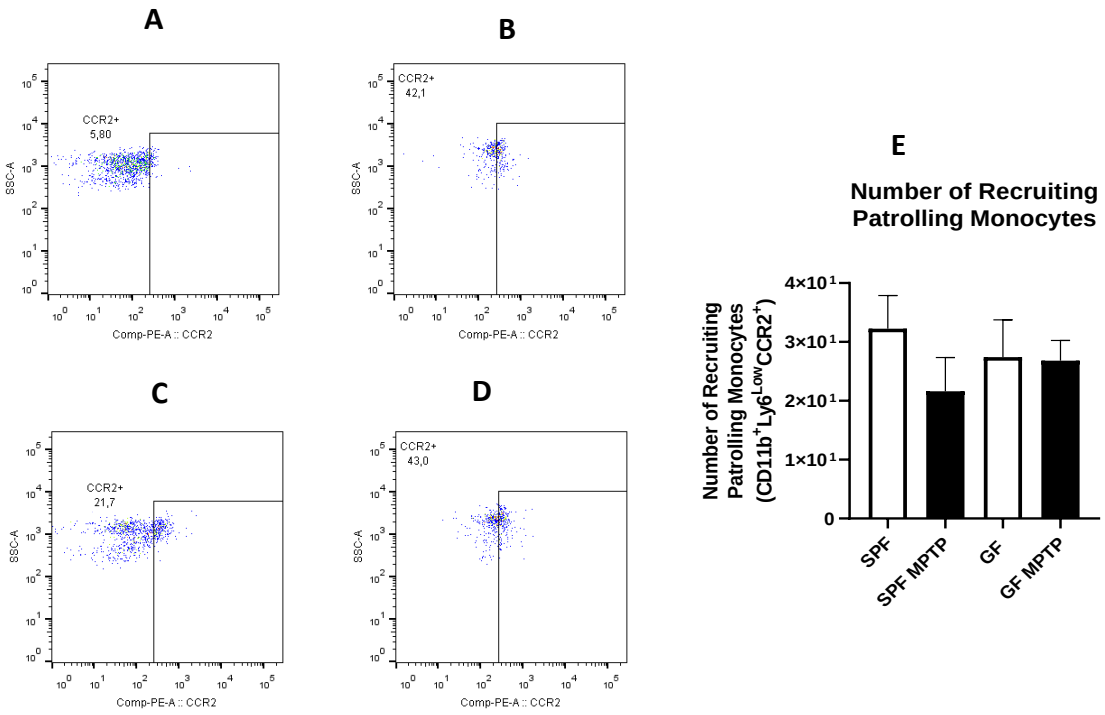

Figure 24 Fluorescence activated cell sorting analysis of myeloid immune cells in the brain. Mice were kept in GF conditions and flow cytometry was used to compare immune cells brain profiles to SPF animal models, upon being treated with MPTP. Gating strategy for isolation of recruiting patrolling monocytes from **(A)** SPF (control), **(B)** SPF-MPTP, **(C)** GF and **(D)** GF-MPTP mice. Histograms represent the number of cells obtained for each population: **(E)** Patrolling monocytes. There was no significant change between conditions tested. Mean values of 2 to 4 mice for each animal group. Error bars indicate standard deviation, while the asterisk refers to a statistically significant difference. *p<0.05; **p<0.01.

After characterizing the myeloid compartment, we then proceeded to the analysis of the distribution of the lymphoid cells. Again, using the T mix in the same brain samples previously presented, we obtained results for the following cells: B Lymphocytes, T Lymphocytes, Th cells, CTLs and their corresponding activation status. This was accomplished using the gating strategy presented in **Figure 13**.

We can see by analyzing **figures 25** and **26** the distribution of the two classes of lymphocytes, b and t cells, respectively.

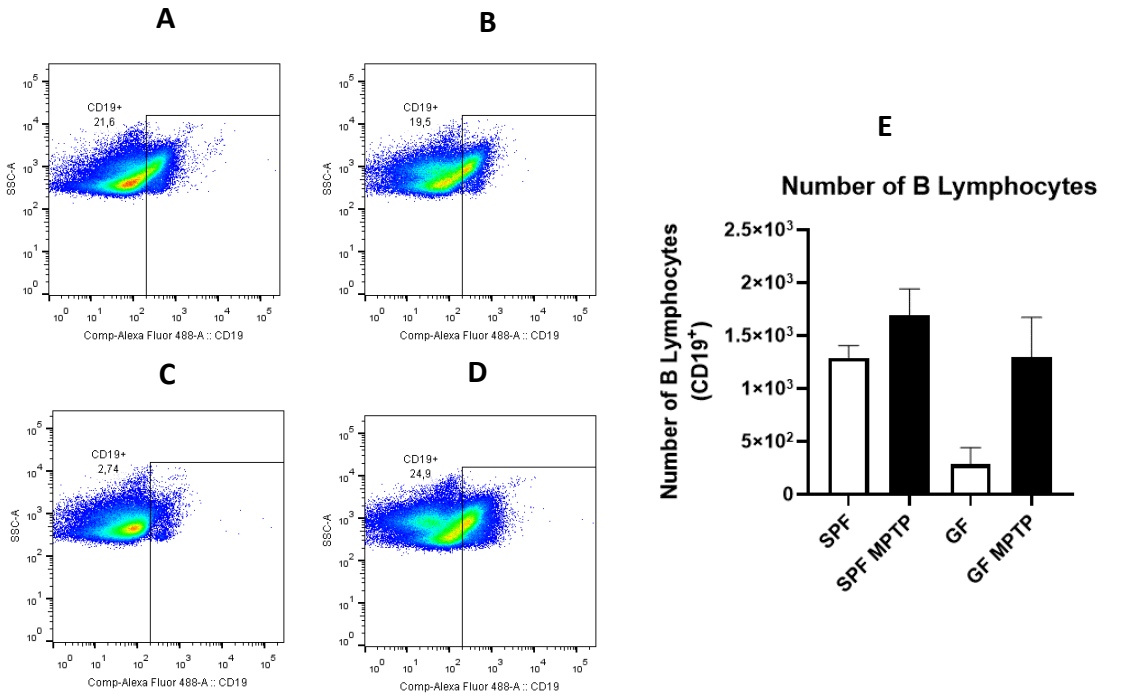

Figure 25 Fluorescence activated cell sorting analysis of lymphoid immune cells in the brain. Mice were kept in GF conditions or treated with antibiotic in order to eliminate possible pathogenic bacteria (SPF) then treated with MPTP. Flow cytometry was used to study cells of the immune system in the brain of our animal models. Gating strategy for isolation of B lymphocytes from **(A)** SPF (control), **(B)** SPF-MPTP, **(C)** GF and **(D)** GF-MPTP mice. Histograms represent the number of cells obtained for each population: **(E)** B lymphocytes. There was no significant change between conditions tested. Mean values of 2 to 4 mice for each animal group. Error bars indicate standard deviation, while the asterisk refers to a statistically significant difference. *p<0.05; **p<0.01.

Starting with the analysis of the B cell population, we observe that a small decrease in the numbers of these cells seem to occur between MPTP-induced SPF and GF. However, the results obtained are not statistically significant (**Figure 25 E**). Moreover, it appears that the number of these cells are increased when compared to the non-modulated control groups, yet statistical significance is still required.

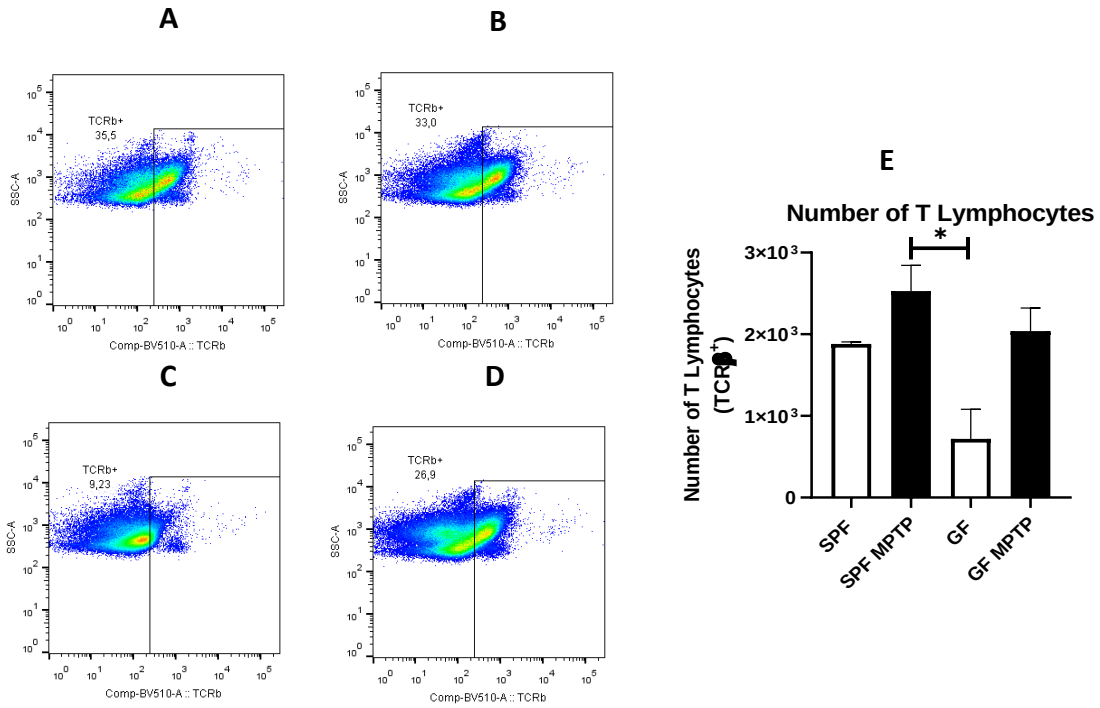

Figure 26 Fluorescence activated cell sorting analysis of lymphoid immune cells in the brain. Mice were kept in GF conditions and flow cytometry was used to compare immune cells brain profiles to SPF animal models, upon being treated with MPTP. Gating strategy for the isolation of T lymphocytes from **(A)** SPF (control), **(B)** SPF-MPTP, **(C)** GF and **(D)** GF-MPTP mice. Histograms represent the number of cells obtained for each population: **(E)** T lymphocytes. A significant decrease was obtained when comparing the SPF-MPTP and GF mice. There was no significant change between any other conditions tested. Mean values of 2 to 4 mice for each animal group. Error bars indicate standard deviation, while the asterisk refers to a statistically significant difference. *p<0.05; **p<0.01.

In the analysis of the T cells, we can observe that these seem to follow the same tendency previously described for the B cells. We noted that not only do they seem to, again, decrease between MPTP-treated models, but that there is also a significant increase in the number of these cells, when comparing NM mice vs. MPTP treated models in both SPF and GF groups (**Figure 26 E**).

Next, we sought to further characterize the two identifiable sub-population of T lymphocytes, T helper cells ($CD4^+$) and cytotoxic T cells ($CD8^+$). The results obtained are presented in **Figure 27**.

By analyzing this figure, we can observe that there is a marked difference in the distribution of Th cells when comparing the SPF with the GF mouse model, as the percentage of these cells drops by almost 50% (**Figures 27 A and C**). This drop in cell numbers we also observed in the statistics (**Figures 27 E**), yet, the only significant difference obtained was between the non-modulated GF and the SPF-MPTP treated models.

In regard to the distribution of the CTL sub-population, there was no statistically significant difference. Nonetheless, we can see that in the GF-MPTP model, their distribution and numbers seem to follow the same tendency of the Th cells, as both of them are diminished compared to the SPF-MPTP treated counterpart (**Figure 27 F**).

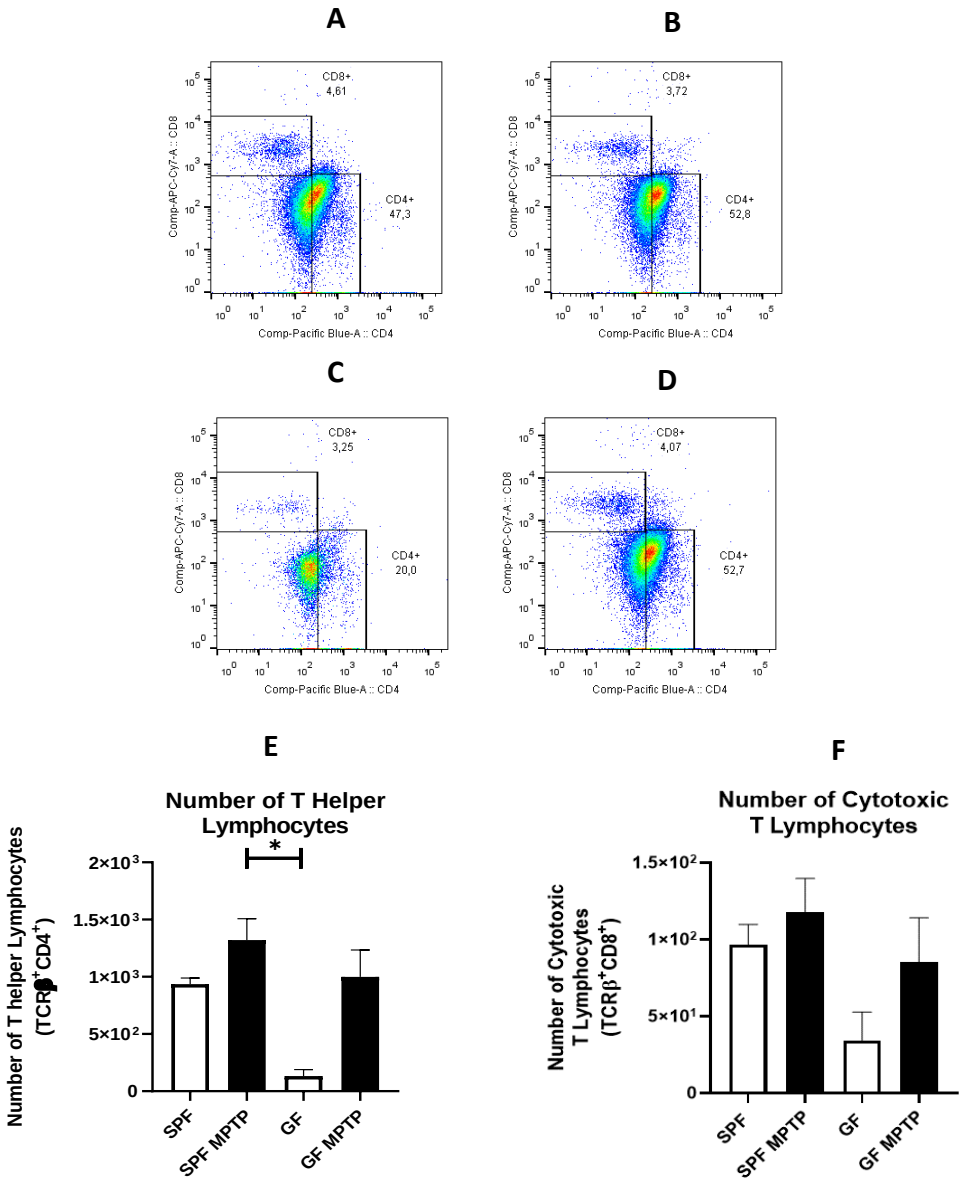

Figure 27 Fluorescence activated cell sorting analysis of lymphoid immune cells in the brain. Mice were kept in GF conditions and flow cytometry was used to compare immune cells brain profiles to SPF animal models, upon being treated with MPTP. Gating strategy for isolation of Th lymphocytes and CTLs from **(A)** SPF (control), **(B)** SPF-MPTP, **(C)** GF and **(D)** GF-MPTP mice. Histograms represent the number of cells obtained for each population: **(E)** Th lymphocytes, (**F**) CTLs. A significant decrease in the Th population was obtained when comparing the SPF-MPTP and GF mice. There was no significant change between any other conditions tested. Mean values of 2 to 4 mice for each animal group. Error bars indicate standard deviation, while the asterisk refers to a statistically significant difference. *p<0.05; **p<0.01.

To finish this set of experiments, we then looked at the activation levels of different populations. The results corresponding to these experiments are shown in **Figures 28, 29 and 30.**

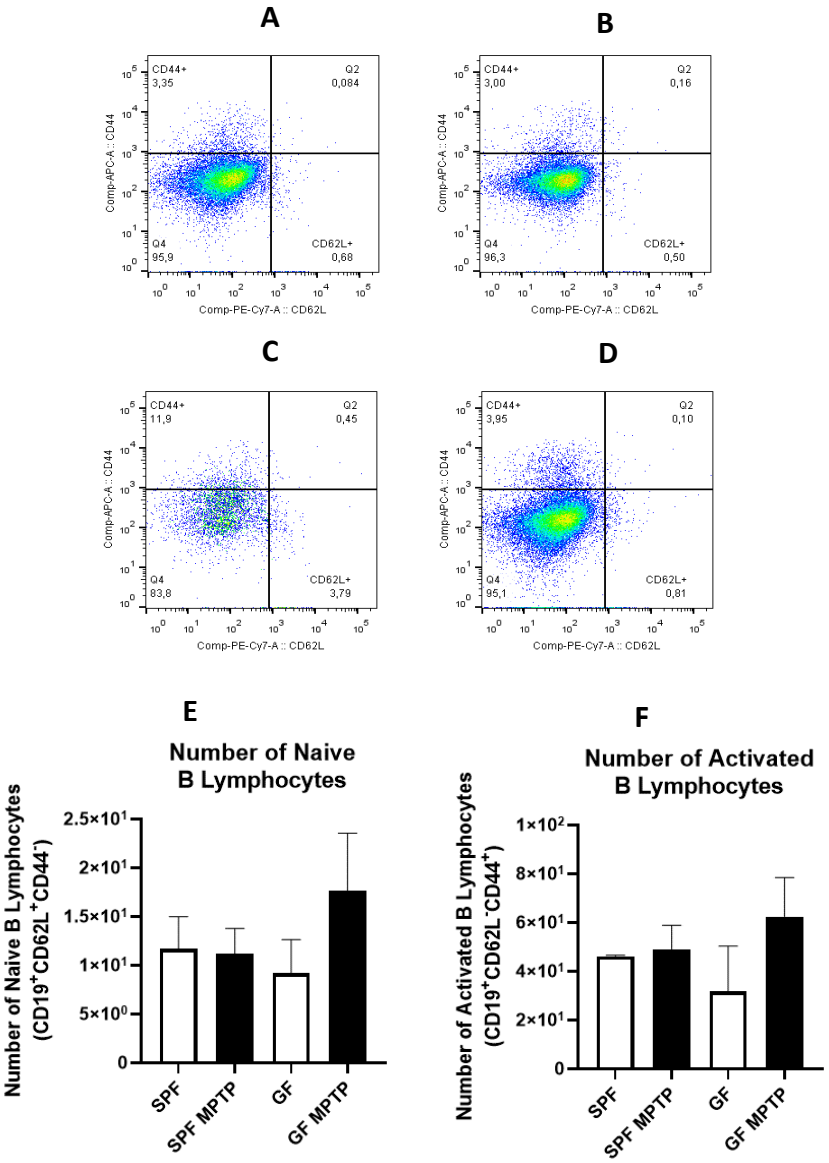

Figure 28 Fluorescence activated cell sorting analysis of lymphoid immune cells in the brain. Mice were kept in GF conditions and flow cytometry was used to compare immune cells brain profiles to SPF animal models, upon being treated with MPTP. Gating strategy for isolation of naïve and activated B lymphocytes from **(A)** SPF (control), **(B)** SPF-MPTP, **(C)** GF and **(D)** GF-MPTP mice. Histograms represent the number of cells obtained for each population: **(E)** Naïve B lymphocytes, (**F**) Activated B lymphocytes. A significant decrease in the Th population was obtained when comparing the SPF-MPTP and GF mice. There was no significant change between any other conditions tested. Mean values of 2 to 4 mice for each animal group. Error bars indicate standard deviation, while the asterisk refers to a statistically significant difference. *p<0.05; **p<0.01.

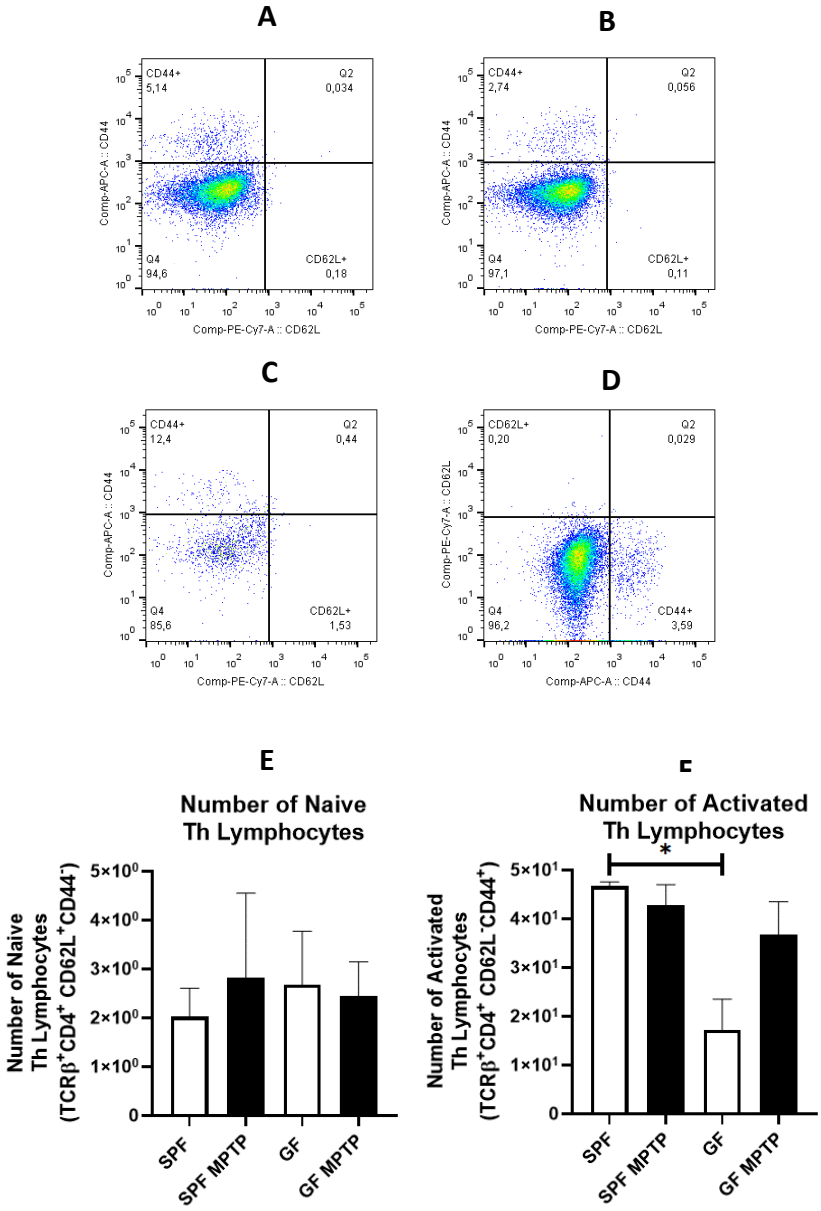

Figure 29 Fluorescence activated cell sorting analysis of lymphoid immune cells in the brain. Mice were kept in GF conditions and flow cytometry was used to compare immune cells brain profiles to SPF animal models, upon being treated with MPTP. Gating strategy for isolation of naïve and activated Th lymphocytes from **(A)** SPF (control), **(B)** SPF-MPTP, **(C)** GF and **(D)** GF-MPTP mice. Histograms represent the number of cells obtained for each population: **(E)** Naïve Th lymphocytes, (**F**) Activated Th lymphocytes. A significant decrease in the Th population was obtained when comparing the SPF and GF mice. There was no significant change between any other conditions tested. Mean values of 2 to 4 mice for each animal group. Error bars indicate standard deviation, while the asterisk refers to a statistically significant difference. *p<0.05; **p<0.01.

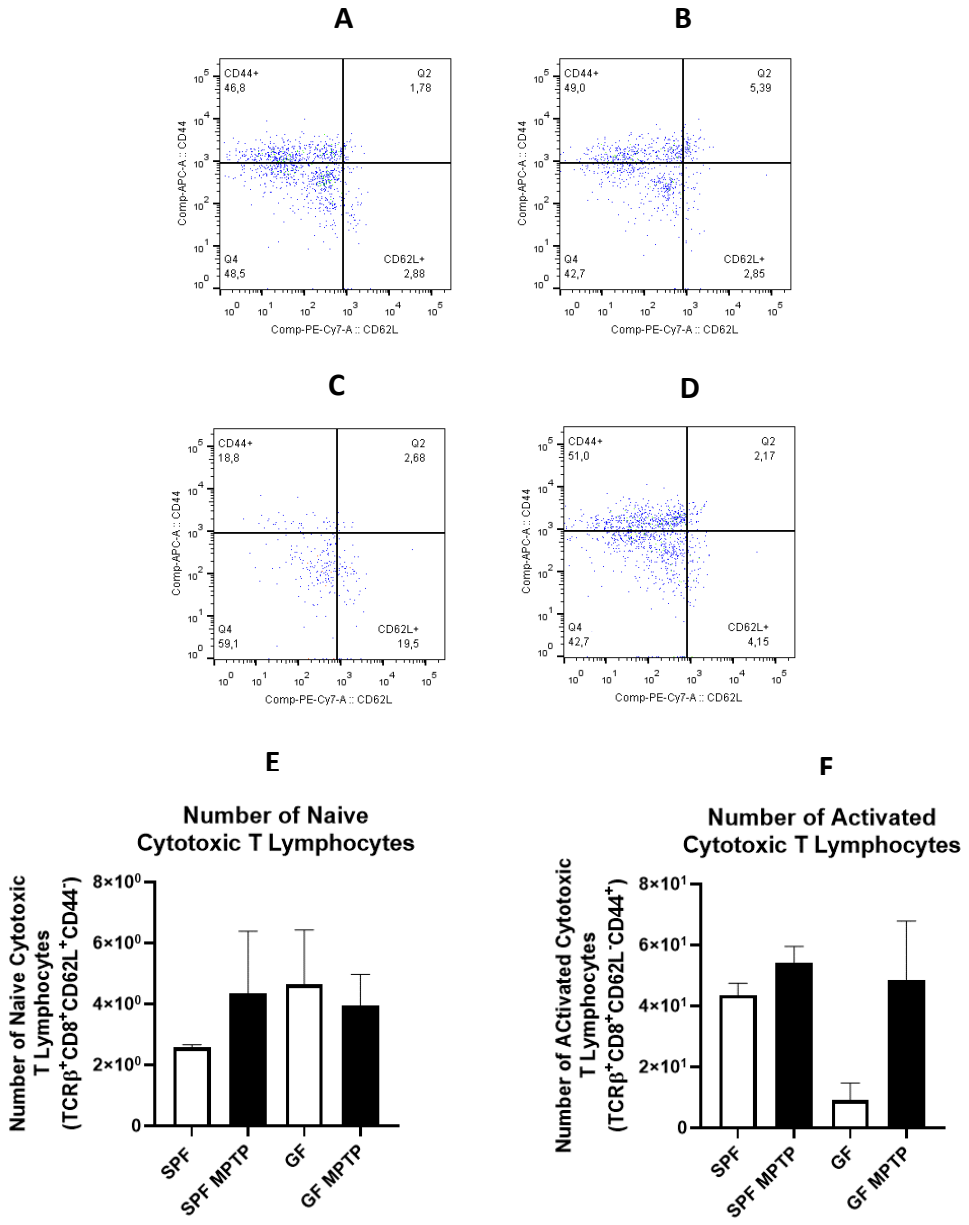

Figure 30 Fluorescence activated cell sorting analysis of lymphoid immune cells in the brain. Mice were kept in GF conditions and flow cytometry was used to compare immune cells brain profiles to SPF animal models, upon being treated with MPTP. Gating strategy for isolation of naïve and activated CTLs from **(A)** SPF (control), **(B)** SPF-MPTP, **(C)** GF and **(D)** GF-MPTP mice. Histograms represent the number of cells obtained for each population: **(E)** Naïve CTLs, (**F**) Activated CTLs. There was no significant change between any conditions tested. Mean values of 2 to 4 mice for each animal group. Error bars indicate standard deviation, while the asterisk refers to a statistically significant difference. *p<0.05; **p<0.01.

One observation that can be made from all of these conditions is that no significant difference could be observed when comparing the MPTP-treated models.

Still, the B cell population seems to be a little increased (**Figure 28 E and F)** in the GF-MPTP treated model. On the other hand, the activation of the different T cell sub-populations seems to be maintained in similar levels to those of the SPF-MPTP model, as no statistical or visible change could be found in these experiments (**Figures 29 and 30 E and F**).

Although some cellular populations seemed increased, no statistical significance was observed. Hence, these results suggest that these animals were resistant to PD induced by MPTP. However, new experiments should be conducted to corroborate these results.

Neuroinflammatory profile in animals maintained in specific pathogen free (SPF) vs. germ-free (GF) conditions, upon colonization and PD induction

It is well established that gut microbiota plays a crucial role in PD pathophysiology. *Sampson et al.* demonstrated that the colonization of animals with microbiota collected from individuals with PD increases motor dysfunction and neuroinflammation, when compared to their non-colonized counterparts. Moreover, this work also demonstrated that the results obtained by supplementing GF with short-chain fatty acids (SCFAs), a known microbial metabolite capable of modulating microglia, were similar to those observed in colonized animals [45]. However, a genetic model was used. As such, the role that the aging microbiota plays in the susceptibility to develop sporadic PD remained to be addressed.

Since our GF mice were previously shown to be resistant to MPTP-induction, we hypothesized that this could be manipulated through gut colonization. The reasoning is based on the notion that aging decreases gut microbial diversity, becoming the highest the risk factor for the development of sporadic PD. As such, in order to evaluate the role of aged microbiota in the susceptibility to PD, we colonized gnotobiotic animals with stool samples collected from their old SPF counterparts. Upon fecal transplantation, mice were treated with MPTP. This allowed to compare not only the effect that colonization alone played in the neuroinflammatory profile of these animals, but also its role in modulating PD susceptibility.

Motor dysfunction was assessed in GF colonized, MPTP treated mice, in order to evaluate if gut colonization could influence their susceptibility to develop PD-like symptoms, namely, motor dysfunction. The results are presented in **Figure 33**.

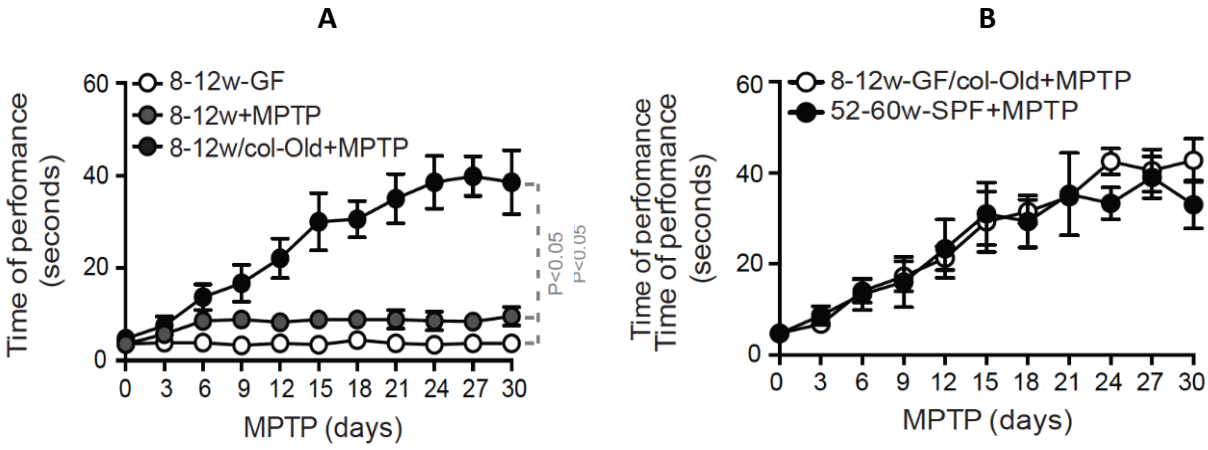

Figure 33 Motor dysfunction assessment. Exacerbated motor dysfunction was measured as time of performance of mice placed up-side-down on a vertical pole. Motor performance evaluated for **(A)** young colonized GF mice. **(B)** Comparison between colonized GF and SPF-MPTP mice. 10 mice per group. Significance has been observed, according to t-test.

These data demonstrated that we could now see a reduced motor dysfunction in these animals. Even young animals, when treated with MPTP and colonized with stool samples

from old animals showed a motor behavioral alteration. (**Figure 33 A**). However, if not colonized, they were protected against this alteration.

Nevertheless, the most unexpected result is observed in **Figure 33 B**, as we can clearly observe that not only young animals, colonized, developed motor dysfunction, but their phenotype was extraordinarily similar to that of old SPF-mice treated with MPTP. Yet, other histological and biochemical processes should be applied in order to complement these results and provide proof that these alterations may be linked to PD susceptibility.

As such we used the previously described antibody mixes in order to categorize both the myeloid and lymphoid compartments of these gnotobiotic animal models. Starting with the analysis of the myeloid cells, we can see a dramatic difference in the first condition tested.

Figure 34 depicts the results obtained for the distribution of both microglial cells and peripheric leukocytes. We detected a marked increase in both cellular populations in GF colonized MPTP-treated mice when compared with their non-colonized counterpart, suggesting that neuroinflammation is increasing in this condition.

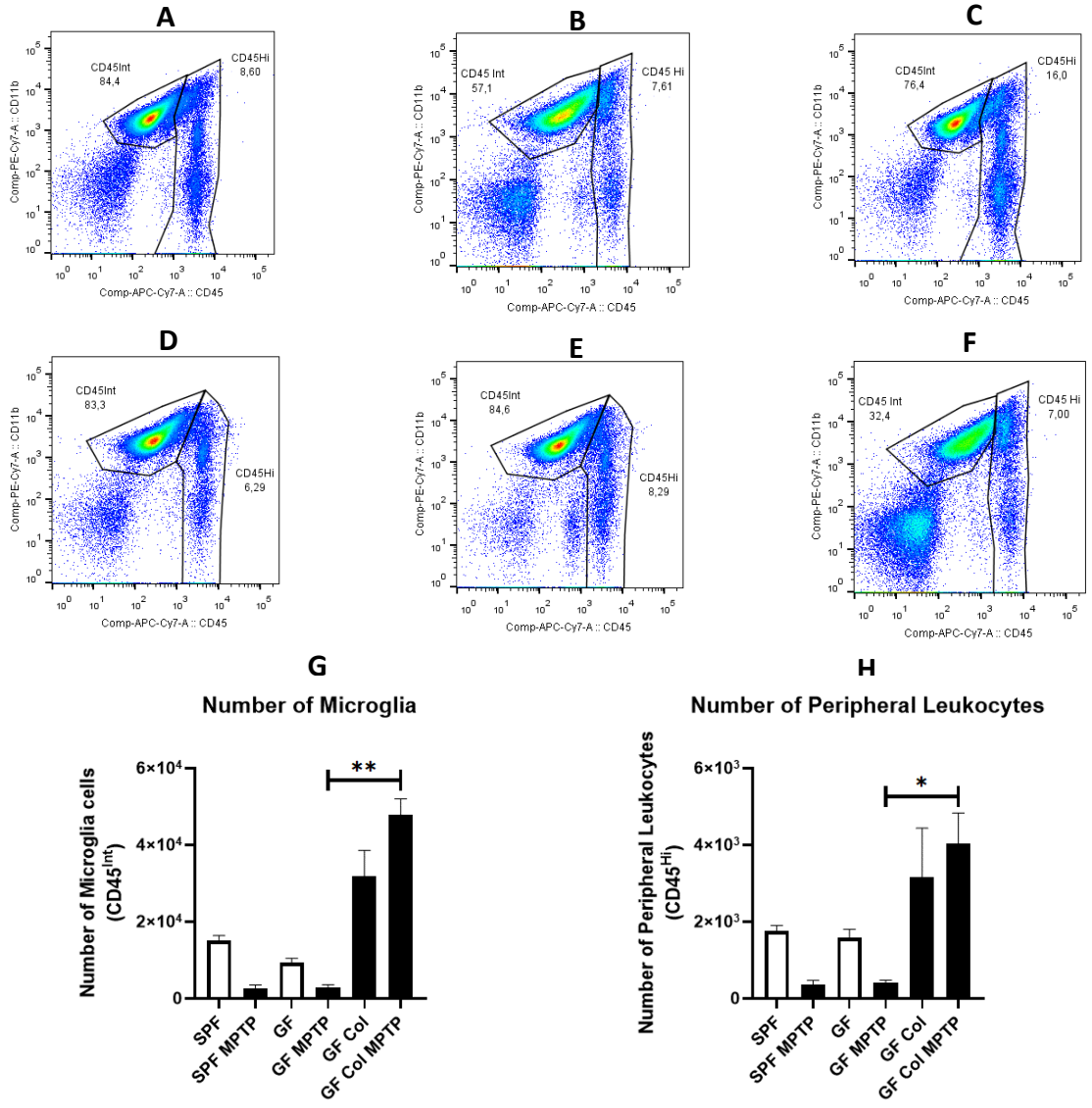

Figure 34 Fluorescence activated cell sorting analysis of brain immune cells. Mice were kept in GF conditions, colonized and treated with MPTP. Flow cytometry was used to study cells of the immune system in the brain of our animal models. Gating strategy for isolation of microglia and peripheral leukocytes from **(A)** SPF (control) and **(B)** SPF-MPTP; **(C)** GF, **(D)** GF-MPTP mice **(E)** GF-Col and **(F)** GF-Col-MPTP. Histograms represent the number of cells obtained for each population: **(G)** Microglia, **(H)** Peripheral Leukocytes. A significant increase in both populations occurred when comparing the GF with the GF-Col-MPTP mice. Mean values of 2 to 4 mice for each animal group. Error bars indicate standard deviation, while the asterisk refers to a statistically significant difference. *p<0.05; **p<0.01.

Next, after isolating the remaining cell types (natural killer cells and lymphocytes **Figure 10**) we looked at the results obtained regarding the different monocyte subsets.

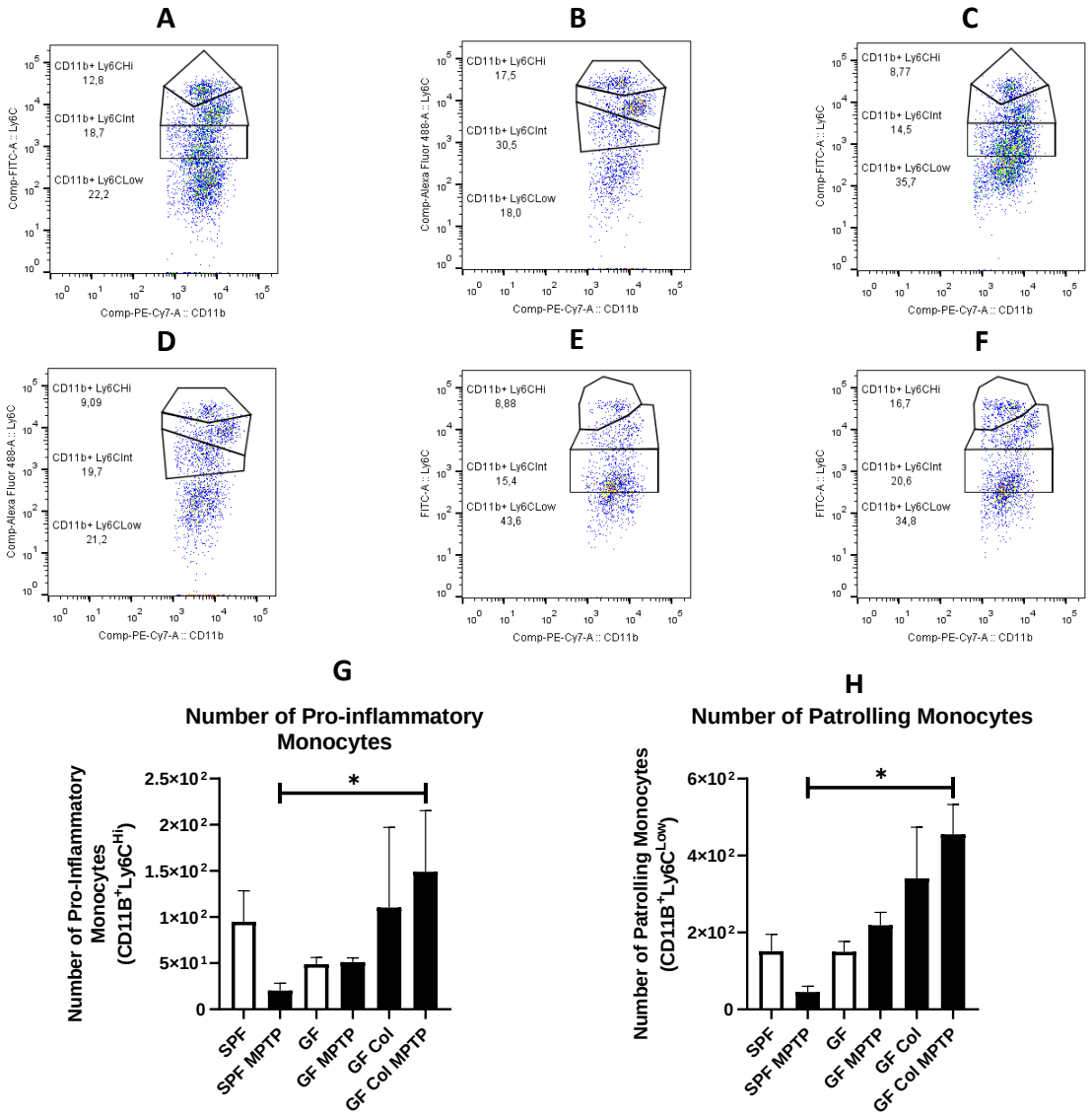

Figure 35 Fluorescence activated cell sorting analysis of myeloid immune cells in the brain. Mice were kept in GF conditions, colonized and treated with MPTP. Flow cytometry was used to study cells of the immune system in the brain of our animal models. Gating strategy for isolation of monocytic subsets from **(A)** SPF (control) and **(B)** SPF-MPTP; **(C)** GF, **(D)** GF-MPTP mice **(E)** GF-Col and **(F)** GF-Col-MPTP. Histograms represent the number of cells obtained for each population: **(G)** Pro-inflammatory monocytes, **(H)** Patrolling monocytes. Significant changes were observed between the SPF-MPTP and GF-Col-MPTP mice. Mean values of 2 to 4 mice for each animal group. Error bars indicate standard deviation, while the asterisk refers to a statistically significant difference. *p<0.05; **p<0.01.

By analyzing **Figure 35** we can observe that, once again, both cell types are drastically increased in GF colonized MPTP-treated mice. Moreover, this increase seems to follow a tendency throughout the GF models, despite not statistically significant. For both cell types, when comparing these models with the SPF-MPTP animals (**Figure 35 G and H**), significant data were obtained. However, due to the low number of cells collected in this model (SPF-MPTP), further experiments would need to be conducted to assess their reproducibility.

Afterwards, we proceeded to attain the values for the number of recruited cells for both monocytic subsets. The results are depicted in **Figure 36**.

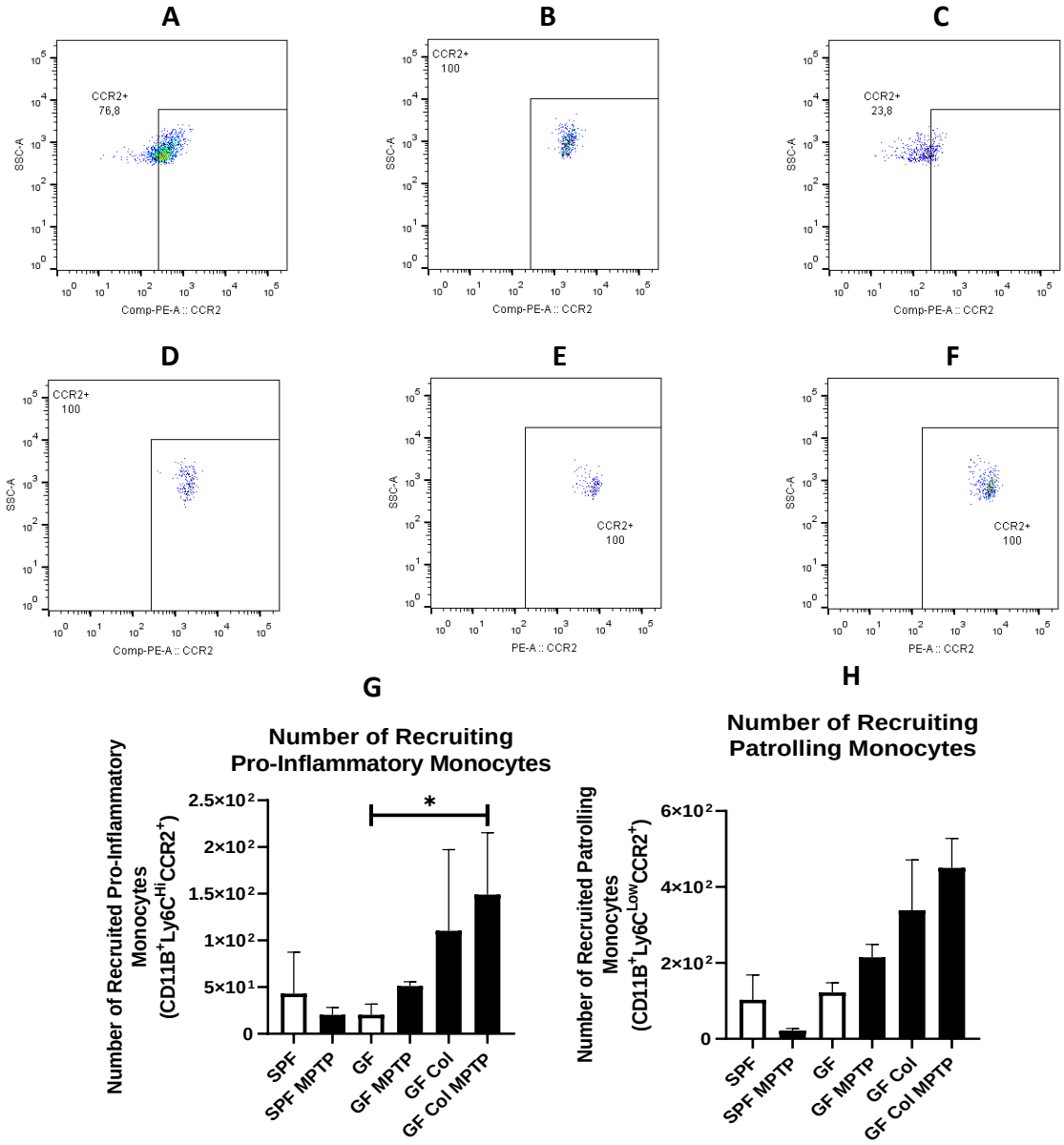

Figure 36 Fluorescence activated cell sorting analysis of myeloid immune cells in the brain. Mice were kept in GF conditions, colonized and treated with MPTP. Flow cytometry was used to study cells of the immune system in the brain of our animal models. Gating strategy for isolation of monocyte subsets from **(A)** SPF (control), **(B)** SPF-MPTP **(C)** GF, **(D)** GF-MPTP mice **(E)** GF-Col and **(F)** GF-Col-MPTP. Histograms represent the number of cells obtained for each population: **(G)** Recruiting pro-inflammatory monocytes, **(H)** Recruiting patrolling monocytes. Significant changes were observed between the GF and GF-Col-MPTP mice. Mean values of 2 to 4 mice for each animal group. Error bars indicate standard deviation, while the asterisk refers to a statistically significant difference. *p<0.05; **p<0.01.

By analyzing these results, we can clearly see that these populations present the same tendency. The results are similar to those illustrated in **Figure 35,** as both monocytic subsets significantly increased in the GF colonized MPTP-treated models, when compared with the GF non-modulated animals (**Figure 36 G** and **H**). Our gnotobiotic animal models also recapitulated the results obtained for patrolling monocytes

populations, as these were also increased when compared to the SPF mice. Moreover, it is worth mentioning that by looking at the percentages of recruited cells, these suggest that inflammation increased in these animals, as all analyzed monocytes were recruited from the periphery (with percentages close to 100%).

Having characterized the myeloid compartment, and showing an increased neuroinflammation , we then started to assess the lymphoid subsets.

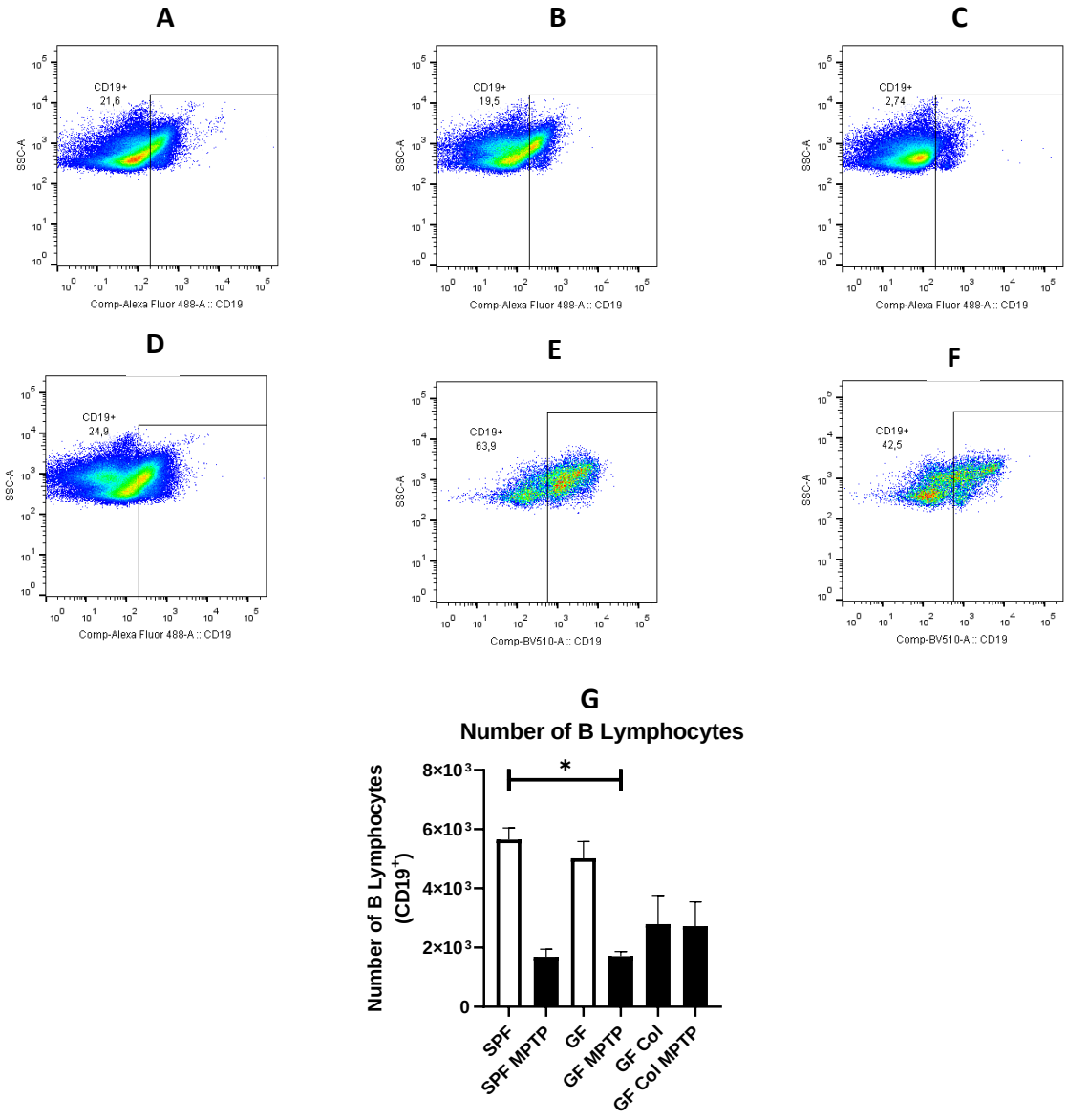

Figure 37 Fluorescence activated cell sorting analysis of lymphoid immune cells in the brain. Mice were kept in GF conditions, colonized and treated with MPTP. Flow cytometry was used to study cells of the immune system in the brain of our animal models. Gating strategy for isolation of B lymphocytes from **(A)** SPF (control), **(B)** SPF-MPTP **(C)** GF, **(D)** GF-MPTP mice **(E)** GF-CoI and **(F)** GF-CoI-MPTP. Histograms represent the number of cells obtained for each population: **(G)** B lymphocytes. Significant changes were observed between the SPF and GF-MPTP mice. Mean values of 2 to 4 mice for each animal group. Error bars indicate standard deviation, while the asterisk refers to a statistically significant difference. *p<0.05; **p<0.01.

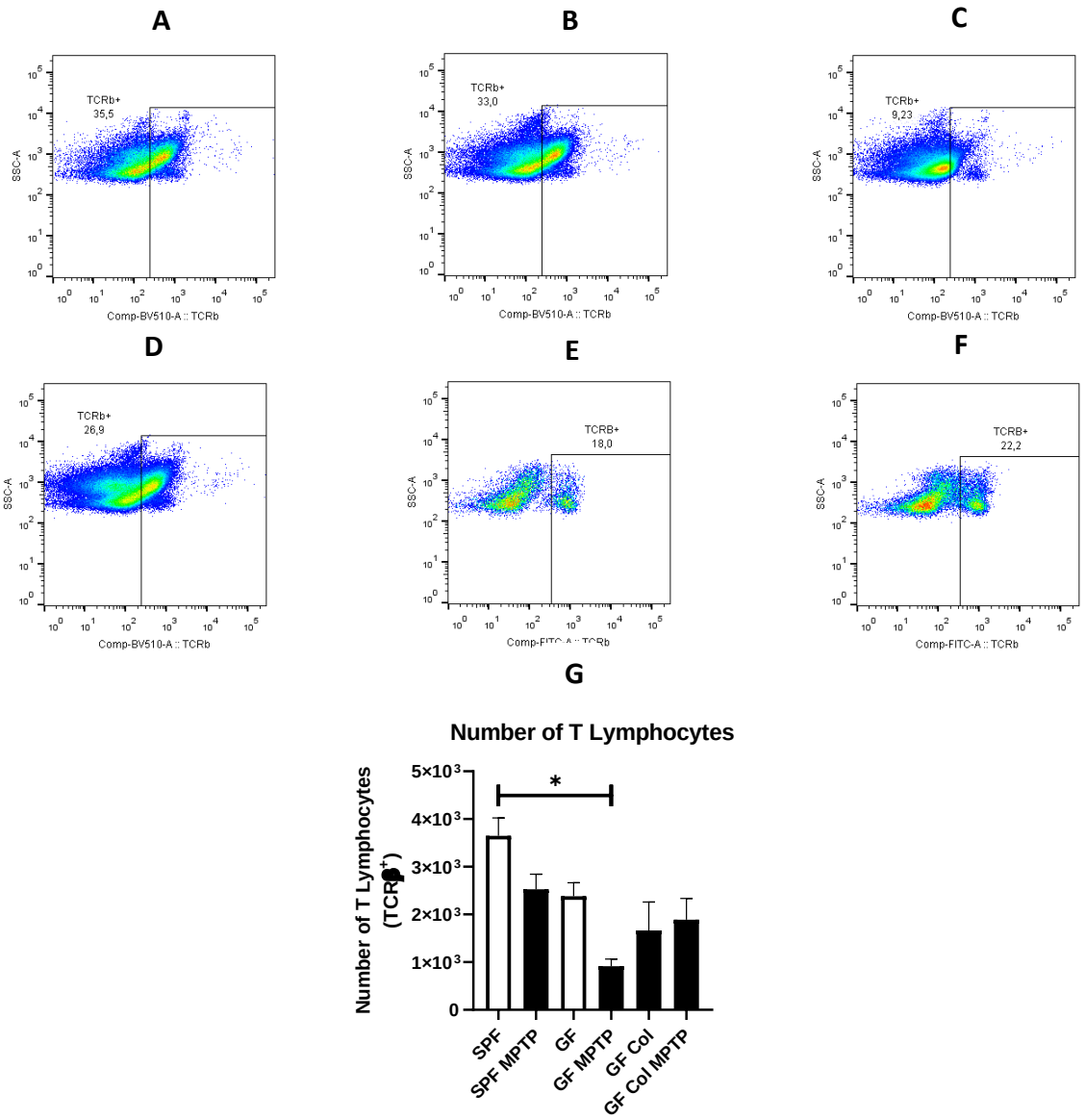

Figure 38 Fluorescence activated cell sorting analysis of lymphoid immune cells in the brain. Mice were kept in GF conditions, colonized and treated with MPTP. Flow cytometry was used to study cells of the immune system in the brain of our animal models. Gating strategy for isolation of T lymphocytes from **(A)** SPF (control), **(B)** SPF-MPTP **(C)** GF, **(D)** GF-MPTP mice **(E)** GF-Col and **(F)** GF-Col-MPTP. Histograms represent the number of cells obtained for each population: **(G)** B lymphocytes. Significant changes were observed between the SPF and GF-MPTP mice. Mean values of 2 to 4 mice for each animal group. Error bars indicate standard deviation, while the asterisk refers to a statistically significant difference. *p<0.05; **p<0.01.

Figures 37 and 38 show the distribution of B and T cells, respectively. No significant differences are observed between the conditions tested, since both GF conditions presented similar numbers of cells. However, objective of this experience was also to examine the role that the gut microbiota may play in colonized mice and their colonized MPTP challenged counterparts, which revealed no significant difference (**Figure 37 G and 38 G**).

Next, we assessed whether these results were maintained also with regards to different T cell subsets and their activation.

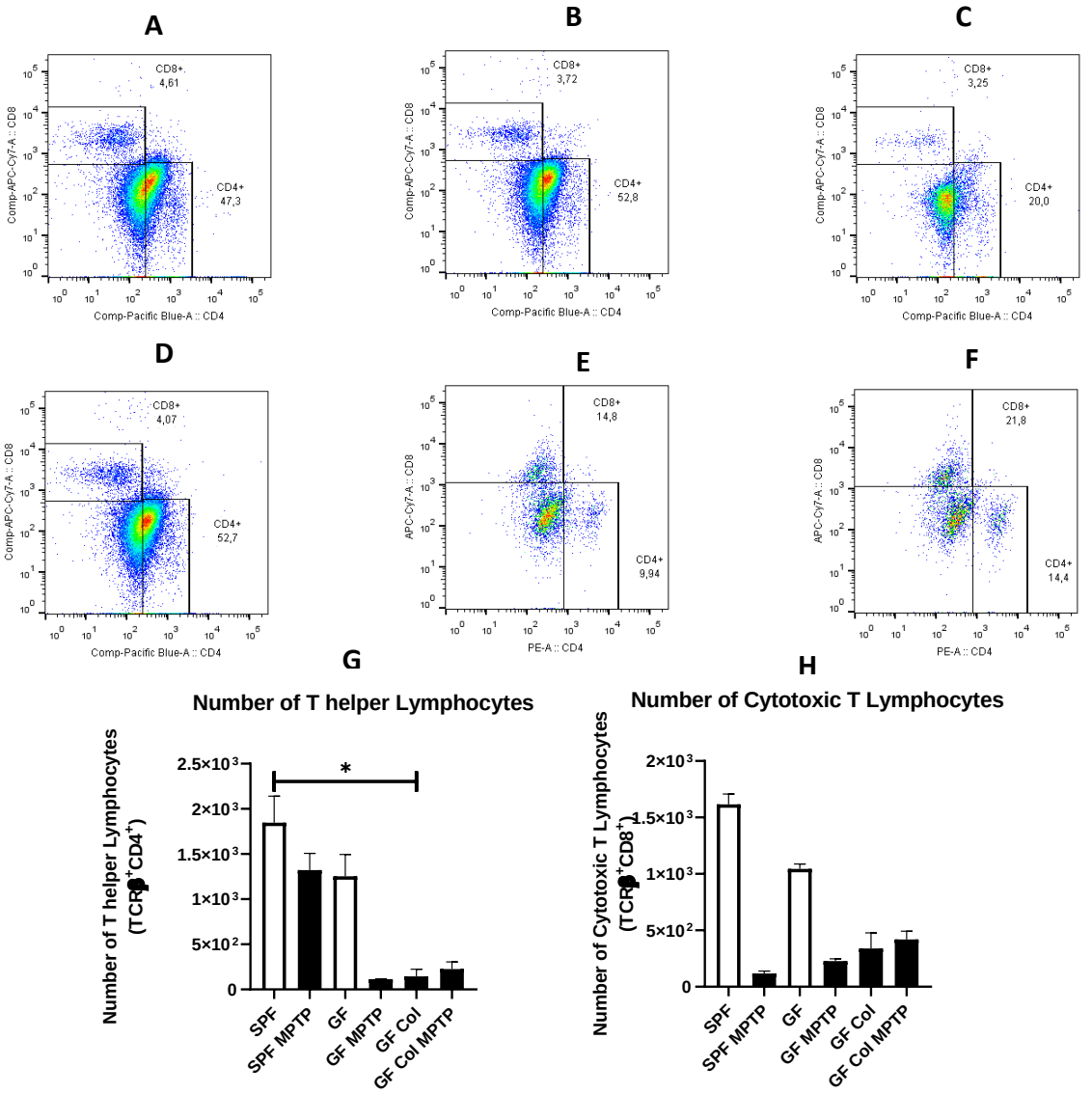

Figure 39 Fluorescence activated cell sorting analysis of lymphoid immune cells in the brain. Mice were kept in GF conditions, colonized and treated with MPTP. Flow cytometry was used to study cells of the immune system in the brain of our animal models. Gating strategy for isolation of Th lymphocytes or CTLs from **(A)** SPF (control), **(B)** SPF-MPTP **(C)** GF, **(D)** GF-MPTP mice **(E)** GF-Col and **(F)** GF-Col-MPTP. Histograms represent the number of cells obtained for each population: **(G)** Th lymphocytes, (**H**) CTLs. Significant changes were observed between the SPF and GF-Col mice. Mean values of 2 to 4 mice for each animal group. Error bars indicate standard deviation, while the asterisk refers to a statistically significant difference. *p<0.05; **p<0.01.

Figure 39 shows that the results obtained, when T cell subsets were analyzed. Once again, no major difference was observed between tested conditions. Although statistical significance is found between GF control and the GF-Col mice (**Figure 39 G**) for the Th cells, no difference was shown between GF colonized mice and GF colonized, MPTP treated animals. CTL levels remained low and similar between conditions (**Figure 39 H**). Hence, we then assessed the activation status of our different populations.

Figures 40, 41 and 42 depict the outcomes obtained when evaluating the activation status of the different lymphoid populations analyzed.

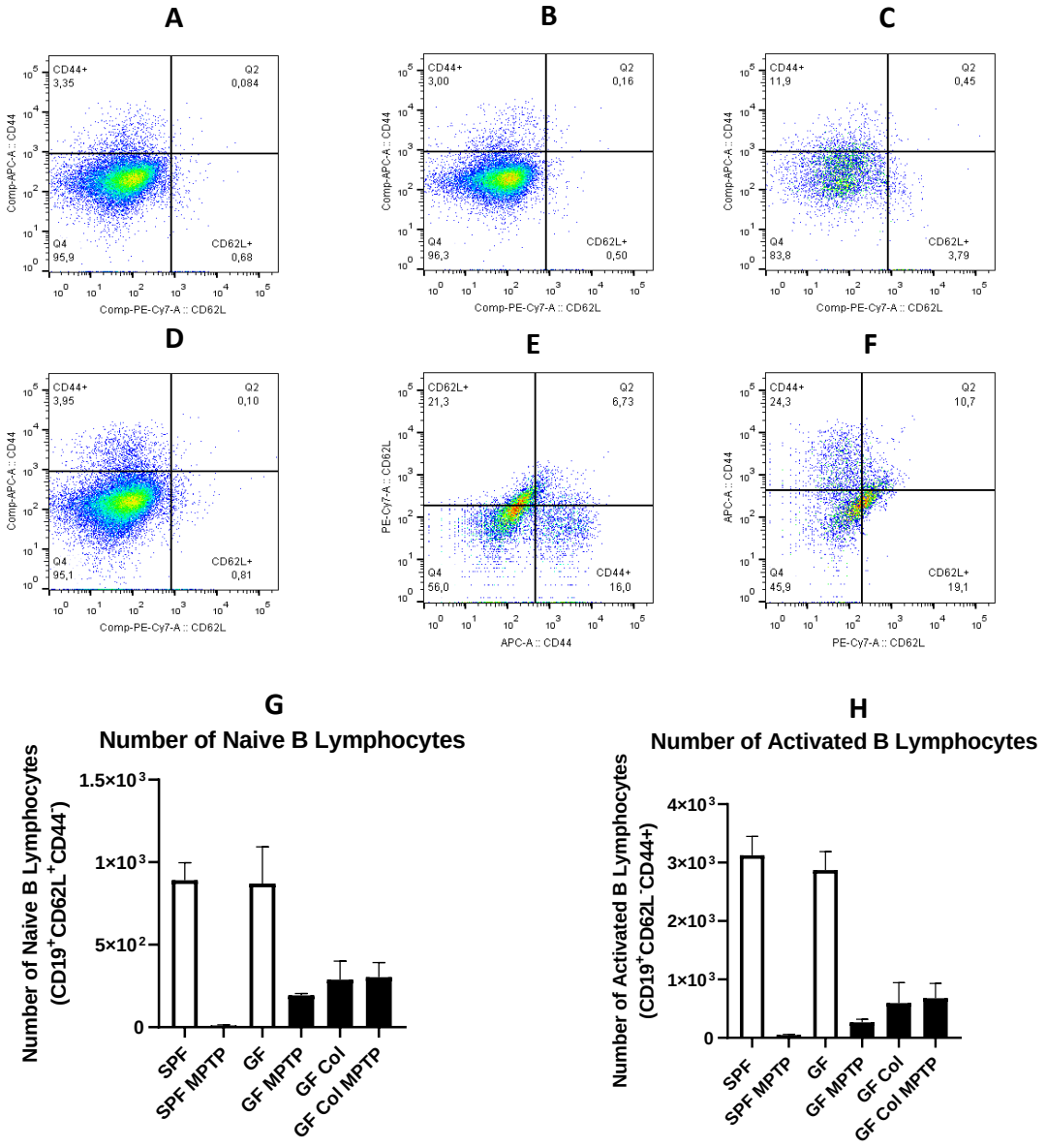

Figure 40 Fluorescence activated cell sorting analysis of lymphoid immune cells in the brain. Mice were kept in GF conditions, then colonized and treated with MPTP. Flow cytometry was used to study cells of the immune system in the brain of our animal models. Gating strategy for isolation of naïve or activated B lymphocytes from **(A)** SPF (control), **(B)** SPF-MPTP **(C)** GF, **(D)** GF-MPTP mice **(E)** GF-Col and **(F)** GF-Col-MPTP. Histograms represent the number of cells obtained for each population: **(G)** Naïve B lymphocytes, (**H**) Activated B lymphocytes. No significant changes were observed between conditions tested. Mean values of 2 to 4 mice for each animal group. Error bars indicate standard deviation, while the asterisk refers to a statistically significant difference. *p<0.05; **p<0.01.

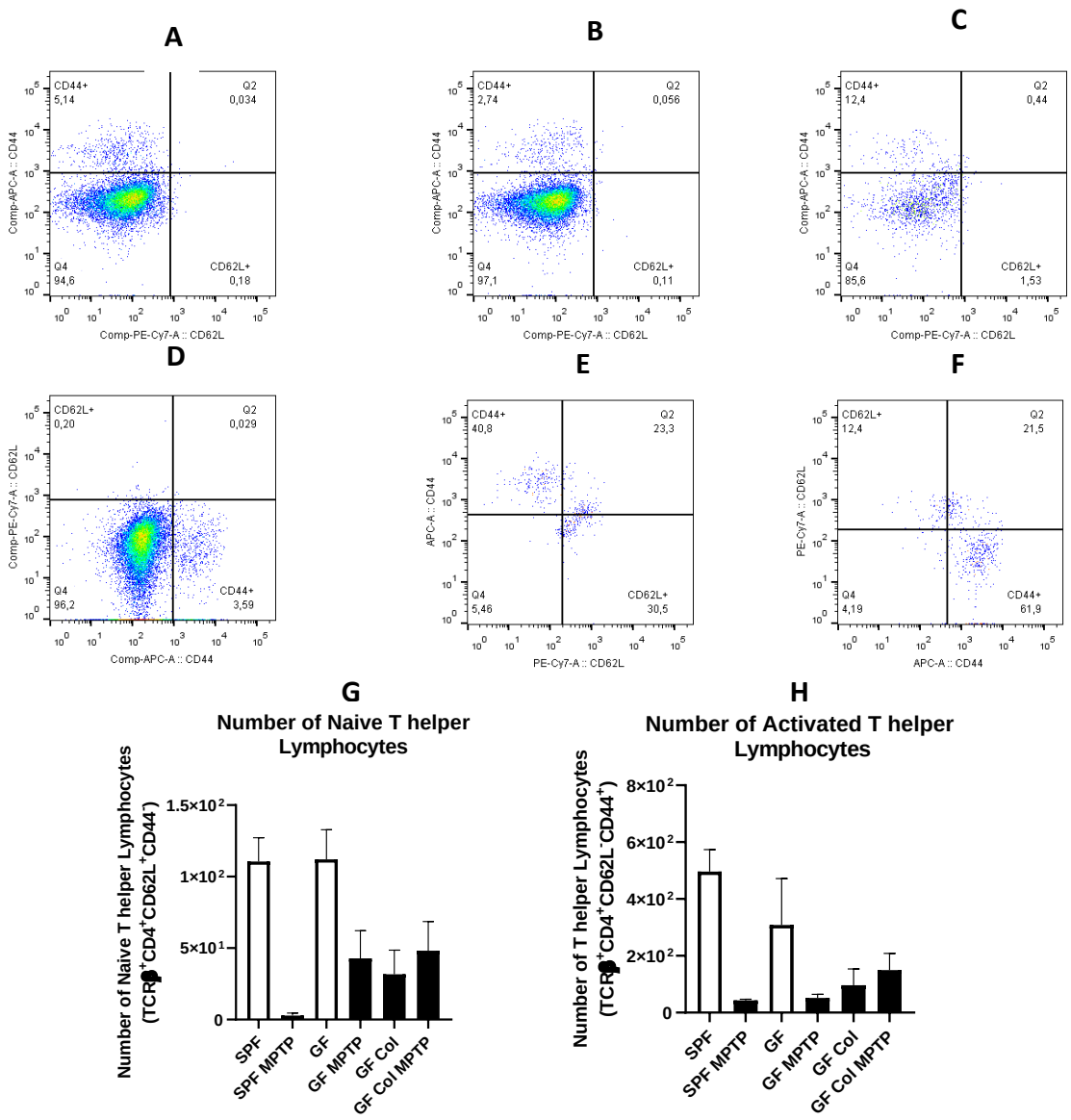

Figure 41 Fluorescence activated cell sorting analysis of lymphoid immune cells in the brain. Mice were kept in GF conditions, then colonized and treated with MPTP. Flow cytometry was used to study cells of the immune system in the brain of our animal models. Gating strategy for isolation of naïve or activated Th lymphocytes from **(A)** SPF (control), **(B)** SPF-MPTP **(C)** GF, **(D)** GF-MPTP mice **(E)** GF-Col and **(F)** GF-Col-MPTP. Histograms represent the number of cells obtained for each population: **(G)** Naïve Th lymphocytes, (**H**) Activated Th lymphocytes. No significant changes were observed between conditions tested. Mean values of 2 to 4 mice for each animal group. Error bars indicate standard deviation, while the asterisk refers to a statistically significant difference. *p<0.05; **p<0.01.

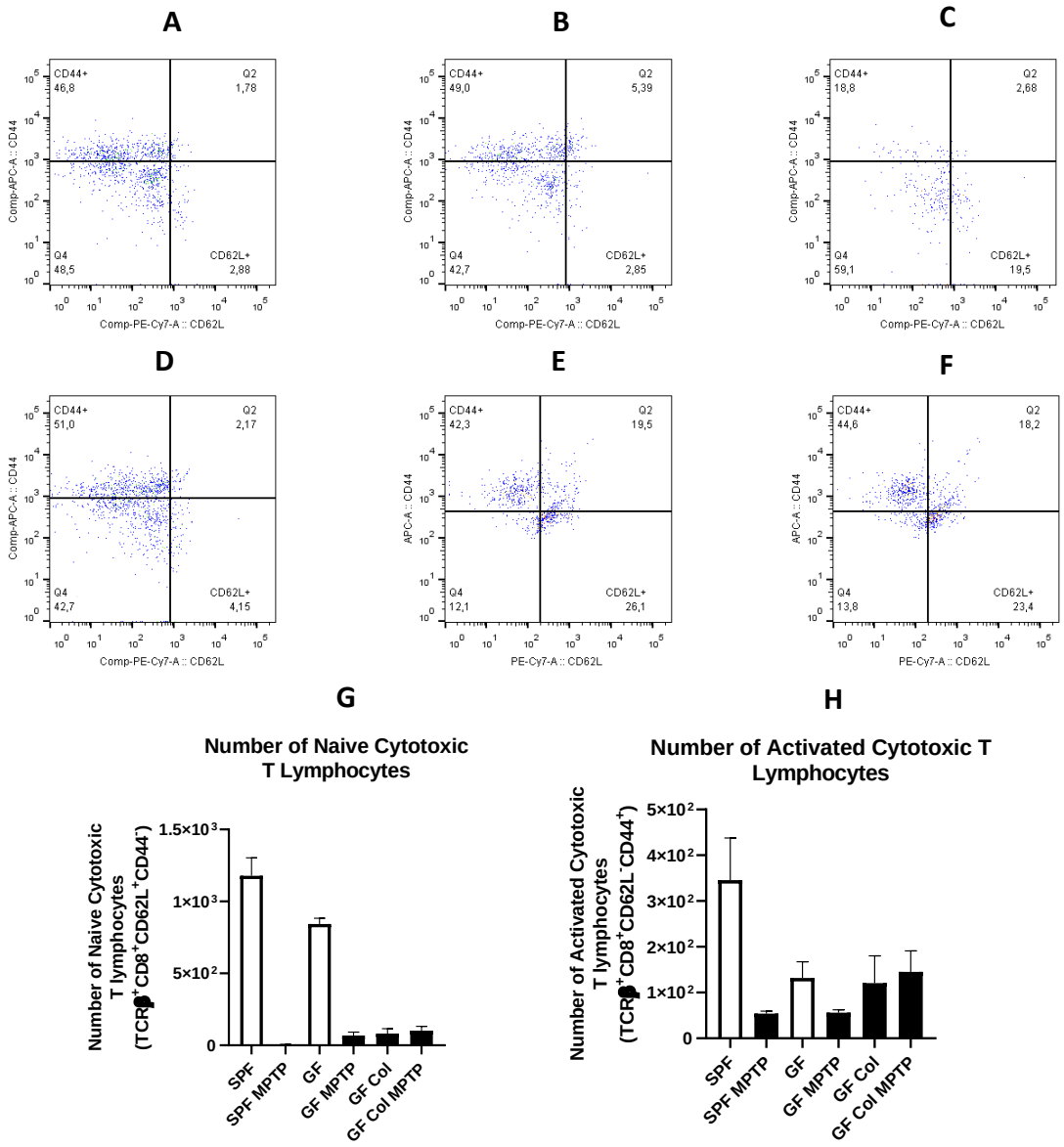

Figure 42 Fluorescence activated cell sorting analysis of lymphoid immune cells in the brain. Mice were kept in GF conditions, then colonized and treated with MPTP. Flow cytometry was used to study cells of the immune system in the brain of our animal models. Gating strategy for isolation of naïve or activated CTLs from **(A)** SPF (control), **(B)** SPF-MPTP **(C)** GF, **(D)** GF-MPTP mice **(E)** GF-Col and **(F)** GF-Col-MPTP. Histograms represent the number of cells obtained for each population: **(G)** Naïve CTLs, (**H**) Activated CTLs. No significant changes were observed between conditions tested. Mean values of 2 to 4 mice for each animal group. Error bars indicate standard deviation, while the asterisk refers to a statistically significant difference. *p<0.05; **p<0.01.

In all results, no major changes were observed. Although several results show us a significant difference between the controls and certain conditions, it is statistically incongruent (**Figure 40/41/42 G** and **H**). This was not shown in the experimental groups of interest, namely, the GF colonized mice and their MPTP challenged counterpart. Furthermore, we can also observe that in these conditions, lymphocyte cell numbers seem to remain quite similar, showing no increase or decrease even upon neuronal insult.

However, the results from the myeloid lineage followed the opposite tendency. We payed particular interest to the results referring to microglia (**Figure 34**) and pro-inflammatory monocytes (**Figure 35**). Moreover, in many experiments, statistical significance was not achieved and this was possibly due to the limited number of animals. Yet, the statistical significance obtained in some cell populations, as microglia (**Figure 34 G**), could underlie the phenotypic changes observed when mice develop motor dysfunction (**Figure 33**). Thus, colonization with gut microbiota collected from older animals increases PD susceptibility.

Brain Iron Accumulation

As previously mentioned, Fe metabolism needs to be strictly controlled in the brain. In this organ, this metal can be involved both in neurotransmission and neurodegeneration, highlighting its dual role as both necessary and dangerous. It is known that Fe accumulates in the brain with aging, and even more so in the brains of PD patients [91], [92]. This can be particularly troublesome, as Fe may be needed for dopamine (DA) synthesis, but it can be toxic when reacting with the metabolites from DA metabolism [93]. As such, our aim was to assess the accumulation of brain iron occurring with aging in these animals.

As mentioned in the Methodology session, along with the M and T mixes, the levels of intracellular Fe were measured through calcein quenching.

This set of experiments implied using a mix that did not allow to discriminate among different populations. Still, we succeeded in assessing the accumulation of iron in microglia ($CD45^{Int}$), peripheral leukocytes ($CD45^{Hi}$), T lymphocytes ($TCR\beta^{+}$), T helper cells ($CD4^{+}$) and B lymphocytes ($CD19^{+}$). Due to time constraints and especially because COVID-19 pandemic, we were not able to perform further experiments. Yet results regarding brain Fe accumulation with aging and intracellular Fe accumulation will be depicted, as follows, given previous work carried out in the laboratory.

The results obtained regarding intracellular Fe accumulation are shown in **Figure 43**.

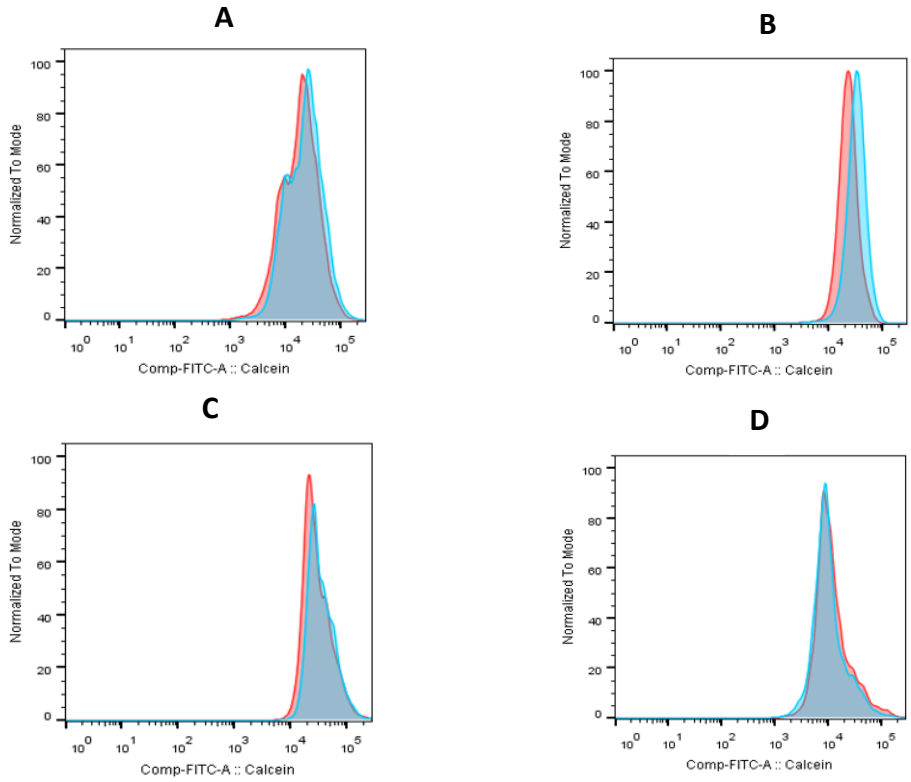

Figure 43 Calcein Quenching. Intracellular Fe levels were evaluated through through calcein quenching. Red curves are relative to the SPF mice, while the blue correspond to the GF. **(A)** $CD45^{Hi}$ **(B)** $CD45^{Int}$ **(C)** $CD19^{+}$ **(D)** $TCR\beta^{+}$.

In this figure we can observe that it is likely that Fe accumulates more in SPF than GF mice, as it could be observed by the shift of the distribution curve to the left. These results are further corroborated by **Figure 44**, where we can clearly see that the GF mouse model accumulates less Fe in the brain with advancing age, when compared to its SPF counterpart, as measured by colleagues in the laboratory.

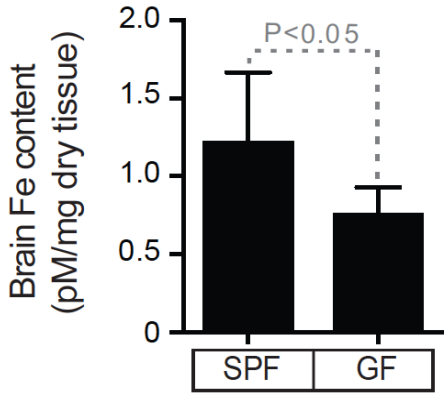

Figure 44 Brain Fe accumulation. Total brain Fe content. SPF vs GF.

DISCUSSION

GF or axenic is a term used for animal models that grow in the absence of microorganisms and therefore all tissues are preserved from pathogens-host interactions, throughout their life. These animals must be housed under special conditions (in isolators) and in recent years have been primarily used in studies related with the role of the gut microbiota. Both models (SPF and GF) have their advantages and disadvantages, however, the most compelling evidence linking the gut microbiota with human health has come from GF studies [94]–[96].

As such, in our first set of experiments we sought to characterize the aged neuroinflammatory profile of GF animals, in order to pre-establish a baseline to which we could compare subsequent results.

GF animals have been described as having a broadly impaired development in several different compartments, although reports are not consistent. For instance, in the gut, the microbiota is responsible for driving specific differentiation of a subset of T lymphocytes [97], while, at the same time, it promotes epithelial integrity through an immune-glial crosstalk [98]. Moreover, their antimicrobial peptide production in the intestine is also reduced [94]. Despite that, the absence of gut microbiota has been shown to have a profound impact on several organismal systems. Indeed, GF mice show a decreased number of myeloid cells, which provoke a reduced immune response [94], possibly due to a decreased ability to induce cytokine/chemokine signaling [99].

Furthermore, the interactions between the microbiota and microglia have been becoming increasingly important [100]. Altered cellular proportions and a generalized hampered microglial immune response has been reported in GF mice [101]. It was even shown that colonization of GF animals with a reduced microbiota is not sufficient to restore proper morphology [101] and immune response, pointing to a causal link between gut microbiota diversity and proper CNS function. When regarding their CNS, axenic animal models show, also demonstrate other defects, such as reduced levels of 5-HT (serotonin) [101].

In our experiments, we could indeed observe a decrease in microglia levels when comparing GF and SPF animals, probably due to lack of important signaling molecules, such as butyrate. Moreover, when analyzing peripheric immune cells not only did their numbers decrease as well, but also their activation, as we could see a decrease in activated cytotoxic T cells. The outcome obtained was in accordance with the literature, as microbiota is known to be able to communicate with both the host microglia and peripheral immune cells [101] [102].

As previously mentioned, the brain is not the only organ affected throughout the course of PD pathogenesis. Comorbid GI symptoms often occur in parallel with neurodegeneration, with constipation even being associated with ENS neurodegeneration [103]. Moreover, gut dysbiosis has been observed in PD patients, as a direct correlation between *Enterobacteriaceae* abundance and severity of postural instability and gait difficulty was established [39].

As such, we also set out to evaluate if the gut microflora could be related to the susceptibility to develop behavioral alterations such as motor dysfunction. Surprisingly, MPTP treatment did not induce them in the GF animal model, raising the possibility that somehow MPTP induction may be connected, or at least exacerbated, by the presence of the gut microbiota. On the other hand, since these animals have underperforming microglia, these cells could simply be incapable of sustaining a chronic neuroinflammation, not developing the disease. Taken together with the fact that BBB permeability is decreased due to lack of bacterial metabolites, such as SCFA, this observed neuroprotective effect could in fact just be a side effect of unproper differentiation, maturation and activation of these cells [104] [105].

With this in mind, using the aged neuroinflammatory profile as a baseline value, we sought to further evaluate the role that the microbiota could play in dysfunction susceptibility. As such, fecal microbiota transplantation was used (as described in the methodology) in order to colonize GF animals with the microbiota of their SPF counterparts. With this new procedure, we could treat them with MPTP and observed if animals developed behavioral deficits.

The results obtained were not expected, as we could clearly distinguish between the effects of colonization with gut microbiota, or not. Keeping in accordance with preliminary data presented, we also observed that mice colonized with their old counterparts microbiota increased the animals motor dysfunction, suggesting a possible increase to disease susceptibility, although further histological and biochemical techniques are required. In these animals, the levels of circulating innate immune cells, namely pro-inflammatory monocytes, drastically increased in their brains, fostering a neuroinflammatory cycle that translated in the development of some behavioral deficits, upon MPTP induction.

Since saccharolytic bacterial strains are the main producers of SCFA's in the gut and, remembering that the aging process promotes a decreased microbe variability, these results suggest that the changes observed in the susceptibility to develop motor symptoms can be mainly attributed to this factor [31]. The mechanism through which this molecule may exert its effect is still questionable though.

With all of the previous results in mind, we wanted to analyze one more piece of this complex puzzle, the role of Fe availability. As previously mentioned, Fe metabolism needs to be strictly controlled in the brain. It is known that Fe accumulates in the brain with aging, and even more so in the brains of PD patients [91], [92].

As such, our last set of experiments aimed at looking at the accumulation of Fe in the brain with aging. However, our hypothesis points to the fact that changing the Fe content available to the gut microbiota is sufficient to ameliorate motor symptoms. Therefore, in the last set of experiments, mice were going to be orally treated with deferiprone in order to diminish the Fe content in their gut. However, due to time limitations, this experience was not possible to realize, although a very small cohort of Fe accumulation results points to the fact that this hypothesis may be correct.

It is also worth mentioning that despite the great clinical results achieved with deferiprone, an antioxidant supplementation should also be considered due to the crucial role oxidative stress plays in PD pathogenesis [12]. Furthermore, when looking at Fe levels in the previous set of experiments, two major findings were observed: i) GF mice have a decreased brain Fe deposition with aging, and ii) colonization with old microbiota increases Fe accumulation in the peripheral leukocytic populations. These observations are in accordance with what is described in the literature as increased levels of iron are capable of inducing bacterial pathogenicity and inflammation, specifically, gut inflammation [81].

Since the discovery of the microbiome, and how it can affect and crosstalk with several systems in our body, particularly the immune and neuronal systems, certain diseases of the CNS have been looked at under a new light [106]. Although the dysbiosis of the gut flora in such diseases has been well established [107]–[109], the fact is that we are still not sure about it being a trigger, a consequence, or a contributing factor. Indeed, GF colonization with PD-patient derived fecal samples exacerbates motor dysfunction in a mouse model of the disease but there is a need for a cautious extrapolation of pre-clinical findings [45].

Nevertheless, by the time motor symptoms are observable in humans, the disease is usually in an advanced state, making the need for early disease biomarkers or therapies ever more pressing. With this in mind, GI non-motor symptoms have emerged has the greatest candidate for both early disease diagnosis, and a possible disease-modifying target, as the link between these symptoms, PD and a dysbiotic microbiota becomes more and more evident [39], [103], [110].

In fact, in recent years, it has been postulated that the trigger for this disease does not occur in the CNS but rather in the gut lumen and the ENS [111] . This hypothesis defends that an increase in pathogenic bacteria in the gut promotes chronic gut inflammation,

and, as such, increases intestinal permeability. This increased permeability, leads to the extraversion of several bacterial metabolites to the luminal surface of the ENS, activating PPR's (pattern recognition receptors) such as the TLR's, involved in recognizing pathogenic bacteria and mounting a pro-inflammatory response. As such, this chronic inflammatory signal that has now reached the ENS will propagate at a systemic level and affect CNS inflammatory responses. Some authors even propose that α-synuclein aggregation begins in the nerve cells of the ENS due to this chronic insult, and then propagates in a prion-like manner via the vagus nerve, to the CNS. Some evidence can be found that is in check with this hypothesis, as for instance, people with a truncated vagus nerve seem to have a lower probability of developing PD. However, they may still develop the disease in latter stages of life, showing the complexity of this pathological condition [112].

We also need to mention the fact that increases in pathogenic bacteria in the gut with increasing age, will also result in a decrease in anti-inflammatory producing bacterial strains [31] . As such, the permeability of the BBB also becomes compromised due to this dysbiosis in the GI resident microflora. This in turn may further promote neuroinflammation, as circulating pro-inflammatory molecules and immune cells may cross into the brain and foster a positive-feedback loop of microglia activation [113]. Our last set of experiments corroborates this hypothesis, as colonized GF mice, although it not being statistically significant, seemed to show an increase in the numbers of pro-inflammatory cells.

Additionally, it is important to remember that Fe accumulation in the brain will add even more detrimental effects than the ones that may be a result of gut dysbiosis. In fact, and as it was previously mentioned, immune cells tend to accumulate excess Fe, in order to maintain homeostasis [57]. As such, Fe levels in the brain will become extremely high throughout the course of PD as not only microglia, but also infiltrating immune cells will be saturated with this metal.

With this in mind, the role that ferroptosis may play in PD progression needs to be better understood. This is an autonomous, non-apoptotic type of cell death that still needs further explanation when regarding its molecular mechanisms [114]. However, its dependence on Fe and oxidative stress is well established [115] [116]. Accumulation of ROS along with lipid peroxidation shows that the mitochondria are also deeply affected by this process [60] [117] and although this process is yet to be observable *in vivo,* the role that it might play in this disease has recently been reviewed by our lab [118].

To conclude, and summing up all of the information previously mentioned, we can strongly postulate that the aims of this thesis were achieved.

First and foremost, we present exploratory data that characterizes the different immune cell populations that increase in the brain of GF animals with normal aging. Then by transplanting the fecal microbiota of SPF animals, we could analyze the changes that gut colonization would promote in animals devoid of any microbial life. Moreover, we were able to identify the difference in immune cells between colonized and non-colonized mice, particularly, the microbiota of old animals was able to increase the susceptibility of GF animals to develop motor dysfunction.

Finally, with this work we wanted to provide a safe and secure basis that modulating Fe levels in the periphery of these animals, would be enough to decrease their colonization-induced motor deficits. Unfortunately, this part of the work could not be done due to time limitations, and a particular difficult year. In the future, the role that deferiprone, or other Fe chelator, may play in modulating the observed effects needs to be assessed. Yet, this work provided a strong basis from which several other works can build upon, not being able to provide a proof of concept, but establishing a groundwork for future studies.

CONCLUDING REMARKS

In this work, a comprehensive description of the interplay between aging, microbiota, and iron metabolism was reported. Understanding the molecular basis of this complex cross-talk might unravel the role that each play in health and disease, and the association that could exist between each other. Iron is of vital importance for life. However its accumulation in tissues favors an inflammatory state that is capable to modulate the composition of gut microbiota and exacerbates mitochondrial dysfunction, which results in oxidative damage and neuronal death.

This project provided new insights into the role of the gut microbiota, and how it may modulate PD susceptibility. The results obtained demonstrated that not only are GF mice resistant to MPTP induction, but also that that phenotype could be abrogated through fecal microbiota transplantation from an old donor, linking once again, aging, neurodegeneration and the intestinal microbiota

Future research to reveal the molecular mechanisms clarifying how Fe accumulates in the brain and affect all phenomena described herein will be of particular interest to the scientific community, due to the positive results of Fe chelation therapy clinically. The development of techniques to better characterize the changes occurring in the composition of gut microbiota could most certainly be used as early diagnostic tool, against PD progression, or even as a potential future biomarker.

REFERENCES

[1] World Health Organization (WHO), "WHO statistics overview 2019," *World Health Organization*, vol. 8, no. 5, pp. 1–9, 2019.

[2] "PORDATA - Esperança de vida à nascença: total e por sexo." [Online]. Available: https://www.pordata.pt/Europa/Esperança+de+vida+à+nascença+total+e+por+sexo-1260. [Accessed: 26-Oct-2020].

[3] R. Suzman and J. Beard, "Preface Overview Humanity's Aging Living Longer New Disease Patterns Longer Lives and Disability New Data on Aging and Health Assessing the Cost of Aging and Health Care Changing Role of the Family Suggested Resources," 2011.

[4] X. Shi, *Physiological Basis of Aging and Geriatrics*, vol. 28, no. 7. 1996.

[5] G. De Winter, "Aging as Disease," *Med. Heal. Care Philos.*, vol. 18, no. 2, pp. 237–243, 2015.

[6] D. Harman, "Aging: a theory on free radical radiation chemistry," *J. Gerontol.*, vol. 11, pp. 298–300, 1956.

[7] B. T. Weinert and P. S. Timiras, "Invited Review: Theories of aging," *J. Appl. Physiol.*, vol. 95, no. 4, pp. 1706–1716, 2003.

[8] C. López-Otín, M. A. Blasco, L. Partridge, M. Serrano, and G. Kroemer, "The hallmarks of aging," *Cell*, vol. 153, no. 6, p. 1194, 2013.

[9] C. Franceschi and J. Campisi, "Chronic inflammation (Inflammaging) and its potential contribution to age-associated diseases," *Journals Gerontol. - Ser. A Biol. Sci. Med. Sci.*, vol. 69, pp. S4–S9, 2014.

[10] A. Salminen, K. Kaarniranta, and A. Kauppinen, "Inflammaging: Disturbed interplay between autophagy and inflammasomes," *Aging (Albany. NY).*, vol. 4, no. 3, pp. 166–175, 2012.

[11] D. Twelves, K. S. M. Perkins, and C. Counsell, "Systematic review of incidence studies of Parkinson's disease," *Mov. Disord.*, vol. 18, no. 1, pp. 19–31, 2003.

[12] A. Navarro and A. Boveris, "Brain mitochondrial dysfunction in aging, neurodegeneration, and Parkinson's disease," *Front. Aging Neurosci.*, vol. 2, no. SEP, pp. 1–11, 2010.

[13] A. H. Schapira, "Mitochondria in the aetiology and pathogenesis of Parkinson's disease," *Lancet Neurol.*, vol. 7, no. 1, pp. 97–109, 2008.

[14] H.-M. Gao, P. T. Kotzbauer, K. Uryu, S. Leight, J. Q. Trojanowski, and V. M.-Y. Lee, "Neuroinflammation and Oxidation/Nitration of -Synuclein Linked to Dopaminergic Neurodegeneration," *J. Neurosci.*, vol. 28, no. 30, pp. 7687–7698, 2008.

[15] E. C. Hirsch and S. Hunot, "Neuroinflammation in Parkinson's disease: a target for neuroprotection?," *Lancet Neurol.*, vol. 8, no. 4, pp. 382–397, 2009.

[16] Richard M. Ransohoff, "How neuroinflammation contributes to neurodegeneration," *Science (80-.).*, vol. 353, no. 6301, pp. 772–777, 2016.

[17] W. Poewe *et al.*, "Parkinson disease," *Nat. Rev. Dis. Prim.*, vol. 3, no. 1, p. 17013, Dec. 2017.

[18] M. C. Houser and M. G. Tansey, “The gut-brain axis: is intestinal inflammation a silent driver of Parkinson’s disease pathogenesis?,” *npj Park. Dis.*, vol. 3, no. 1, 2017.
[19] M. Lubomski, A. H. Tan, S. Y. Lim, A. J. Holmes, R. L. Davis, and C. M. Sue, “Parkinson’s disease and the gastrointestinal microbiome,” *J. Neurol.*, no. 0123456789, 2019.
[20] A. Heintz-Buschart *et al.*, “The nasal and gut microbiome in Parkinson’s disease and idiopathic rapid eye movement sleep behavior disorder,” *Mov. Disord.*, vol. 33, no. 1, pp. 88–98, 2018.
[21] K. L. Adams-Carr, J. P. Bestwick, S. Shribman, A. Lees, A. Schrag, and A. J. Noyce, “Constipation preceding Parkinson’s disease: A systematic review and meta-analysis,” *J. Neurol. Neurosurg. Psychiatry*, vol. 87, no. 7, pp. 710–716, 2016.
[22] A. E. Bharucha and W. A. Rocca, “Medical records documentation of constipation preceding Parkinson disease,” 2010.
[23] X. Gao, H. Chen, M. A. Schwarzschild, and A. Ascherio, “A prospective study of bowel movement frequency and risk of parkinson’s disease,” *Am. J. Epidemiol.*, vol. 174, no. 5, pp. 546–551, 2011.
[24] J. M. Rodríguez *et al.*, “The composition of the gut microbiota throughout life, with an emphasis on early life,” *Microb. Ecol. Heal. Dis.*, vol. 26, p. 26050, 2015.
[25] E. Thursby and N. Juge, “Introduction to the human gut microbiota,” *Biochem. J.*, vol. 474, no. 11, pp. 1823–1836, 2017.
[26] R. Corrêa-Oliveira, J. L. Fachi, A. Vieira, F. T. Sato, and M. A. R. Vinolo, “Regulation of immune cell function by short-chain fatty acids,” *Clin. Transl. Immunol.*, vol. 5, no. 4, pp. 1–8, 2016.
[27] P. Hugon, J. C. Dufour, P. Colson, P. E. Fournier, K. Sallah, and D. Raoult, “A comprehensive repertoire of prokaryotic species identified in human beings,” *Lancet Infect. Dis.*, vol. 15, no. 10, pp. 1211–1219, 2015.
[28] J. Li *et al.*, “An integrated catalog of reference genes in the human gut microbiome,” *Nat. Biotechnol.*, vol. 32, no. 8, pp. 834–841, 2014.
[29] M. J. Claesson *et al.*, “Composition, variability, and temporal stability of the intestinal microbiota of the elderly,” *Proc. Natl. Acad. Sci.*, vol. 108, no. Supplement_1, pp. 4586–4591, 2011.
[30] M. Lu and Z. Wang, “Linking gut microbiota to aging process: a new target for anti-aging,” *Food Sci. Hum. Wellness*, vol. 7, no. 2, pp. 111–119, 2018.
[31] P. B. Simone Rampelli , Marco Candela , Silvia Turroni , Elena Biagi , Sebastiano Collino , Claudio Franceschi , Paul W O’Toole *et al.*, “Functional metagenomic profiling of intestinal microbiome in extreme ageing,” *Aging (Albany. NY).*, vol. 5, no. 12, pp. 902–912, 2013.
[32] L. Desbonnet, L. Garrett, G. Clarke, J. Bienenstock, and T. G. Dinan, “The probiotic Bifidobacteria infantis: An assessment of potential antidepressant properties in the rat,” *J. Psychiatr. Res.*, vol. 43, no. 2, pp. 164–174, 2008.
[33] T. G. Dinan and J. F. Cryan, “Gut instincts: microbiota as a key regulator of brain development, ageing and neurodegeneration,” *J. Physiol.*, vol. 595, no. 2, pp. 489–503, 2017.
[34] F. Turco *et al.*, “Enteroglial-derived S100B protein integrates bacteria-induced Toll-like receptor signalling in human enteric glial cells,” *Gut*, vol. 63, no. 1, pp.

105–115, 2014.
[35] A. Barcelos Morais Da Silveira *et al.*, “Enteroglial cells act as antigen-presenting cells in chagasic megacolon,” *Hum. Pathol.*, vol. 42, no. 4, pp. 522–532, 2011.
[36] L. Seguella, R. Capuano, G. Sarnelli, and G. Esposito, *Play in advance against neurodegeneration: exploring enteric glial cells in gut-brain axis during neurodegenerative diseases*, vol. 12, no. 6. Taylor & Francis, 2019.
[37] A. Cattaneo *et al.*, “Association of brain amyloidosis with pro-inflammatory gut bacterial taxa and peripheral inflammation markers in cognitively impaired elderly,” *Neurobiol. Aging*, vol. 49, pp. 60–68, 2017.
[38] A. Keshavarzian *et al.*, “Colonic bacterial composition in Parkinson’s disease,” *Mov. Disord.*, vol. 30, no. 10, pp. 1351–1360, 2015.
[39] F. Scheperjans *et al.*, “Gut microbiota are related to Parkinson’s disease and clinical phenotype,” *Mov. Disord.*, vol. 30, no. 3, pp. 350–358, 2015.
[40] S. Ghaisas, J. Maher, and A. Kanthasamy, “Gut microbiome in health and disease: Linking the microbiome-gut-brain axis and environmental factors in the pathogenesis of systemic and neurodegenerative diseases,” *Pharmacol. Ther.*, vol. 158, pp. 52–62, 2016.
[41] H. Braak, U. Rüb, W. P. Gai, and K. Del Tredici, “Idiopathic Parkinson’s disease: Possible routes by which vulnerable neuronal types may be subject to neuroinvasion by an unknown pathogen,” *J. Neural Transm.*, vol. 110, no. 5, pp. 517–536, 2003.
[42] T. Clairembault *et al.*, “Structural alterations of the intestinal epithelial barrier in Parkinson’s disease,” *Acta Neuropathol. Commun.*, vol. 3, p. 12, 2015.
[43] A. Mulak and B. Bonaz, “Brain-gut-microbiota axis in Parkinson’s disease,” *World J. Gastroenterol.*, vol. 21, no. 37, pp. 10609–10620, 2015.
[44] E. M. M. Quigley, “Microbiota-Brain-Gut Axis and Neurodegenerative Diseases,” *Curr. Neurol. Neurosci. Rep.*, vol. 17, no. 12, 2017.
[45] T. R. Sampson *et al.*, “Gut Microbiota Regulate Motor Deficits and Neuroinflammation in a Model of Parkinson’s Disease,” *Cell*, vol. 167, no. 6, pp. 1469-1480.e12, 2016.
[46] H. J. H. Fenton, “Oxidation of tartartc acid in presence of iron,” 1894.
[47] A. C. Martins, J. I. Almeida, I. S. Lima, A. S. Kapitão, and R. Gozzelino, “Iron Metabolism and the Inflammatory Response,” *IUBMB Life*, vol. 69, no. 6, pp. 442–450, 2017.
[48] S. Recalcati, E. Gammella, P. Buratti, and G. Cairo, “Molecular regulation of cellular iron balance,” *IUBMB Life*, vol. 69, no. 6, pp. 389–398, 2017.
[49] A. T. McKie *et al.*, “An iron-regulated ferric reductase associated with the absorption of dietary iron,” *Science (80-.).*, vol. 291, no. 5509, pp. 1755–1759, 2001.
[50] S. R. Tenhunen R, Marver HS, “The enzymatic conversion of heme to bilirubin by microsomal heme oxygenase,” *Proc. Natl. Acad. Sci.*, vol. 61, pp. 748–755, 1968.
[51] H. Drakesmith, E. Nemeth, and T. Ganz, “Ironing out Ferroportin,” *Cell Metab.*, vol. 22, no. 5, pp. 777–787, 2015.
[52] D. J. R. Lane *et al.*, “Cellular iron uptake, trafficking and metabolism: Key molecules and mechanisms and their roles in disease,” *Biochim. Biophys. Acta - Mol. Cell Res.*, vol. 1853, no. 5, pp. 1130–1144, 2015.

[53] T. Ganz and E. Nemeth, “Hepcidin and iron homeostasis,” *Biochim. Biophys. Acta - Mol. Cell Res.*, vol. 1823, no. 9, pp. 1434–1443, 2012.
[54] M. Wessling-Resnick, “Iron Homeostasis and the Inflammatory Response,” *Annu. Rev. Nutr.*, vol. 30, no. 1, pp. 105–122, 2010.
[55] T. Ganz and E. Nemeth, “Iron homeostasis in host defence and inflammation,” *Nat. Rev. Immunol.*, vol. 15, no. 8, pp. 500–510, 2015.
[56] R. Gozzelino and P. Arosio, “Iron homeostasis in health and disease,” *Int. J. Mol. Sci.*, vol. 17, no. 1, pp. 2–14, 2016.
[57] I. Nnah and M. Wessling-Resnick, “Brain Iron Homeostasis: A Focus on Microglial Iron,” *Pharmaceuticals*, vol. 11, no. 4, p. 129, 2018.
[58] J. Hagemeier, J. J. G. Geurts, and R. Zivadinov, “Brain iron accumulation in aging and neurodegenerative disorders,” *Expert Rev. Neurother.*, vol. 12, no. 12, pp. 1467–1480, 2012.
[59] S. Levi and V. Tiranti, “Neurodegeneration with brain iron accumulation disorders: Valuable models aimed at understanding the pathogenesis of Iron deposition,” *Pharmaceuticals*, vol. 12, no. 1, 2019.
[60] B. R. Stockwell *et al.*, “Ferroptosis: A Regulated Cell Death Nexus Linking Metabolism, Redox Biology, and Disease,” *Cell*, vol. 171, no. 2, pp. 273–285, 2017.
[61] W. S. Yang and B. R. Stockwell, “Ferroptosis : Death by Lipid Peroxidation,” *Trends Cell Biol.*, vol. 26, no. 3, pp. 165–176, 2016.
[62] J. H. O. Barbosa *et al.*, “Quantifying brain iron deposition in patients with Parkinson’s disease using quantitative susceptibility mapping, R2 and R2*,” *Magn. Reson. Imaging*, vol. 33, no. 5, pp. 559–565, 2015.
[63] M. Daglas and P. A. Adlard, “The Involvement of Iron in Traumatic Brain Injury and Neurodegenerative Disease,” *Front. Neurosci.*, vol. 12, no. December, 2018.
[64] M. A. Smith, P. L. R. Harris, L. M. Sayre, and G. Perry, “Iron accumulation in Alzheimer disease is a source of redox-generated free radicals,” *Proc. Natl. Acad. Sci.*, vol. 94, no. 18, pp. 9866–9868, 2002.
[65] A. Ashraf, M. Clark, and P. W. So, “The aging of iron man,” *Front. Aging Neurosci.*, vol. 10, no. MAR, pp. 1–23, 2018.
[66] J. Anderson, J. A. Blair, and R. Armstrong, “The effect of age on tetrahydrobiopterin metabolism in the human brain,” *J. Neurol. Neurosurg. Psychiatry*, vol. 50, no. 2, p. 231, 1987.
[67] L. I. Wallis *et al.*, “MRI assessment of basal ganglia iron deposition in Parkinson’s disease,” *J. Magn. Reson. Imaging*, vol. 28, no. 5, pp. 1061–1067, 2008.
[68] N. Ostrerova-Golts, L. Petrucelli, J. Hardy, J. M. Lee, M. Farer, and B. Wolozin, “The A53T α-Synuclein Mutation Increases Iron-Dependent Aggregation and Toxicity,” *J. Neurosci.*, vol. 20, no. 16, pp. 6048–6054, 2000.
[69] W. Li, H. Jiang, N. Song, and J. Xie, “Oxidative stress partially contributes to iron-induced alpha-synuclein aggregation in SK-N-SH cells,” *Neurotox. Res.*, vol. 19, no. 3, pp. 435–442, 2011.
[70] B. Do Van *et al.*, “Ferroptosis, a newly characterized form of cell death in Parkinson’s disease that is regulated by PKC,” *Neurobiol. Dis.*, vol. 94, pp. 169–178, 2016.
[71] A. Sfera, K. Bullock, A. Price, L. Inderias, and C. Osorio, “Ferrosenescence: The

iron age of neurodegeneration?," *Mech. Ageing Dev.*, vol. 174, pp. 63–75, 2018.
[72] M. Abdalkader, R. Lampinen, K. M. Kanninen, T. M. Malm, and J. R. Liddell, "Targeting Nrf2 to suppress ferroptosis and mitochondrial dysfunction in neurodegeneration," *Front. Neurosci.*, vol. 12, no. JUL, pp. 1–9, 2018.
[73] F. A. Zucca *et al.*, "Interactions of iron, dopamine and neuromelanin pathways in brain aging and Parkinson's disease," *Prog. Neurobiol.*, vol. 155, pp. 96–119, 2017.
[74] J. C. Deschemin *et al.*, "The microbiota shifts the iron sensing of intestinal cells," *FASEB J.*, vol. 30, no. 1, pp. 252–261, 2016.
[75] B. S. Reddy, J. R. Pleasants, and B. S. Wostmann, "Effect of Intestinal Microflora on Calcium, Phosphorus and Magnesium Metabolism in Rats," *J. Nutr.*, vol. 99, no. 3, pp. 353–362, 1969.
[76] M. Knutson, E. Johnson, S. Chlosta, M. Wessling-Resnick, L. Harrington, and D. Fishman, "The Iron Efflux Protein Ferroportin Regulates the Intracellular Growth of Salmonella enterica," *Infect. Immun.*, vol. 74, no. 5, pp. 3065–3067, 2006.
[77] O. Olakanmi, L. S. Schlesinger, and B. E. Britigan, " Hereditary hemochromatosis results in decreased iron acquisition and growth by Mycobacterium tuberculosis within human macrophages ," *J. Leukoc. Biol.*, vol. 81, no. 1, pp. 195–204, 2007.
[78] P. N. Paradkar *et al.*, "Iron depletion limits intracellular bacterial growth in macrophages Iron depletion limits intracellular bacterial growth in macrophages," *Growth (Lakeland)*, vol. 112, no. 3, pp. 866–874, 2011.
[79] B. Yilmaz and H. Li, "Gut microbiota and iron: The crucial actors in health and disease," *Pharmaceuticals*, vol. 11, no. 4, pp. 1–20, 2018.
[80] K. N. Goran, C. Nindjin, A. Dostal, M. B. Zimmermann, C. Chassard, and F. Rohner, "The effects of iron fortification on the gut microbiota in African children : a randomized controlled trial in Co," *Am. J. Clin. Nutr.*, pp. 1406–1415, 2010.
[81] T. Jaeggi *et al.*, "Iron fortification adversely affects the gut microbiome, increases pathogen abundance and induces intestinal inflammation in Kenyan infants," *Gut*, vol. 64, no. 5, pp. 731–742, 2015.
[82] M. T. Nuñez and P. Chana-Cuevas, "New perspectives in iron chelation therapy for the treatment of neurodegenerative diseases," *Pharmaceuticals*, vol. 11, no. 4, pp. 5–9, 2018.
[83] A. A. Belaidi and A. I. Bush, "Iron neurochemistry in Alzheimer's disease and Parkinson's disease: targets for therapeutics," *J. Neurochem.*, pp. 179–197, 2016.
[84] P. Dusek, S. A. Schneider, and J. Aaseth, "Iron chelation in the treatment of neurodegenerative diseases," *J. Trace Elem. Med. Biol.*, vol. 38, pp. 81–92, 2016.
[85] D. Devos *et al.*, "Targeting Chelatable Iron as a Therapeutic Modality in Parkinson's Disease," *Antioxid. Redox Signal.*, vol. 21, no. 2, pp. 195–210, 2014.
[86] A. H. Paolini *et al.*, "Metal-protein attenuation with iodochlorhydroxyquin (Clioquinol) targeting AB amyloid deposition and toxicity in Alzheimer's disease : a pilot Phase 2 clinical trial," *Arch. Neurol.*, vol. 60, 2003.
[87] S. Rose, A. Misharin, and H. Perlman, "A novel Ly6C/Ly6G-based strategy to analyze the mouse splenic myeloid compartment," *Cytom. Part A*, vol. 81 A, no. 4, pp. 343–350, 2012.

[88] C. V. Jakubzick, G. J. Randolph, and P. M. Henson, “Monocyte differentiation and antigen-presenting functions,” *Nat. Rev. Immunol.*, vol. 17, no. 6, pp. 349–362, 2017.
[89] N. V. Serbina, T. Jia, T. M. Hohl, and E. G. Pamer, “Monocyte-mediated defense against microbial pathogens,” *Annu. Rev. Immunol.*, vol. 26, pp. 421–452, 2008.
[90] P. B. Narasimhan, P. Marcovecchio, A. A. J. Hamers, and C. C. Hedrick, “Nonclassical Monocytes in Health and Disease,” *Annu. Rev. Immunol.*, vol. 37, pp. 439–456, 2019.
[91] Y. Anzai *et al.*, “Brain iron concentrations in regions of interest and relation with serum iron levels in Parkinson disease,” *J. Neurol. Sci.*, vol. 378, pp. 38–44, 2017.
[92] J. H. Lee and M. S. Lee, “Brain iron accumulation in atypical parkinsonian syndromes: In vivo MRI evidences for distinctive patterns,” *Front. Neurol.*, vol. 10, no. FEB, pp. 1–9, 2019.
[93] D. L. Abeyawardhane and H. R. Lucas, “Iron Redox Chemistry and Implications in the Parkinson’s Disease Brain,” *Oxid. Med. Cell. Longev.*, vol. 2019, 2019.
[94] E. A. Kennedy, K. Y. King, and M. T. Baldridge, “Mouse microbiota models: Comparing germ-free mice and antibiotics treatment as tools for modifying gut bacteria,” *Front. Physiol.*, vol. 9, no. OCT, pp. 1–16, 2018.
[95] P. Luczynski, K. A. M. V. Neufeld, C. S. Oriach, G. Clarke, T. G. Dinan, and J. F. Cryan, “Growing up in a bubble: Using germ-free animals to assess the influence of the gut microbiota on brain and behavior,” *Int. J. Neuropsychopharmacol.*, vol. 19, no. 8, pp. 1–17, 2016.
[96] M. Al-Asmakh and F. Zadjali, “Use of germ-free animal models in microbiota-related research,” *J. Microbiol. Biotechnol.*, vol. 25, no. 10, pp. 1583–1588, 2015.
[97] I. I. Ivanov *et al.*, “Specific Microbiota Direct the Differentiation of IL-17-Producing T-Helper Cells in the Mucosa of the Small Intestine,” *Cell Host Microbe*, vol. 4, no. 4, pp. 337–349, 2008.
[98] A. Mortha *et al.*, “Microbiota-dependent crosstalk between macrophages and ILC3 promotes intestinal homeostasis,” *Science (80-.).*, vol. 343, no. 6178, 2014.
[99] A. Khosravi *et al.*, “Gut microbiota promote hematopoiesis to control bacterial infection,” *Cell Host Microbe*, vol. 15, no. 3, pp. 374–381, 2014.
[100] D. Erny, A. L. Hrabě de Angelis, and M. Prinz, “Communicating systems in the body: how microbiota and microglia cooperate,” *Immunology*, vol. 150, no. 1, pp. 7–15, 2017.
[101] D. Erny *et al.*, “Host microbiota constantly control maturation and function of microglia in the CNS,” *Nat. Neurosci.*, vol. 18, no. 7, pp. 965–977, 2015.
[102] K. Honda and D. R. Littman, “The microbiota in adaptive immune homeostasis and disease,” *Nature*, vol. 535, no. 7610, pp. 75–84, 2016.
[103] M. G. Cersosimo and E. E. Benarroch, “Pathological correlates of gastrointestinal dysfunction in Parkinson’s disease,” *Neurobiol. Dis.*, vol. 46, no. 3, pp. 559–564, 2012.
[104] T. J. Wenzel, E. J. Gates, A. L. Ranger, and A. Klegeris, “Short-chain fatty acids (SCFAs) alone or in combination regulate select immune functions of microglia-like cells,” *Mol. Cell. Neurosci.*, vol. 105, no. March, p. 103493, 2020.
[105] L. Hoyles *et al.*, “Microbiome–host systems interactions: Protective effects of propionate upon the blood–brain barrier,” *bioRxiv*, pp. 1–13, 2017.

[106] C. R. Martin, V. Osadchiy, A. Kalani, and E. A. Mayer, “The Brain-Gut-Microbiome Axis,” *Cmgh*, vol. 6, no. 2, pp. 133–148, 2018.
[107] J. F. Cryan and T. G. Dinan, “Mind-altering microorganisms: The impact of the gut microbiota on brain and behaviour,” *Nat. Rev. Neurosci.*, vol. 13, no. 10, pp. 701–712, 2012.
[108] H. E. Vuong and E. Y. Hsiao, “Emerging Roles for the Gut Microbiome in Autism Spectrum Disorder,” *Biol. Psychiatry*, vol. 81, no. 5, pp. 411–423, 2017.
[109] K. Berer *et al.*, “Commensal microbiota and myelin autoantigen cooperate to trigger autoimmune demyelination,” *Nature*, vol. 479, no. 7374, pp. 538–541, 2011.
[110] M. F. Sun and Y. Q. Shen, “Dysbiosis of gut microbiota and microbial metabolites in Parkinson’s Disease,” *Ageing Res. Rev.*, vol. 45, no. February, pp. 53–61, 2018.
[111] E. Fitzgerald, S. Murphy, and H. A. Martinson, “Alpha-synuclein pathology and the role of the microbiota in Parkinson’s disease,” *Front. Neurosci.*, vol. 13, no. APR, pp. 1–13, 2019.
[112] E. Svensson *et al.*, “Vagotomy and subsequent risk of Parkinson’s disease,” *Ann. Neurol.*, vol. 78, no. 4, pp. 522–529, 2015.
[113] R. Jones, “NIH Public Access,” *Bone*, vol. 23, no. 1, pp. 1–7, 2014.
[114] S. J. Dixon *et al.*, “Ferroptosis : An Iron-Dependent Form of Nonapoptotic Cell Death,” *Cell*, vol. 149, no. 5, pp. 1060–1072, 2012.
[115] J. Wu, Q. Tuo, and P. Lei, “Ferroptosis , a Recent Defined Form of Critical Cell Death in Neurological Disorders,” pp. 197–206, 2018.
[116] B. R. Stockwell, X. Jiang, and W. Gu, “Emerging Mechanisms and Disease Relevance of Ferroptosis,” *Trends Cell Biol.*, vol. 30, no. 6, pp. 478–490, 2020.
[117] W. Seok, K. J. Kim, M. M. Gaschler, M. Patel, and M. S. Shchepinov, “Peroxidation of polyunsaturated fatty acids by lipoxygenases drives ferroptosis,” 2016.
[118] I. S. Lima, A. C. Pêgo, J. T. Barros, A. R. Prada, and R. Gozzelino, “Cell death-osis of dopaminergic neurons and the role of iron in Parkinson’s disease,” *Antioxid. Redox Signal.*, pp. 1–61, 2020.
[119] “World Population Prospects - Population Division - United Nations.” [Online]. Available: https://population.un.org/wpp/Graphs/Probabilistic/POP/65plus/900. [Accessed: 26-Oct-2020].
[120] C. P. Anderson, M. Shen, R. S. Eisenstein, and E. A. Leibold, “Mammalian iron metabolism and its control by iron regulatory proteins,” *Biochim. Biophys. Acta - Mol. Cell Res.*, vol. 1823, no. 9, pp. 1468–1483, 2012.

APENDIXES

FORUM REVIEW ARTICLE

Cell death-osis of dopaminergic neurons and

the role of iron in Parkinson's disease

Illyane Sofia Lima*[1] & Ana Catarina Pêgo*[1], Tomas Barros[1], Ana Rita Prada[1], Raffaella Gozzelino[1,2]

[1] Laboratório de Inflamação e Neurodegeneração, Centro de Estudos de Doenças Cronicas (CEDOC) / NOVA Medical School, NOVA University of Lisbon, Lisbon, 1150-082, Portugal.

[2] Atlantic Technical University (UTA), Campus de Ribeira de Julião, CP.163, São Vicente, Cabo Verde.

*equal contribution

§correspondent author: Raffaella Gozzelino, (CEDOC) / NOVA Medical School, NOVA University of Lisbon, Lisbon, 1150-082, Portugal, Phone number: +351 967190669, Fax number: +351 218803010.

E-mail: raffaella.gozzelino@nms.unl.pt; raffaellagozzelino@gmail.com

Abbreviated title: Programmed cell death in Parkinson's disease

Keywords: Parkinson's disease, cell death, iron, apoptosis, necroptosis, ferroptosis.

Word count: 7082

Reference number: 199

Number of greyscale illustrations: 6

Number of colour illustrations: 0

Number of tables: 4

Abstract

Significance

There is still no cure for neurodegenerative diseases, like Parkinson's disease (PD). Current treatments are based on the attempt to reduce dopaminergic neuronal loss and multidisciplinary approaches have been used to provide only a temporary symptoms' relief. In addition to the difficulties of drugs developed against PD to access the brain, the specificity of those inhibitory compounds could be a concern. This because neurons might degenerate by activating distinct signalling pathways, which are often initiated by the same stimulus.

Recent Advances

Apoptosis, necroptosis and ferroptosis were shown to significantly contribute to PD progression and, so far, are the main death programs described as capable to alter brain homeostasis. Their activation is characterized by different biochemical and morphological features, some of which might even share the same molecular players.

Critical Issues

If there is a pathological need to engage, in PD, multiple death programs, sequentially or simultaneously, is not clear yet. Possibly, the activation of apoptosis, necroptosis and/or ferroptosis correlates to different PD stages and symptom severities. This would imply that the efficacy of therapeutic approaches against neuronal death might depend on the death program they target and the relevance of this death pathway on a specific PD phase.

Future Directions

In this review, we describe the molecular mechanisms underlying the activation of apoptosis, necroptosis and ferroptosis in PD. Understanding the interrelationship between different death pathways' activation in PD is of utmost importance for the development of therapeutic approaches against disease progression.